



Universiteit Utrecht

Influence of climate and oceanography on Cretaceous sedimentation in the North Atlantic.

A dissertation

By

Godert De Keijzer

Submitted to the Department of Earth Sciences

Utrecht University

Budapestlaan 4, 3584 CD Utrecht

The Netherlands

Influence of climate and oceanography on Cretaceous sedimentation in the North Atlantic.

Abstract

Sedimentation in the North Atlantic Ocean underwent fundamental changes during the Cretaceous. From a Late Jurassic restricted basin regime, characterized by a large influx of siliciclastics, to a Mid – Late Cretaceous widening basin with open circulation and a prominent biogenic component. A systematic analysis of sediment and mineral composition of the Cretaceous cores in IODP sites was made. The study covers; Moroccan offshore, Iberian offshore, Celtic Sea Basin, Grand Banks, Blake Bahama Basins, and Demerara Rise Basins. This dissertation aims to enhance the understanding of the effect of climatic and oceanographic changes on the general sedimentary infill of the North Atlantic during the Cretaceous.

The western and eastern Early Cretaceous North Atlantic commenced as wet and humid, the northern North Atlantic was prone to strong terrigenous deposition. Aptian large eustatic sea level rise, shoaling CCD and heating climate led to widespread clay deposition. The climatic and oceanographic changes led to OAE formation, from the Aptian onward. The western and southeastern margins behave differently. Continued warming climate, eustatic sea level rise and shoaling CCD were responsible for the continued shale deposition and carbonate deposition on the eastern margin influenced by upwelling. Turonian change to a ventilated margin caused by the deep water connection to the South Atlantic and cooling climate led to a carbonate dominated western North Atlantic and a zeolitic clay dominance in the southeastern North Atlantic. The Late Cretaceous was characterized by marl deposition in the western margin, and clay deposition in the southeastern North Atlantic. The western and northern continental humidity, continental weathering and high temperatures created optimum surface for high oceanic primary production. Ventilated oceans on the southeastern North Atlantic margin led to adverse conditions; less nutrient input and shoaling CCD leading to large-scale clay deposition.

Table of Content

I.	Introduction	5
II.	Methods	6
	2.1. Site Selection	6
	2.2. Processing IODP data	7
III.	Geological setting	9
	3.1. Formation of the North Atlantic Ocean	9
	3.2. Basin physiography	10
	3.2.1. North Atlantic	10
	3.2.2. West African offshore	12
	3.2.3. Iberia	12
	3.2.4. Irish Sea	14
	3.2.5. Grand Banks	14
	3.2.6. Blake Bahama Basins	15
IV.	Stratigraphy	16
	4.1. North Atlantic lithostratigraphy	17
	4.3. Large scale basin histories.	22
	4.3.1. Morocco	22
	4.3.2. Iberia	22
	4.3.3. Celtic Sea Basin	23
	4.3.4. Grand Banks	24
	4.3.6. Blake Bahama/Cape Hatteras	24
V.	Observations	25
	5.1. Lower Cretaceous	30
	5.1.1. Earliest Lower Cretaceous	30
	5.1.2. Late Early Cretaceous	32
	5.2. Mid Cretaceous	34
	5.2.1. Earliest Mid Cretaceous	34
	5.2.2. Mid Cretaceous	35
	5.2.3. Latest Mid Cretaceous	36
	5.4. Upper Cretaceous	38
VI.	Interpretation	40
	6.1. Oceanic Anoxic Events (OAE's)	40
	6.1.1. OAE interpretation per site	41

6.2. <i>Water depth</i>	46
6.2.1. Water depth interpretation per site	48
6.3. <i>Eustatic Sea Level and CCD</i>	54
6.3.1. Eustatic sea level and CCD per site	56
VII. Discussion	59
7.1. <i>Limitations</i>	59
7.1.1. Limitations on the interpretation of core data	59
7.1.2. Limitations on the interpretation of OAE's	62
7.1.3. Limitations on the interpretation of water depth	62
7.2 <i>Cretaceous climate and oceanography</i>	63
7.2.1 Lower Cretaceous	63
7.2.2. Mid Cretaceous	65
7.2.3. Upper Cretaceous	75
VIII. Conclusions	76
IX. Acknowledgements	76
X. References	77
XI. Appendixes	82
11.1. <i>Legend</i>	82
11.2. <i>Appendix A</i>	82
11.3. <i>Appendix B</i>	83
11.4. <i>Appendix C</i>	84
11.5. <i>Appendix D</i>	84
11.6. <i>Appendix E</i>	85
11.7. <i>Appendix F</i>	86
11.8. <i>Appendix G</i>	87
11.9.1. Clay mineralogy	87

I. Introduction

Since the 1970's sedimentation in the North Atlantic Ocean has attracted great academic and industrial attention. The proceedings of the IODP (International Ocean Drilling Program) provide extensive data on the deep sea and continental shelf infill of the North Atlantic Ocean. Academia and industry focused their studies on individual DSDP and ODP legs or on selective continental regions. As a consequence few studies focused on the large scale sedimentary development of the North Atlantic Ocean during the Cretaceous.

The current understanding of the North Atlantic was laid out by Jansa et al., (1979). Jansa et al., (1979) delineated the general sedimentological relationships for the Mesozoic Western and Eastern North Atlantic by defining six lithostratigraphic formations and two members, in the Figure 1 we depict only the Cretaceous formations (Rothe & Tucholke 1981): 1) Cat Gap Formation, greenish gray argillaceous limestone and calcareous claystone (Oxfordian - Tithonian) (Figure 1), 2) Blake – Bahama Formation, white chalky limestone, (Tithonian – Barremian) (Figure 1), 3) Hatteras Formation, dark green-gray claystones and shales (Barremian - Cenomanian), 4) Plantagenet Formation, zeolitic varicolored claystones (Cenomanian – Eocene) (Figure 1), 4b) Cresnet Peaks Member, olive gray chalk marl and limestone (Maastrichtian - Paleocene), 5) Bermuda Rise Formation, green siliceous oozes, claystone and cherts (Paleocene – Eocene), 6) Blake Ridge Formation, green gray hemipelagic muds with sand and silt beds (Eocene – Quaternary), 6b) Great Abaco Member, light gray carbonates (Miocene) (Jansa et al., 1979, Rothe & Tucholke 1981). This subdivision of the Mesozoic forms the pillar of the North Atlantic sedimentological classification (Tucholke et al., 2004).

Formation/Member	Lithostratigraphy	Principal Mineral Components (Rothe et al., 1981)	Formation	Schematic Stratigraphic Column	Bathyal CCD level Abyssal (Jansa et al., 1978)	Age
Cresnet Peak Mb.	Nannofossil Marl	Montmorillonite, Illite				Eocene
Plantagenet Fm.	Varicolored zeolitic clay	silty zeolitic clay with montmorillonite				Cenomanian
Hatteras Fm.	Greenish claystone	monmorillinite, illite, kaolinite, chlorite, quartz, opal, zeolite				Cenomanian
	Black bituminous shale grayish green claystone variegated intraclast claystone sandstone subfacies	black shale, marls with mica 40%, montmorillonite 10-25%, illite, quartz, kaolinite, feldspar nannofossil claystone, silty clay with montmorillonite, illite, kaolinite				Barremian
Blake Bahama Fm.	White chalky limestone	organic rich marl with terrigenous elements; illite, quartz palygorskite, feldspar, montmorillonite, cristobalite.				Barremian Tithonian

Figure 1; Stratigraphic characteristics of the Southern North Atlantic, colors refer to different formation/lithostratigraphic units (adapted from Jansa et al., 1978, Rothe et al., 1981)

Other work contributing to the general understanding of the North Atlantic sedimentology was that of Thiede and Ehrmann (1986). Thiede and Ehrmann (1986) subdivided sedimentation of the North Atlantic on the basis of sedimentation rate. Two main phases were identified: 1) Late Jurassic – Early Cretaceous (high sedimentation rate) 2) Early Cretaceous – Cenozoic (slow sedimentation rate). The second phase is characterized by numerous hiatuses and low sedimentation. Rothe & Tucholke (1981), Von Rad & Sarti (1986) and lately Tucholke et al., (2004) tried to find the intradimensional relationships in the Cretaceous North Atlantic linking the western and eastern segments. These

studies proved that strong similarity in sedimentary style and composition in turbidites existed during Early – Mid Cretaceous between the two margins.

This study investigates a selection of North Atlantic IODP data for the Cretaceous. The primary objective is to increase the understanding of large scale sedimentation in the North Atlantic. The IODP data contain sediment and mineral compositions of cores located throughout the North Atlantic Ocean. Investigation of the composition of these records will give data on the climate and oceanographic conditions on these specific locations. It is the aim of this study to study the Cretaceous sedimentary record across the North Atlantic; from north to south and west to east. This research will look in detail at sedimentary patterns and composition to delineate climatic and oceanographic patterns in the North Atlantic Ocean.

By linking the IODP record to literature on the Moroccan, Iberian and Newfoundland margins and the Cape Verde Basin, Demerara Rise and Blake Bahama Basin a generic reconstruction will be made of the Cretaceous North Atlantic infill. The study uses a framework of smear slides, X-ray and lithological interpretation to assign the Jansa et al., (1978) formations, identify and correlate similarities and differences between the different basins of the North Atlantic Ocean. Using the Jansa et al., (1978) classification as a basis a systematic overview and detailed insight in climatic, tectonic and physiographic changes will be constructed.

II. Methods

2.1. Site Selection

This research is based on the investigation of thirteen cores of the Deep Sea Drilling Program (DSDP) and the Ocean Drilling Program (ODP) part of the Integrated Ocean Drilling Program (IODP) (Figure 2). Site and core selection were based on the following criteria:

- 1) Distribution along the different margins of the North Atlantic Ocean. Six sites were chosen in the Western Atlantic and seven in the Eastern Atlantic (Figure 2).
- 2) Sites are selected on different latitudes to cover different paleoclimate belts.
- 3) Sites should represent the longest available Cretaceous succession in that location. Preferably from earliest to latest Cretaceous. Many locations lack such a coverage, in these cases the study opted for the most extensive Cretaceous coverage.
- 4) Sites were selected on the availability of smear slide and X-ray studies.

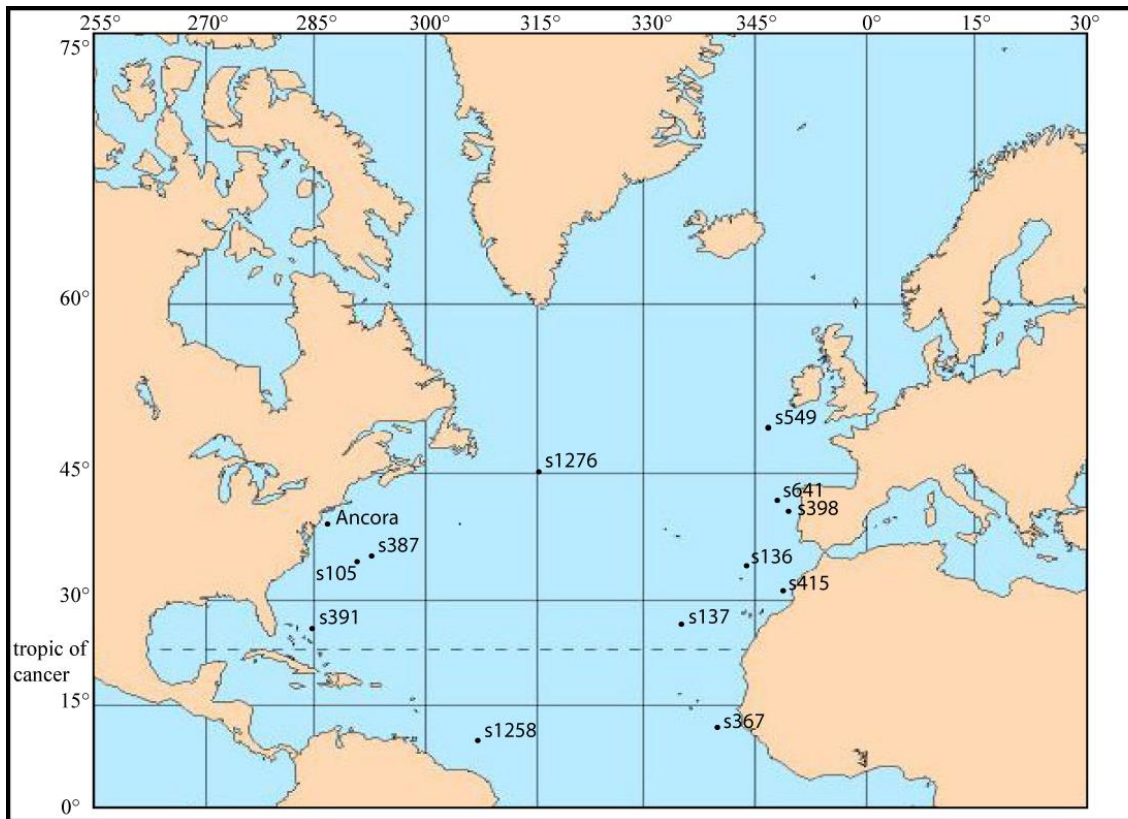


Figure 2; Paleogeographic location of all DSDP and ODP cores

2.2. Processing IODP data

The IODP data were processed to attain results Appendix A - F:

- 1) All relevant data was captured in an Excel database. Relevant data: depth, age, lithology, colour, fauna species (eg. foraminifers), smear slide data (composition and texture), X-ray fractions.
- 2) A standard was deducted from the database. IODP reports present their smear slide data and X-ray fractions either in exact percentages or in relative fractions (Eg: D=Dominant (>50%), A=Abundant (25%-50%), C=Common (10%-25%), R=Rare (2%-10%), and T=Trace (<2%). To construct one single format, relative fractions were calculated to exact percentages. Eg.: Smear Slide, Quartz (A), Clay (A), Mica (A). Results in Quartz (33 $\frac{1}{3}$ %), Clay (33 $\frac{1}{3}$ %), Mica (33 $\frac{1}{3}$ %).
- 3) Smear slide and X-ray fractions were calculated proportionally per ten meter core. IODP records have a strong data density in some cores. Smear slide and X-ray fractions can contain more than 5 measurements per 10 meter. The maximum detail, recorded by the figures created in this study (Appendix A – F), is one measurement per 3 meter. Consequently the abundance of data needs to be averaged to one measurement per 3 meter. In situations with a strong variation in the sediment composition, averages per 3 meter could lead to a blurring of the data (eg. S1276). In these situations a stronger data density was opted or an arbitrary selection to best represent the smear slide composition.
- 4) Excel data is transferred to figures (Adobe Illustrator). The data is represented by different columns: depth, age, lithology, smear slide composition, smear slide texture, X-ray fractions,

comments (Appendix A – F). Different colours illustrate different components of smear slides and X-ray fractions.

- 5) Transferred smear slide and X-ray fractions are represented by a maximum detail of 1 measurement per 3 meter. Which fits the aim of this study, to investigate large scale sedimentary trends.
- 6) Smear slide and X-ray fractions less than 3 % are mentioned in the column comments. Adding fractions < 3 % creates a chaotic diagram and obscures large scale components.
- 7) Backstripping was not considered in this study as a comparable contribution of compaction in all sites is assumed.

The sedimentary history of the North Atlantic Ocean was split into three time segments: 1) Lower Cretaceous; Tithonian / Berriasian boundary - Aptian boundary, 2) Mid Cretaceous; Barremian /Aptian boundary - Turonian / Coniacian boundary, 3) Upper Cretaceous; Turonian / Coniacian boundary - Maastrichtian / Paleogene boundary.

Transects from west to east and north to south were created to study relationships between different basin and margins (Figure 3). The west to east transects are located in different latitudes, the sedimentary composition of the transects will allow a comparison of the effect of different climate and oceanography conditions on the sedimentation. The north south transects will illustrate similarities and difference between the western and eastern margin of the North Atlantic ocean. In this study a series of six transects were constructed (Figure 3). Four extrapolating the Western and Eastern Atlantic margins from west to east (Appendix A-D) and two correlating the Western and Eastern margin from north to south (Appendix E-F). The characteristic formations as defined by Jansa et al., (1979) and Rothe & Tüchle (1981) are placed in plate reconstructions for the different Cretaceous intervals mentioned in the previous paragraph, to illustrate the regional development of different the formations and highlight the tectonic development of the North Atlantic Ocean.

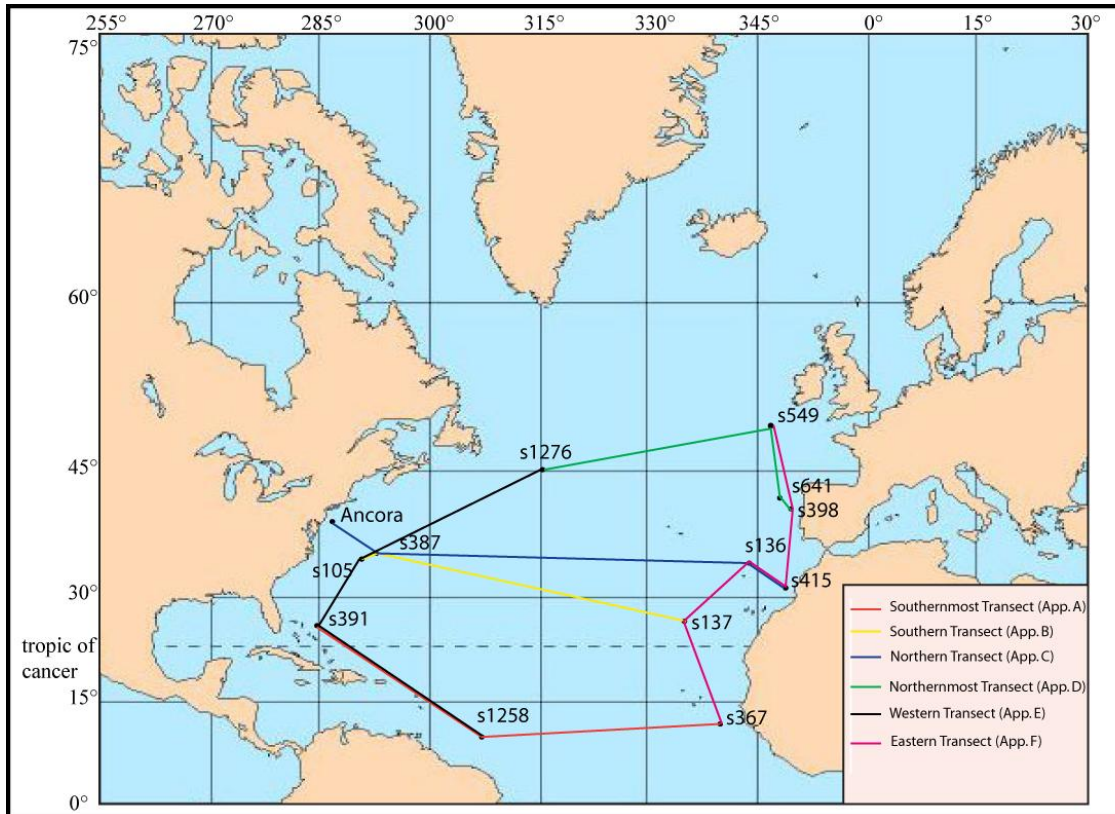


Figure 3; Transects and related appendixes (App.)

III. Geological setting

3.1. Formation of the North Atlantic Ocean

The North Atlantic Ocean formed as a result of Permian - Triassic rifting of pre-Cambrian fold belts (Thiede 1979). The rift followed a belt of weakness along parts of the Variscan, Acadian, Hercynian and Caledonian mountain chains and is related to the southward propagation of the late Palaeozoic Norwegian-Greenland sea rift and the westward propagation of the Permo-Triassic Tethys rifts (Thiede 1979, Ziegler 1989). The first phase formation of the North Atlantic consisted of continental rifting and evaporite precipitation in small North East trending halfgrabens (Hafid et al. 2008, Poag 1978). Hafid et al., (2008) placed the first phase at Late Permian to Early Jurassic. The second phase and a change from continental rifting to the formation of oceanic crust and start of spreading is dated by Robertson & Ogg (1986) as Early Toarcian (oldest crust 170 – 178.7 Ma) (Steiner et al., 1998).

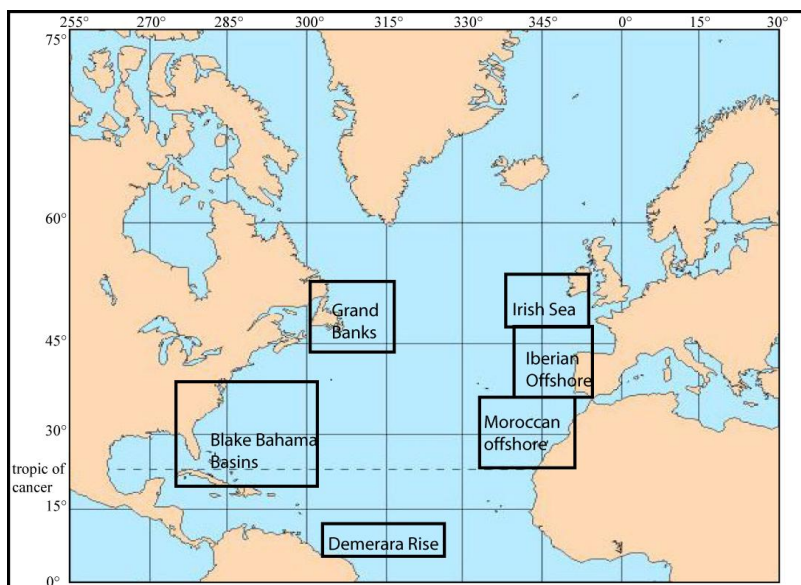


Figure 4; North Atlantic provinces: Grand Banks detail map see figure 8, Iberian offshore detailed map see figure 7, Moroccan offshore detailed map see figure 6, Blake Bahama Basins detailed map see figure 9.

The spreading of the North Atlantic Ocean started between North Africa and North America during late Early Jurassic. During Early Aptian (114 – 125 Ma) the Iberian (Galicia Bank) and Grand Banks margins became separated by the North Atlantic rift (Figure 5) (Blakey 2007, Wilson et al., 1989, Boillot et al., 1989). The Aptian / Early Albian rifting sequence split the Grand Banks (Flemish Cap) and Irish Sea (Goban Spur) (Figure 5) (Mauffret et al., 1988, Tankard & Balkwill 1989, Ziegler 1989). The final important Cretaceous propagation of the North Atlantic spreading axis was the Santonian - Campanian opening of the Labrador Sea, separating New Foundland and Greenland (Ziegler 1989).

Plate tectonics have been responsible for migration and expansion of the North Atlantic Ocean to the north, east and west. The North Atlantic migrated from 0° - 30°N during Berriasian - Valanginian (von Rad & Sarti 1986, Lawver et al., 2002) to 0° - 40°N Early Aptian and 0° - 45°N during Middle Cenomanian (95 Ma) (Lawver et al., 2002). During latest Cretaceous the entire ocean shifted north stretching from 10°N to 55°N (Lawver et al., 2002). Expansion mostly led to a latitudinal change in the Late Cretaceous while the current northern location commenced in the Tertiary with the continental break up between Greenland and the Baltic Shield.

3.2. Basin physiography

3.2.1. North Atlantic

Physiography is one of the basic parameters controlling the stratal architecture in basins (Posamentier & Allen 1993). This subchapter firstly aims to conceive the general characteristics of the North Atlantic Ocean and secondly of the different North Atlantic subbasins. Physiography includes the estimated paleobathymetry and the connection between different basins, including the implications of large-scale physiographic features on the hydrographic regime.

The first physiographic parameter, paleobathymetry, is based on the estimation of the 1D cooling model (Sclater et al., 1971) in combination with literature; Sclater (1977), Thiede (1979), von Rad & Sarti (1986). The 1D cooling model follows the fact that new oceanic crust is produced at the

Mid Atlantic Ridge, implying that the oldest oceanic crust lies adjacent to the continental margins. The 1D cooling model states that subsidence is proportional to square root of age ($2900 + \sqrt{\text{age in Ma}}$) (Sclater et al., 1971). The cooling model requires compensation for anomalous regions; elevated regions of uplifted old sea floor, aseismic ridges (Bahama Plateau) and sediment load (Parsons and Sclater 1977). In a normal situation the assumption is made that crust of 0-80 Ma ranges between 2600-5000 m. Applying the bathymetric charts of Sclater et al., (1971) the 3000, 4000 and 5000 m isobaths correspond to ages of 2, 20 and 50 Ma of normal oceanic crust.

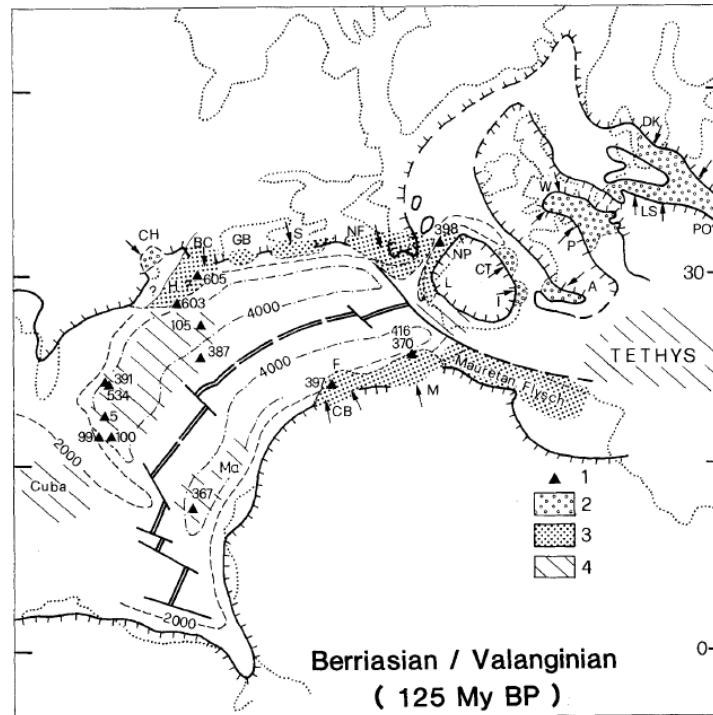


Figure 5; Early Cretaceous paleogeography of the North Atlantic – Tethys Ocean adapted from (van Rad & Sarti 1986)

The connection between basins, the second physiographic effect, discusses the existence and extent of surface- and bottom water exchange based on literature. The earliest east west trending North Atlantic Ocean had a plausible connections with both the Pacific in the west and the Tethys in the east (Thiede 1979, Sclater et al., 1977). The extent of large-scale bottom water exchange to the Pacific depends on the scale and extent of the proto Caribbean Island arc (Sclater et al., 1977). The Western Tethys is considered a mosaic of shallow basin, surface water exchange is undisputed. A deep water passage is debated due to the great complexity around the Gibraltar strait (Figure 5). Holbourn et al., (2001) claimed a deep water link > 2500 m to have existed in the Rifian seaway, this research was based on benthic foraminifera.

The other major basin connection was that between the Northern and Southern Atlantic. A surface water connection between the North and South Atlantic opened in the Mid Cretaceous and a deep water connection developed in the Late Cretaceous (80 Ma) (Thiede 1979). The Norwegian Greenland Sea connection with the North Atlantic was established during the Early Tertiary with the breakup of the Iceland-Faeroe Ridge, a structural high. However, a surface water link may already have existed during the Mesozoic as part of a narrow epicontinental basin (Thiede 1979).

On an intra North Atlantic scale the Mid Oceanic Ridge would have acted as a tectonic divide between the western and eastern subbasins. The Mid Oceanic Ridge could have prevented the large-scale exchange of bottom water. However, transform faults and fracture zones may have enabled local deepwater exchange. Pinpointing if, when, where and how these bypasses were created is troublesome.

3.2.2. West African offshore

The West African offshore is considered here as one subbasin. Offshore West Africa contains no major tectonic elements imposing barriers to the large-scale sediment transport from south to north or west to east (Hafid et al., 2008). The main structural elements are a series of half grabens striking north-northeast to south-southwest separated by crosscutting transfer faults (Heyman 1989). The three main proximal basins in North Morocco from south to north are the Aaiun, Tarfaya and Essaouira Basins (Figure 6). The abyssal plain is subdivided from south to north in the Madeira Abyssal plain, Seine Abyssal plain and Horseshoe Abyssal plain. The current main structural high in the West African offshore is the Canary Island Hotspot, which is supposed to have formed 60 Ma ago and therefore is unlikely to have formed a barrier in the Cretaceous (Figure 6).

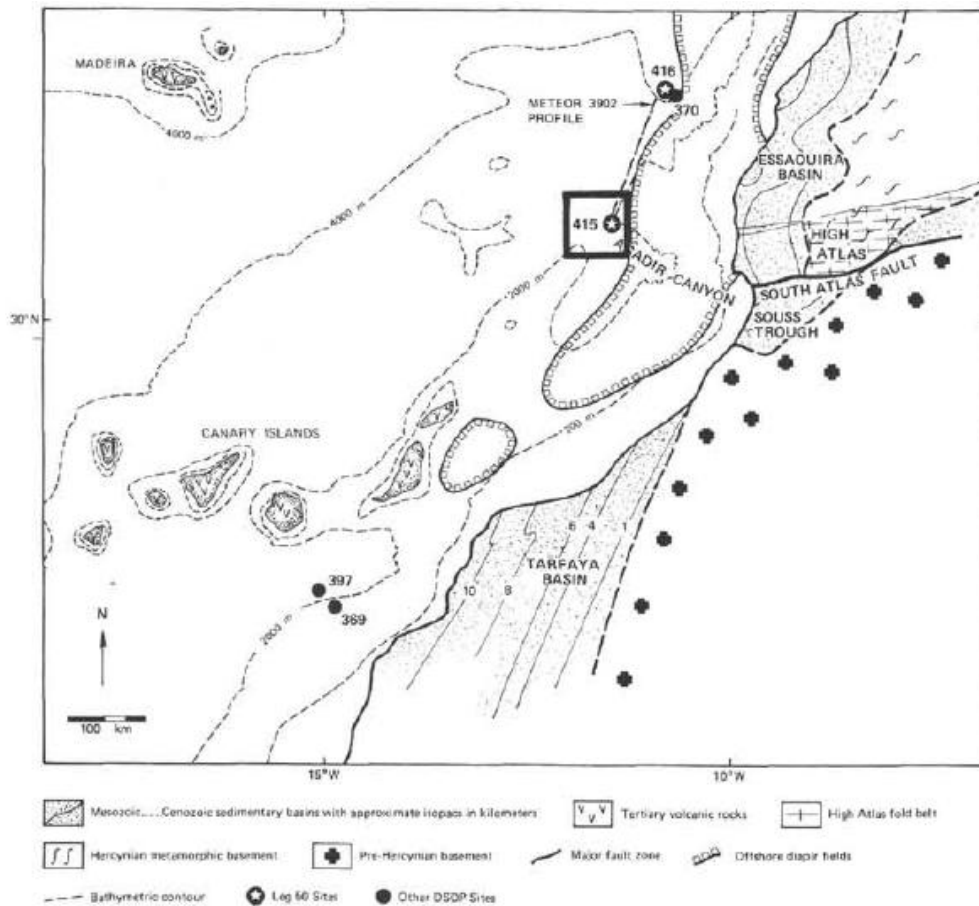


Figure 6; Regional map of Western Morocco including Tarfaya, Essaouira Basins (Site 415 DSDP report)

3.2.3. Iberia

The Iberian offshore consists of two different margins, the western rifted margin and the northern active margin. The western rifted margin formed during Early Cretaceous extension and break up of North America and Iberia. The northern active margin originated from the Palaeogene

convergence between the Iberian and European plates (Boillot et al., 1989). The western Iberian deep offshore consists of two distinct offshore depocenters separated by canyons and tectonic highs; 1) Iberia Abyssal plain, 2) Tagus Abyssal plain (Figure 7) (Pinheiro et al., 1996). The Iberian continental shelf contains two depocentres; 1) Lusitanian Basin, 2) Galicia Interior Basin (Figure 7).

A more detailed subdivision of the Iberian offshore is needed to understand the complicated physiography observed in Figure 7. The West Galician Margin, resulted from Valanginian – Latest Aptian rifting, the main structural highs are the: Vasco da Gama-, Porto-, Tore- and Vigo Sea Mounts, Galicia Bank and Ortegual Spur. These highs form a discontinuous barrier between the West Galician Basin and the Iberian Abyssal plain. Presently these plateaus consist of Mesozoic tilted blocks and half-grabens which were reactivated and uplifted during early Cenozoic (Boillot et al., 1989). The Tagus Abyssal plain to the south of the Iberia Abyssal plain is isolated by the Tore Sea Mount, Estremadura Spur, Madeira – Tore Rise in the north and to the south by the Gorringe Bank (Pinheiro et al., 1996). Paleobathymetry of the Iberian Basins at 108 Ma has a range from 1 to 3 km along the continental margin (Verhoef & Srivastava 1989).

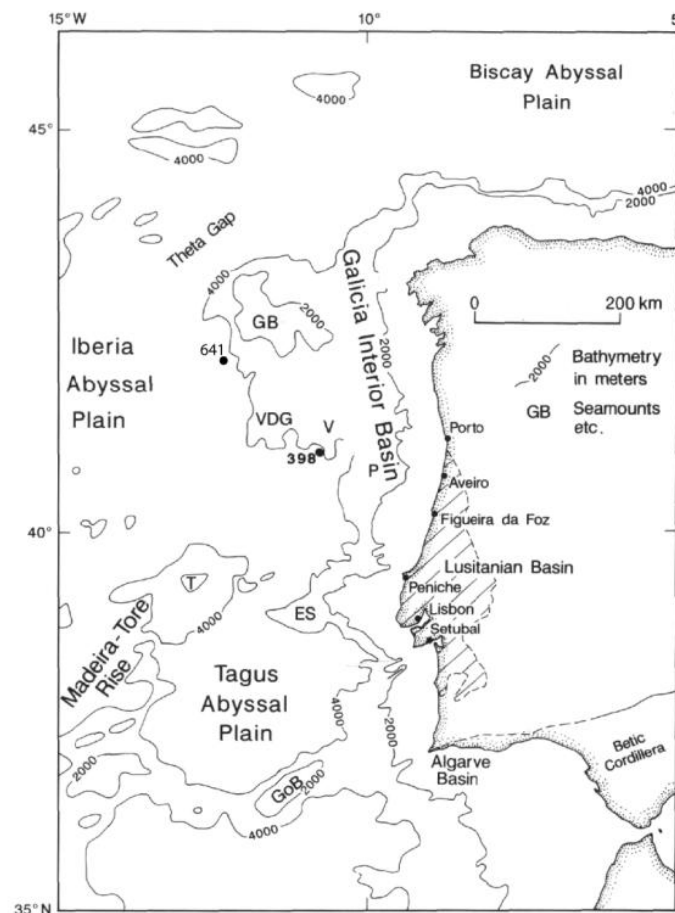


Figure 7; Physiography of West Iberian Margin. Bathymetry is in meters (Lallemand et al., 1985), seamounts: GB: Galicia Bank, P = Porto Seamount, T = Tore Seamount, V = Vigo Seamount, VDG = Vasco da Gama Seamount, ES = Estremadura Spur, GoB = Gorringe Bank (Pinheiro et al., 1996).

3.2.4. Irish Sea

Northern Atlantic offshore Ireland and Great Britain consist of the Porcupine Basin, Celtic Sea Basin and Western Approaches Basin. Structural highs are the Goban Spur and the Porcupine Bank. Fault trends in the Porcupine Basin are NW-SE (Verhoef & Srivastava 1989). Paleobathymetry off the basins at 105 Ma ranges from 1 km in the Celtic Sea and Western Approaches Basins to 3 km in the Porcupine Basin.

4.2.5. Grand Banks

Grand Banks is the northernmost extension of the Cretaceous North Atlantic and is located in the Newfoundland offshore. The proximal Grand Banks region displays a wide variety of tectonic styles (Verhoef & Srivastava 1989). The southern basins developed before and during convergence between Africa and Nova Scotia and are typically narrow and elongate (Whale and Horseshoe Basins). The central Jeanne d’Arc Basin evolved from Late Triassic to mid-late Cretaceous with a typical half-graben asymmetry, whereas the northern Orphan Basin developed during middle to late Cretaceous with a wide stretched shape (Figure 8) (Tankard & Welsink 1987). Fault trends in the central and southern Grand Banks are directed southwest-northeast, whilst the northern Orphan Basin shows a southeast – northwestern trend (Welsink et al., 1989). The basins are separated by a series of ridges and platforms controlled by major bounding faults following the dip slip extensional system that were active from Late Callovian to Aptian (Tankard & Welsink, 1989). Tankard & Welsink (1989) placed the Iberian Grand Banks break up in the Early Aptian, synchronous to the Early Aptian unconformity. The latest Cretaceous rifting pulse, “late Kimmerian,” is related to thermal doming. This doming led to deep truncation of the Jurassic in the Grand Banks (Horseshoe Basin, North- and South Whale Basin) (Ziegler 1989). The major regional tectonic highs from south to north are the Flemish Cap and Orphan Knoll. The abyssal plain is divided between the South Newfoundland Basin and the North Newfoundland Basin (Figure 8).

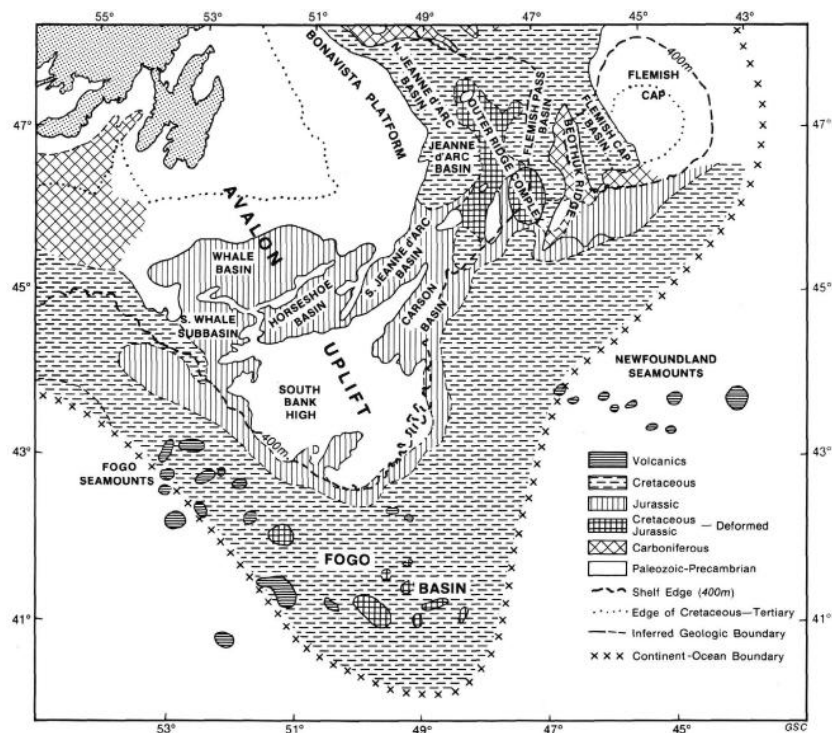


Figure 8; Physiography of the New Foundland offshore, Grand Banks region (Welsink et al., 1989)

Paleobathymetry at 105 Ma (Verhoef & Srivastava 1989) ranged from 1 to 3 km. Structural highs were the Grand Banks (Avalon Uplift) and Flemish Cap. Note that paleobathymetry from Verhoef & Srivastava (1989) is not a paleodepth reconstruction as no sediment backstripping was applied. As such it has to be treated as an indication rather than an exact appreciation of the paleodepth.

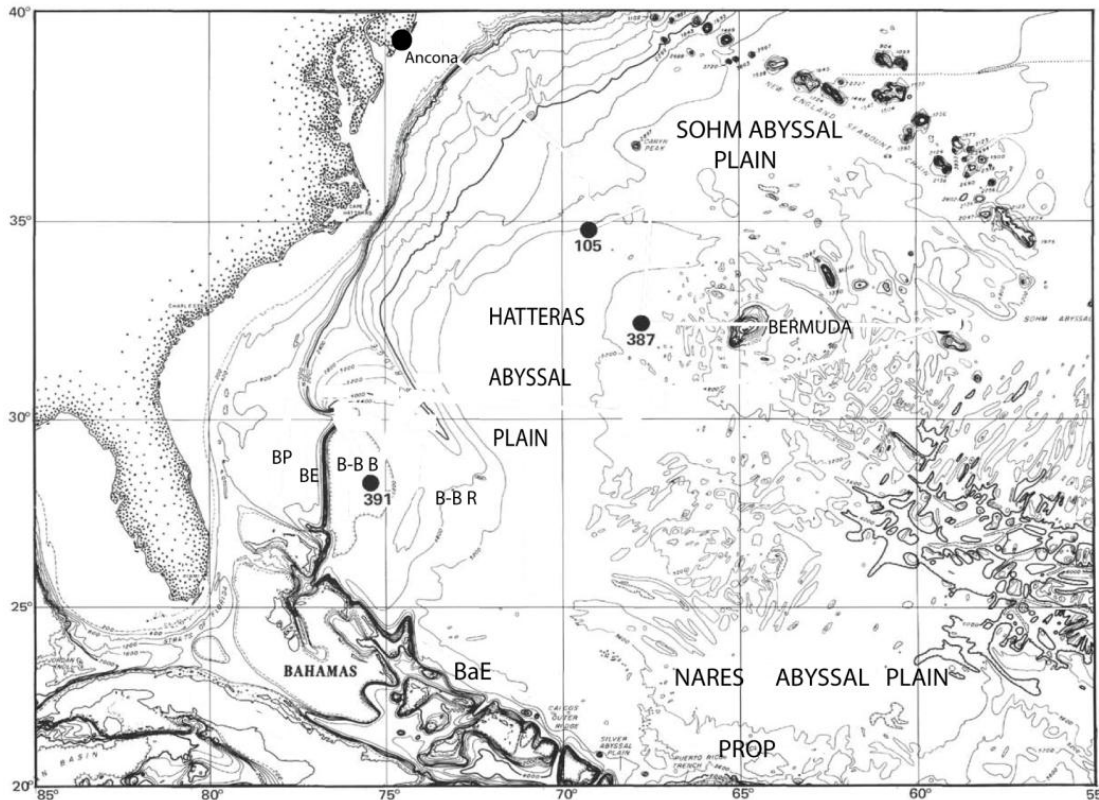


Figure 9; Physiography of North American offshore. BP = Blake Plateau, BE = Blake Escarpment, B-B B = Blake – Bahama Basin, B-B R = Blake Bahama Ridge, BaE = Bahama Escarpment, PROP = Puerto Rico Outer Ridge (Miller et al., 1999)

3.2.6. Blake Bahama Basins

The North American offshore formed as part of the earliest rifting of the North Atlantic. During this episode the North American margin was located adjacent to the present Moroccan margin. The Blake Plateau region can be subdivided in four regions: 1) Blake Plateau (separating Florida Slope from Blake Escarpment) (Figure 9), 2) Blake Escarpment (a cliff that falls from the relatively shallow Blake Plateau to the abyssal plain of the Blake – Bahama Basin) (Figure 9), 3) New Jersey Continental shelf, 4) Hatteras Abyssal Plain (Figure 9).

The Blake Plateau is an elongated North – South trending depression bounded by Cape Fear to the north and by the Bahama uplift to the south (Figure 9). The Bahama uplift formed as a splinter of the continental margin during Middle Jurassic (Sheridan & Crosby 1981) (Figure 9). The Blake Escarpment is the abrupt transition between intermediate waterdepth today (1000 – 2000 m) to the 5000 m deep abyssal plain. This transition was correlated to a change during the rifting of the Blake plateau, based on presence of a magnetic anomaly (Sheridan & Crosby 1981) (Figure 9).

The northern part of the Blake Escarpment is known as the Blake Spur. Central and southern parts of the Blake Spur are oriented parallel to the Blake Plateau. During Early Cretaceous the Bahama uplift, Southern Blake Plateau, Bahama Escarpment, Georges Bank Basin and Scotian Basin developed

extensive carbonate platforms and reefs. Other important physiographic characteristics of the deep North American margin are the Hatteras Abyssal Plain, Sohm Abyssal Plain and the Bermuda and Bahama Highs (Figure 9).

Event	Approximal age	References
Isolated narrow marine basins with a restricted depositional environment ("salts")+ Gulf of Mexico, W/African cont margin, N-American continental margin	Bathonian	Hafid et al., 2008
Establishment of marine connection between the Gulf of Mexico/Caribbean (+Pacific) and the NW European epicontinental seas /Tethys realm	Early L Jurassic -150Ma	Thiede 1979
Separation Africa - North America	Middle Jurassic 165 Ma	Slater et al., 1977
Opening of a pathway through the Caribbean to the Pacific	Tithonian 140 Ma	Thiede 1979
E-W trending central North Atlantic basin as part of Tethys-realm	Tithonian 140Ma - Aptian	Thiede 1979
Separation Iberia – North America	Aptian 110 Ma	Slater et al., 1977, Wilson et al., 1978
Opening of a surface water pathway to the South Atlantic	Aptian 110 Ma	Slater et al., 1977
Opening of a deep water current North – South Atlantic	Early Cenomanian 97 Ma	Graciansky de, et al., 85
Western Interior Seaway	Cenomanian-Santonian 95-80 Ma	Thiede 1979
Part of a N-S stranding Atlantic ocean but virtually closed to the North	Cenomanian 95Ma - Danian 65Ma	Thiede 1979
Trans-Saharan Sea	Latest Cenomanian and Santonian-Palaeocene 80-53 Ma	Thiede 1979
Opening of Labrador Sea	Turonian - Santonian	Srivatava and Verhoef 1992
Opening of the deep connection to the South Atlantic	Santonian / Maastrichtian 65-80 Ma	Thiede 1979

Table 1: Chronological summary of important events for North Atlantic physiography (Thiede 1979)

IV. Stratigraphy

Chapter 4 Stratigraphy will describe the current state of knowledge on the North Atlantic stratigraphy. The first sub-chapter will study the North Atlantic Cretaceous lithostratigraphy. The second sub-chapter will focus on the largescale sedimentary development of the different subbasins.

The in the above mentioned study of Jansa et al., (1979) correlated the Western and Eastern margin of the southern North Atlantic (Figure 10). Jansa et al., (1979) used DSDP data from three legs to correlate the western North Atlantic West African offshore to the Blake Bahama & Hatteras Basin eastern North Atlantic. To do this Jansa defined formations and members as defined in the introduction (Figure 1). In addition to the description of these three formation sub-chapter 4.1. will also describe the three members of the Hatteras Formation reported by Jansa et al., (1978).

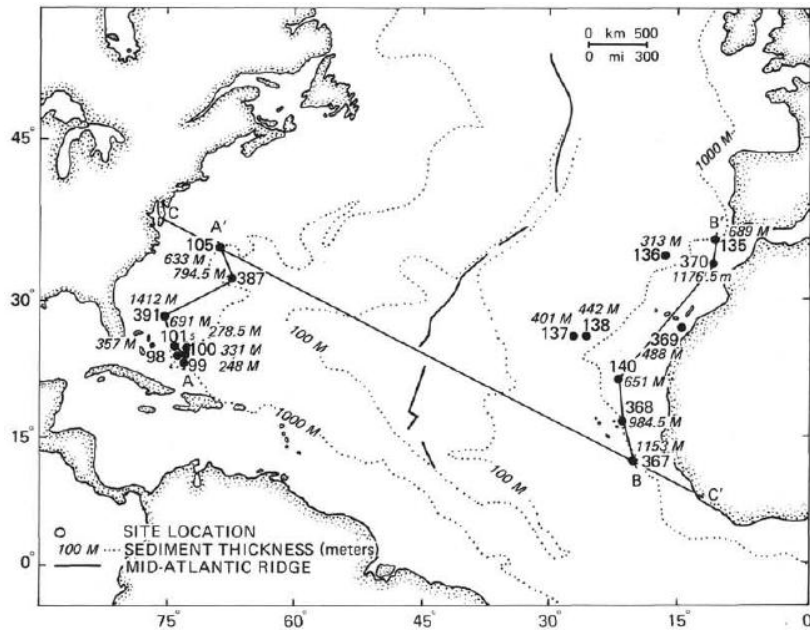


Figure 10; Stratigraphic correlation and cores used by Jansa et al., (1979).

4.1. North Atlantic lithostratigraphy

The Blake – Bahama Formation, white chalky limestone, is mainly composed of rich marl (33 – 99 % carbonate) (Rothe & Tucholke 1981). Characteristically the formation contains the following major terrigenous components; illite, palygorskite, montmorillonite and minor terrigenous components; quartz, plagioclase, mica, pyrite and heavy minerals (Figure 1 & 11, Appendix A – F). This formation is texturally homogenous, contains rare bioturbation and has a scarcity of nannoplankton and radiolarians. These elements point to a pelagic deposition in a deep bathyal depositional environment (Jansa et al., 1978). Deposition must have occurred above the CCD, but below the lysocline related to a dissolution of foraminifera (Jansa et al., 1978). In the Western Atlantic (S105, S391) this unit is characterised by (from bottom to top); clayey limestone (lower part) and sand to silty (upper part, containing Bouma sequences). The Bouma sequences are related to turbidites containing schist and quartz fragments, which links them to the adjacent continental margin (Sheridan et al., 1977).

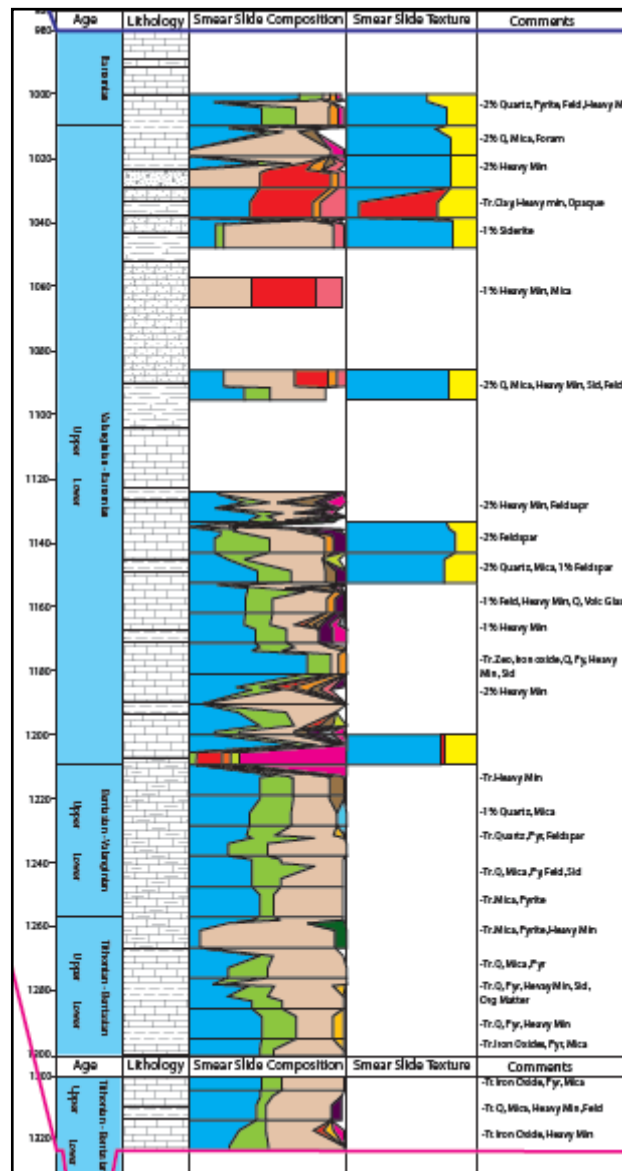


Figure 11: S391 Typical Blake – Bahama Formation (Legend, Appendix E)

The Hatteras Formation as described by Rothe and Tucholke (1981) has been divided by Jansa et al., (1978) into three members (Figure 1): 1) Black Bituminous Shale, 2) Grayish-green Claystone Intraclast Sandstone, 3) Greenish Claystone. These are specified below.

The Hatteras Black Bituminous Shale Member, is mainly composed of black shale, silty laminae and dark-gray marls (Figure 1 & 12, Appendix A – F). The shale is bituminous rich and contains zeolites, organic matter, quartz, pyrite, siderite and mica (Figure 1 & 12, Appendix A - F). Silty laminae are comprised of quartz silt, organic matter from noncalcareous algae, rare pollen, wood fragments and heavy minerals. In the Western Atlantic the clay part (65 %) consists of mainly mica 40 %, montmorillonite 10 – 25 % and minor chlorite and kaolinite < 2 % (Sheridan et al., 1977). The silty laminae are the only parts in the formation consisting of biogenic debris, nannofossils, foraminifers, radiolarians and fish debris. Jansa et al., (1978) interpreted these layers as turbidites. The dark gray marl is thought to represent a transitional facies located between the black shale and silty laminae. The marls are a mixture of nannoplankton, quartz, feldspars and heavy minerals. Deposition must have taken place above the CCD, interpreted from the presence of nannoplankton. In North

American offshore the Hatteras Formation wedges out towards the eastern part of the Bermuda Rise. Of specific interest is the Moroccan Basin influx of terrigenous turbidites. This influx diffuses shale deposition in the Eastern Southern Moroccan offshore. In the Moroccan Basins this terrigenous influx led to the deposition of a sub unit of hemipelagic dark gray silty claystones, which is interbedded by siltstone and fine-grained sandstone laminae (Jansa et al., 1978).

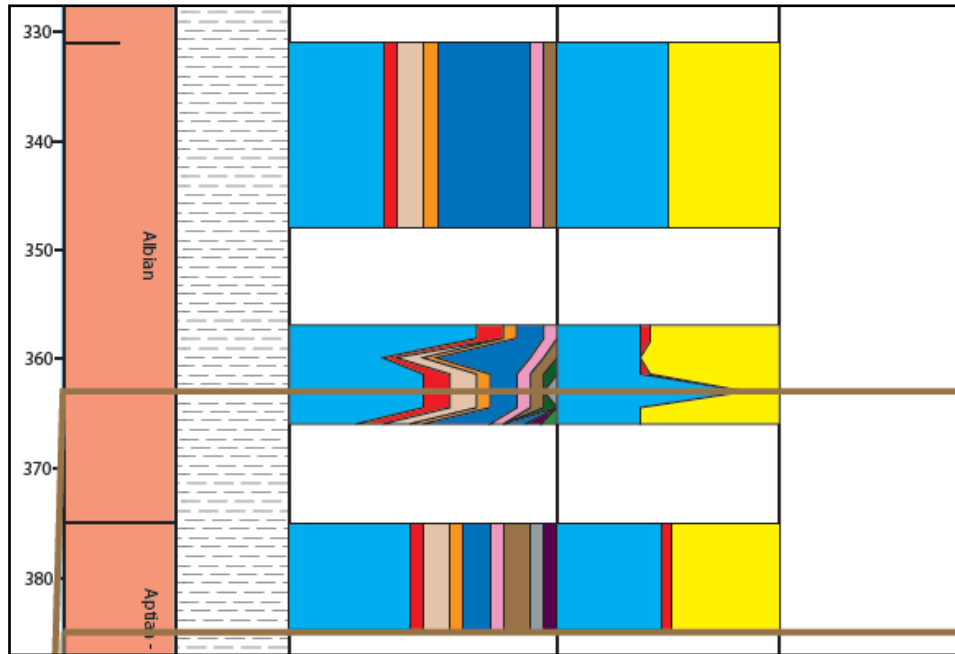


Figure 12: S391 Typical Hatteras Black Bituminous Shale Member (Legend, Appendix E)

The Hatteras Grayish-green Claystone Intraclasts Sandstone Member, is mainly composed of nannofossil claystone and silty clay interbedded by thin siltstone, sandstone and conglomerate beds, hence the name intraclast sandstone (Figure 1 & 13, Appendix A – F) (Jansa et al., 1978). The claystone is primarily composed of montmorillonite, illite, kaolinite, rare chlorite, quartz silt (rare to abundant), pyrite, heavy minerals, glauconite, dolomite, feldspar and heavy minerals. The silty claystone comprises of abundant biogenic remains, nannofossils and foraminifers and also contains coalified wood, fish debris, heavy minerals (concentrated into fine laminae indicating reworking), iron oxide and feldspar. The presence of sandstones and conglomerates indicates reworking of shelf slope sediments. The depositional environment was most likely deposited under alternating low-oxygen and anoxic conditions (Rothe and Tucholke 1981). Scarcity of carbonates apart from the silty layers consisting of biogenic remains, points to deposition below the CCD (Jansa et al., 1978). This unit has been penetrated in the Moroccan Basin (Jansa et al., 1978, Rothe and Tucholke 1981).

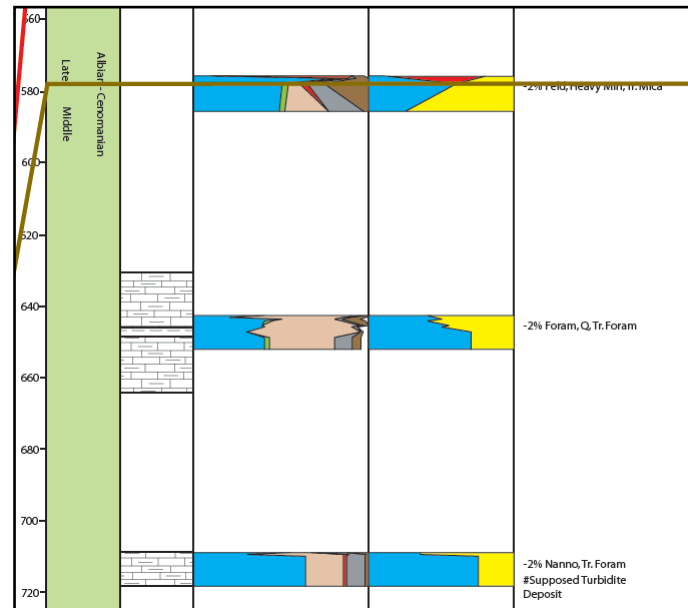


Figure 14: S415 Typical Hatteras Greenish Claystone Member (Legend, Appendix F)

The Plantagenet Formation, varicoloured zeolitic clay, is composed of silty zeolitic clay (Figure 1 & 15, Appendix A – F). Dominant components of this formation are; major montmorillonite with minor palygorskite, illite and rare kaolinite as well as quartz, feldspar, mica, heavy minerals, iron/manganese oxide and pyrite (Figure 1 & 15, Appendix A – F). In the Western Atlantic the formation is strongly enriched in heavy metals, sphalerite, pyrite, goethite, hematite and zeolites (Sheridan et al., 1977), in some cases these are attributed to a volcanic origin (Jansa et al., 1978). Jansa et al., (1978) stress that the Plantagenet Formation does not extend beyond the Western North Atlantic. Though he notes a resemblance to variegated sediments retrieved in the Cape Verde region.

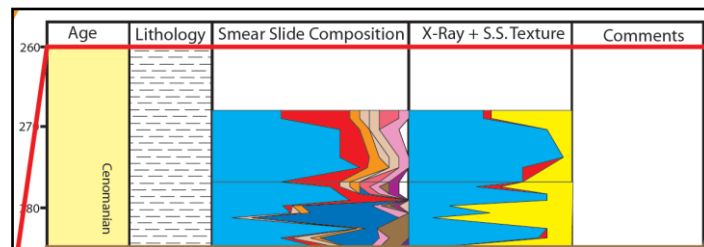


Figure 15: S105 Typical Plantagenet Formation (Legend, Appendix E)

The Crescent Peaks Member, nannofossil marl, is comprised of chalk, marl and limestone (Rothe & Tuscholke 1981) (Figure 16, Appendix B – F). Dominant components are calcite (40 – 60 %) it contains similar to the Plantagenet formation major montmorillonite with minor palygorskite, illite and rare kaolinite as well as quartz, feldspar, mica, heavy minerals, iron/manganese oxide and pyrite (Figure 16, Appendix B – F). However the quantities are much smaller due to dilution by calcite (Rothe & Tuscholke 1981).

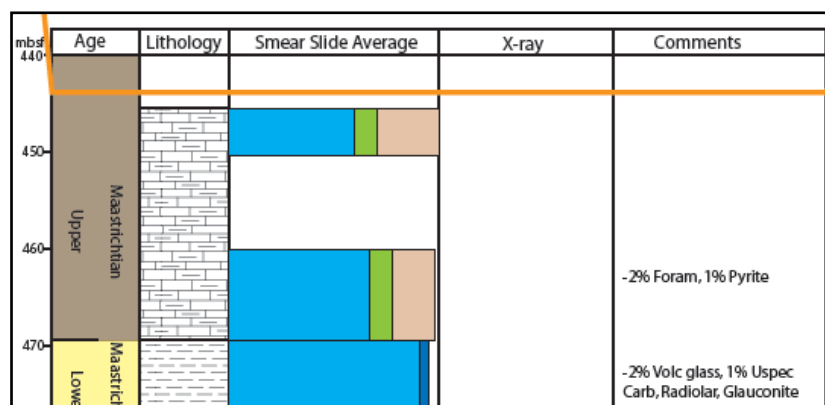


Figure 16: S387 Typical Crescent Peaks member (Legend, Appendix C)

4.3. Large scale basin histories.

4.3.1. Morocco

The Moroccan margin experienced no major tectonic perturbations during the Cretaceous since the Jurassic rifting between North America and Northwest Africa. The Early Cretaceous postrift sedimentation constituted of a restrictive marine environment resulting in increased carbonate deposition (Middle Jurassic – Cretaceous). The Early Berriasian global sea level fall lowered the base level. This event brought an end to the deposition of the Jurassic south Moroccan carbonate reefs (Figure 6) (von Rad & Sarti 1986). The Berriasian sea level fall led to a large flux of clastic material (also known as Wealden clastics) in the western Moroccan offshore (Figure 6). These clastics were deposited from Berriasian to Hauterivian.

During the Berriasian to Hauterivian Northern Morocco remained dominated by pelagic marls, chinks, thinly bedded limestones and black shales. In the Late Cretaceous the northern margin deepened and became deep-marine pelagic, depositing limestones and shales (muds and marls offshore). Apart from local offshore salt tectonics the Moroccan margins remained passive throughout the rest of the Cretaceous.

4.3.2. Iberia

The west Iberian margin accommodates four unconformity bounded formations; 1) Middle Oxfordian – Berriasian, 2) Valanginian – Lower Aptian, 3) Upper Aptian – Turonian 4) Uppermost Cretaceous – Tertiary (Wilson et al., 1989, Pinheiro et al., 1996).

The 1st formation is characterized by red fluvial and debris flow sediments. These sediments are related to rifting and correlate to the onshore Iberian Wealden formation.

The 2nd and 3rd formation blanket the continental shelf and Iberian deep sea (Figure 7). In the proximal northern part of the basin these formations are characterized by fluvial sands. The southern part consists of marine marls and limestones. These sediments greatly increase in thickness to the distal part of the basin. This increase was related to basin movement along boundary faults, during the Late Aptian synrift of the Grand Banks – Iberia opening (Figure 7) (Wilson et al., 1989, Pinheiro et al., 1996).

Similar to the 2nd and 3rd formations the 4th formation is strongly siliciclastic in the proximal northern part. These siliciclastics are contributed to a compressional regime (latest Cretaceous –

Miocene). This compression is also related to the formation of seamounts in western Iberian Trough and the inversion of the Galicia Bank (Figure 7) (Wilson et al., 1989, Pinheiro et al., 1996). The bounding unconformity, dated Cenomanian to Campanian, is related to changes in the continental drainage pattern (Wilson et al., 1989). Canyons (Lisboa, Porto Aveiro, Nazaré and Setúbal) served as conduits for sediment transport from the Iberian shelf to the Iberian abyssal plain (Figure 7) (Pinheiro et al., 1996).

The Galician sedimentary record commences with shallow marine limestone, dolomite, shale and minor sandstone deposition for the Late Jurassic – Early Cretaceous interval (Jansa 1988). Since the onset of rifting, from lower Valanginian to Hauterivian, a marlstone sequence was deposited. The upper Valanginian – Hauterivian sequence which is interbedded by turbiditic sandstone and shale containing allochthonous terrestrial plant debris (Boillot et al., 1989). The Barremian to Aptian was characterized by an alteration of clay / calcareous clay, marl / marlstone and argillaceous limestone interbedded by turbidites and debris flows. Boillot et al., (1989) delineates these mass flow deposits to seamounts and the Galician Bank, which triggered mass flow deposits during the ongoing rifting. Shale, thin turbidites (with plant debris) and calcareous oozes were deposited during the Albian – Cenomanian postrift sedimentation. Gradstein (1985) defined the postrift breakup unconformity at Late Aptian (114 Ma), to which the onset of sea floor spreading between Iberia – Newfoundland was placed (Boillot et al., 1989) (Figure 5).

4.3.3. Celtic Sea Basin

The Cretaceous extension and fault-controlled subsidence of the North Celtic Sea Basin was subdivided by Petrie et al., (1989) in three periods: 1) Tithonian – Early Berriasian, active extension, 2) Berriasian – Aptian, extension, 3) Aptian – Maastrichtian, passive subsidence.

The 1st extensional period led to major erosion, as a response to the uplift of basin margins (Petrie et al., 1989). The northeastern and west-northwestern sedimentation consists primarily of coarse grained clastics and fine-grained red beds, the southern part of the North Celtic sea contains a stronger marine component. The upper sequences in this extensional period are characterized by lacustrine and lagoonal deposits. Petrie et al., (1989) interpreted this as a passive subsiding basin.

During the 2nd stage margin erosion intensified, especially on the northern margin. The first phase of the 2nd stage (Berriasian – Hauterivian) is essentially nonmarine. Deposition was characterized by alluvial fan systems; channel sandstones grading into sand-, silt- and mudstones (Petrie et al., 1989). The second phase (Hauterivian – Aptian) is characterized by a transgression progressing from the southwest, characterized by deposition of marine shelf carbonates in the Goban Spur. To the north the influx is influenced by sediments of a continental origin. Early Aptian fault reactivation led to a maximum transgression followed by an episode of fluvial deltaic sedimentation (Petrie et al., 1989).

The 3rd stage, the passive subsidence unit, distributed marginal marine sediments to the southwestern and central North Celtic Basin. Northern North Celtic Basin sediments became progressively clastic from Aptian – Albian. During the upper Cenomanian the basin progressively deepened, resulting in deposition of marine clastics. The following Early Turonian sea level rise led to a change in sedimentation from the upper Cenomanian marine clastics to the deposition of chalk (Petrie et al., 1989).

4.3.4. Grand Banks

The Grand Banks consists of numerous basins, the largest and best studied are the Jeanne d'Arc, Orphan, Whale and Horseshoe Basins (Figure 8). These basins have been subjected to different stress regimes during the different phases of the North Atlantic opening. Apart from the difference in tectonic regime, they exhibit a largely similar sedimentary infill. The following three paragraphs study the general characteristics.

From Late Kimmeridgian to Early Valanginian the Grand Bank Basins were fluvially dominated. This changed during the Berriasian – Early Valanginian transgression to an absent to weak marine influence (Tankard et al., 1989). The Late Valanginian – Early Aptian transgression led to marine sedimentation, throughout the Valanginian – Hauterivian the basin opened and normal salinity and open marine conditions prevailed. This led to argillaceous deposits with a strong affinity to volcanic chemical influx due to basaltic volcanism (Tankard & Welsink 1989, Tankard et al., 1989). The basaltic volcanism reported by Tankard et al., (1989) is related to the North Atlantic spreading ridge separating Iberia and the Grand Banks (Figure 5). During Aptian – Albian a broad epeiric sea developed on the Grand Banks continental shelf, this sea became starved of terrigenous sediments throughout the Turonian (Figure 8).

The Late Cretaceous is separated from the Late Valanginian – Early Aptian marine sediments by the Barremian – Aptian unconformity (Tankard et al., 1989). The lower bounding unconformity is referred to as the basal Aptian unconformity. This unconformity is identified as the termination point of the synrift (Tankard et al., 1989) and coincides with the separation of Iberia from the Grand Banks (Tankard & Welsink 1989). The breakup of Iberia and Grand Banks during the Aptian is related an episode of uplift and erosion of intrabasinal highs and deposition of deltaic, sandstones and shallow-marine mudstones (Figure 5). From the Barremian – Aptian a postrift sequence developed due to late-stage extensional subsidence and uninterrupted marine sedimentation. The unconformity related change in marine circulation, palynofacies and marine biota were caused by rifting in the Orphan Basin and opening of the Labrador Sea (Mauffret et al., 1989). During this period extensive erosion took place in the southeast corner of the Grand Banks. This is called the basal Cenomanian hiatus which marks the shoaling of the epeiric sea leading to a period of erosion (Tankard et al., 1989). The last Cretaceous major tectonic event is the Santonian opening of the Labrador Sea and separation of Orphan Knoll/Flemish Cap from Rockall and North West Europe (Tucholke et al., 1989).

4.3.6. Blake Bahama/Cape Hatteras

The stratigraphic background of the eastern North American offshore is studied through the following subdivision (Figure 9); 1) Blake – Bahama Basin and Blake Plateau, 2) Hatteras Abyssal Plain, 3) New Jersey continental shelf. Before focusing on the different subbasins the shallow sea covering the continental shelf during Early Cretaceous is pointed out (Poag 1978). Adjacent to this sea extensive carbonate platforms and reefs developed along the Bahama uplift, Southern Blake Plateau, Georges Bank Basin and Scotian Basin (Figure 9) (Poag 1978). These shallow marine environments acted as a barrier/sieve for clastic sediments, preventing clastic sediments to reach the deep oceanic basins.

1) The Blake Plateau consists of Neocomian Berriasian – Aptian backreef to shelf carbonates (Figure 9) (Poag 1978). Carbonate banks extended from the Blake Escarpment to Blake Nose (Figure 9) (Sheridan et al., 1977). The carbonate banks are covered by an Aptian - Albian nannofossil ooze,

which are ended by the Campanian – Albian unconformity. The Campanian – Albian unconformity is a consequence of low sedimentation rates (0,35 – 0,14 cm / 1000 yr), in combination with scouring by deep marine currents (Sheridan et al., 1977). During the Late Albian sea level fall (~100 Ma) the Blake Escarpment became intersected by canyons and gullies and also exposed the carbonate Blake Plateau to erosion (Figure 9) (Sheridan et al., 1977). The Upper Cretaceous Blake Plateau was influenced by an increasing terrigenous fraction. Highest concentrations are found in the northern part of the plateau. This last formation is heavy mineral rich, probably related to volcanic activity (Rothe and Tucholke 1981).

2) The Early Cretaceous Hatteras Abyssal Plain is composed of the Blake Bahama Formation, white and gray limestone, similar to the Blake Plateau and Moroccan Basins (Figure 9) (Lancelot et al., 1972). From Late Valanginian – Early Barremian carbonaceous clays and shales were deposited (Lancelot et al., 1972). The abundance of clays and black shales in the Early Cretaceous led Lancelot et al., (1972) to conclude that stagnation was accompanied by subsidence. The repetitive character of the clays and silty laminae indicates that stagnation was interrupted by periods of slow bottom water oxidizing conditions (Lancelot et al., 1972). The Early Cretaceous Hatteras Abyssal Plain experienced a relatively small influx of detrital terrigenous material.

The Upper Cretaceous was prone to deposition of the Plantagenet Formation, varicoloured clays (fossil barren) and black clays. The Hatteras Abyssal Plain varicoloured clays contain large amounts of montmorillonite and micaceous clay, the black zones contain iron oxide and manganese oxide. These sediments are related to low sedimentation rates, hiatuses and volcanogenic sediment influx. The volcanic influence is directly relatable to a metal enrichment as a result of direct precipitation from concentrated solution (Lancelot et al., 1972).

3) The Early Cretaceous New Jersey continental shelf is composed of shallow siliciclastics (Figure 9) (Poag 1977, Sheridan et al., 1977). Proximal sequences are composed of nonmarine sandstone and shale with coal beds (Olsson 1977). Sediment was sourced from Appalachians and deposited in delta to estuary type systems (Sheridan et al., 1977). During the Barremian – Aptian / Cenomanian period the New Jersey plain was covered by deltaic swamps. Sheridan et al., (1977) claims that these swamps contributed to organic rich layers in the Western Atlantic.

The Mid and Upper Cretaceous contains calcareous sands and shale's, filling up the backreef basin, burying reefs and spilling into the ocean basin. The Upper Cretaceous (Cenomanian – Santonian) transgression and later Campanian – Maastrichtian subsidence led to a deepening of the New Jersey shelf. During this interval, fine grained sand and shale were deposited.

V. Observations

The chapter observations studies and identifies the major characteristics of the data presented in Appendix A-F. In important cases a snapshot of a core was made, in all other situations the author refers to the core and depth / interval depth of the specific feature. The chapter is separated in three subchapters; Lower Cretaceous, Mid Cretaceous and Upper Cretaceous. Within the subchapters subdivisions are made between earliest, mid and latest part of the specific part of the Cretaceous e.g. earliest Lower Cretaceous (Tithonian – Hauterivian). This chapter refers to figures and for the detailed results to the appendixes.

Influence of climate and oceanography on Cretaceous sedimentation in the North Atlantic

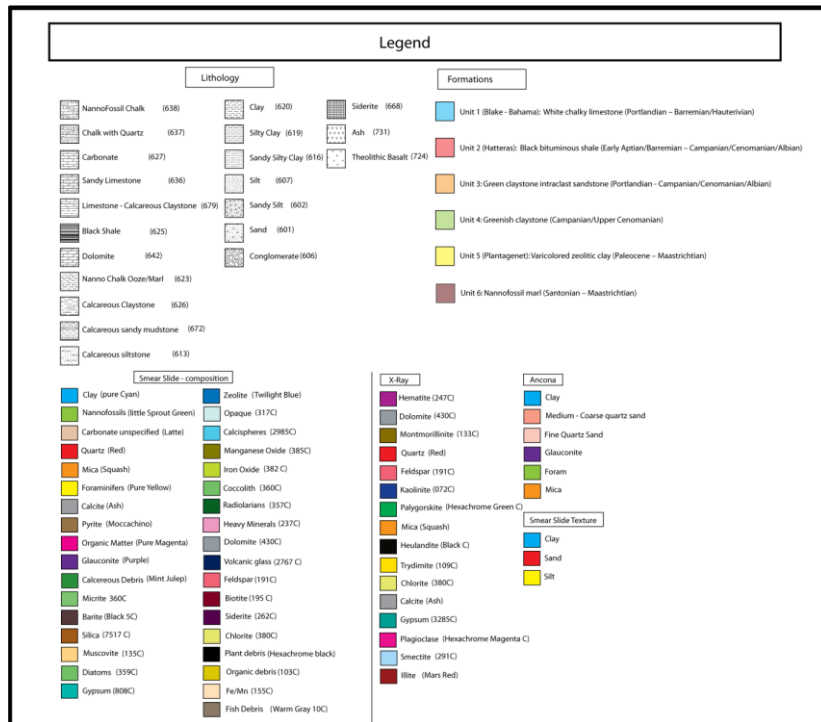


Figure 17: Legend for Figures 18, 19, 20 & 21

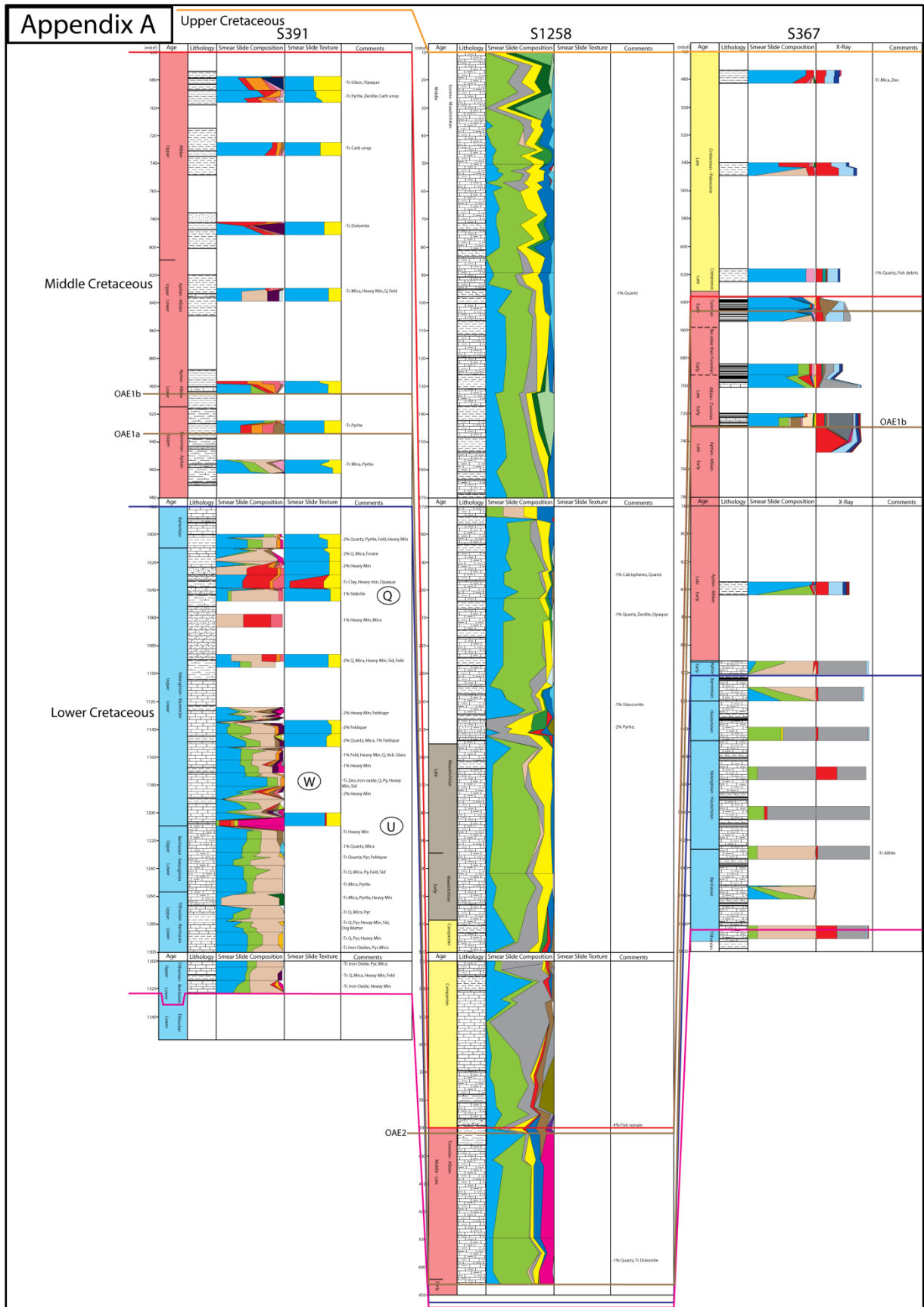


Figure 18: Southernmost transect Legend Figure 17 (Figure 3, Appendix A)

Influence of climate and oceanography on Cretaceous sedimentation in the North Atlantic

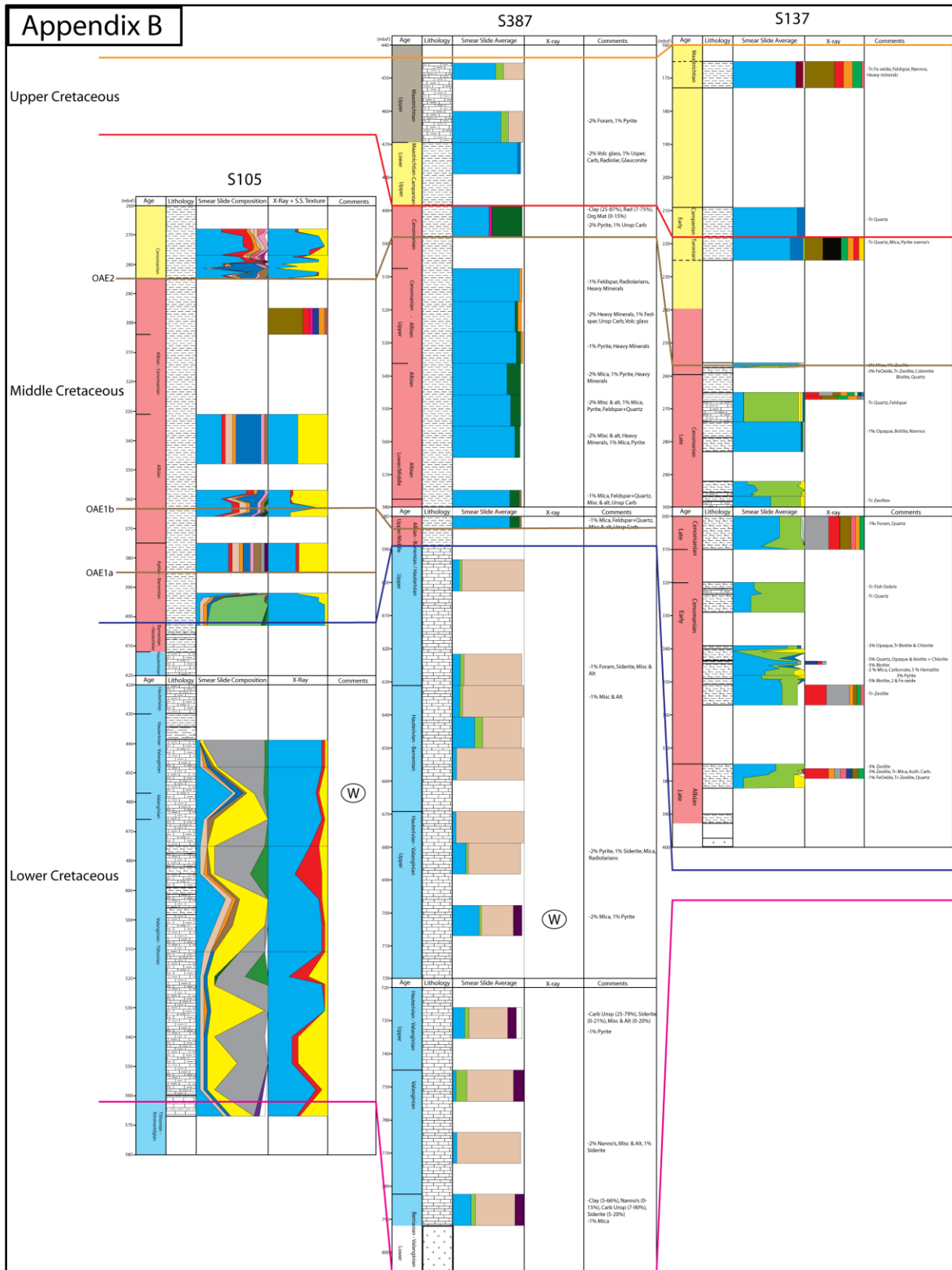


Figure 19: Southern transect Legend Figure 17 (Figure 3, Appendix B)

Influence of climate and oceanography on Cretaceous sedimentation in the North Atlantic

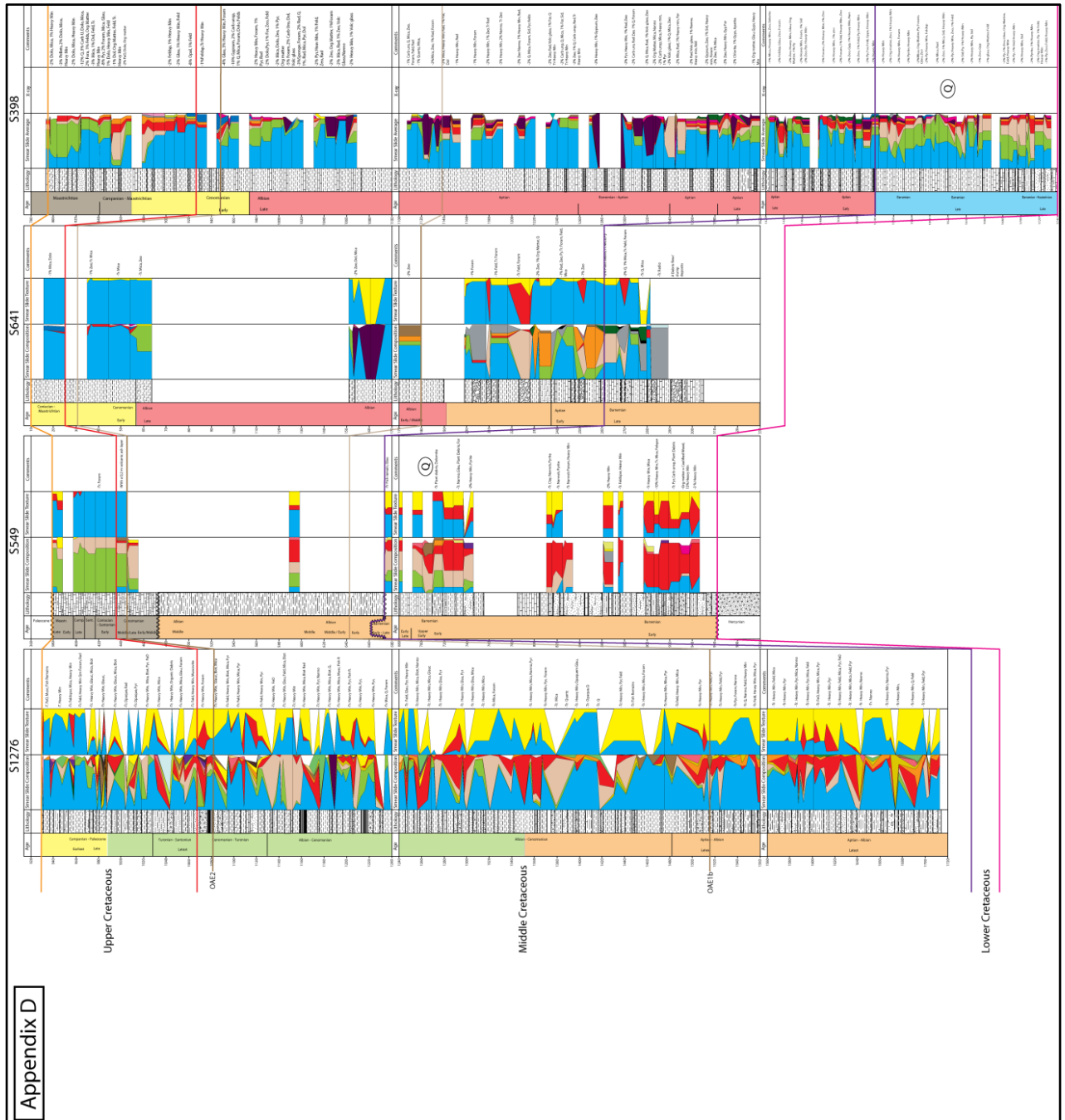


Figure 21: Northernmost transect Legend Figure 17 (Figure 3, Appendix D)

5.1. Lower Cretaceous

5.1.1. Earliest Lower Cretaceous

Tithonian – Hauterivian: S105 (Hatteras), S387 (Hatteras), S391 (Bahama) and S367 (Cape Verde).

S105, S387 and S391 (Figure 2) are mostly calcareous, they contain two large clay peaks. These peaks are referred to as event W: S105 at 455 mbsf (50 % clay), S387 at 700 mbsf (40 % clay) and S391 at 1170 mbsf (80 % clay) (Figure 2, 18, 19 & 23). In S105 radiolarians peaks (484 & 519 mbsf) coincide with an increasing grainsize (Figure 19, Appendix B & E). S105 and S387 are barren of quartz but not of mica. S391 is predominantly consisting of a clayey (40 %), carbonate (60 %) over the whole Tithonian – lower Valanginian (Figure 19, Appendix B & E). At the boundary Lower Valanginian –

Upper Valanginian S391 (1210 mbsf), a markedly large organic matter excursion (70 %) in combination with quartz (15 %) and mica (4 %) is encountered (Figure 18, Appendix A & E). This excursion is further referred to as event U. Quartz in Tithonian – Hauterivian is only found in minor fractions in both S367 and S391 (2 – 3 %) (Figure 18, Appendix A, E & F). Organic matter (4 – 5 %) is present from the lower Valanginian up to Barremian in all four sites. S387 shows a consistent siderite fraction (5 – 10 %) from Berriasian – Hauterivian (Figure 19 & 20, Appendix B & C). Overall the Tithonian – Hauterivian period is characterized as strongly calcareous, with minor terrigenous (mica, quartz, pyrite, feldspar) influx in S105 (Hatteras), S387 (Hatteras), S391 (Bahama) and S367 (Cape Verde) (Figure 2, 18, 19 & 20) (Appendix A, B, C, E & F).

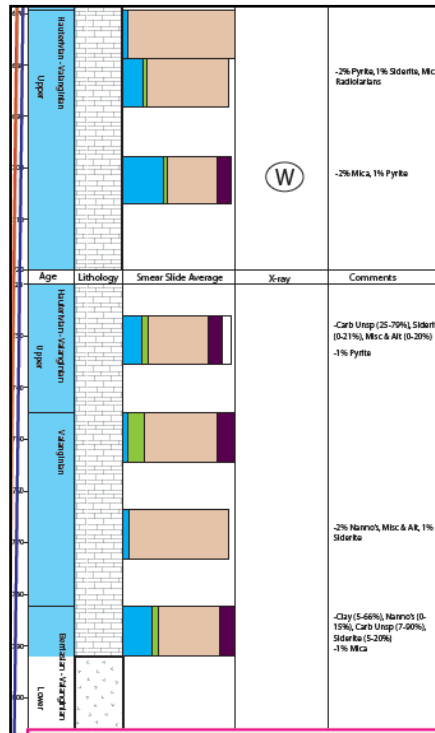


Figure 22; S387, W identifies event W (see Appendix C)

The Barremian - Aptian boundary is distinguished by a pyrite, feldspar, organic matter and clay peak (S398, S391, S105, S549) (Figure 2, 18, 19 & 20, Appendix A, B, D, E & F). An important change occurs in site S391, the Lower Barremian (1040 mbsf) is identified as a large flux of clay (80 %) followed by a feldspar (15 %) quartz (30 %) and mica (4 %) episode 1040-1020 mbsf (Figure 18, Appendix A & E). Another important excursion, entitled event U, is retrieved in the Lower – Upper Valanginian episode. Event U is characterized by an extremely large positive organic matter excursion in combination with quartz and mica. The event assigned to as Q (Figure 22, 23, 24 & 25), is significant for its high pyrite/organic matter peak in the Early Late Barremian (S549, S398, S391) (Figure 2, 18 & 21, Appendix A, D, E, & F). This event is recognizable by a strong mica fraction (10 – 15 %), a large pyrite or organic matter (5 – 10 %) flux and feldspar presence (up to 8 %).

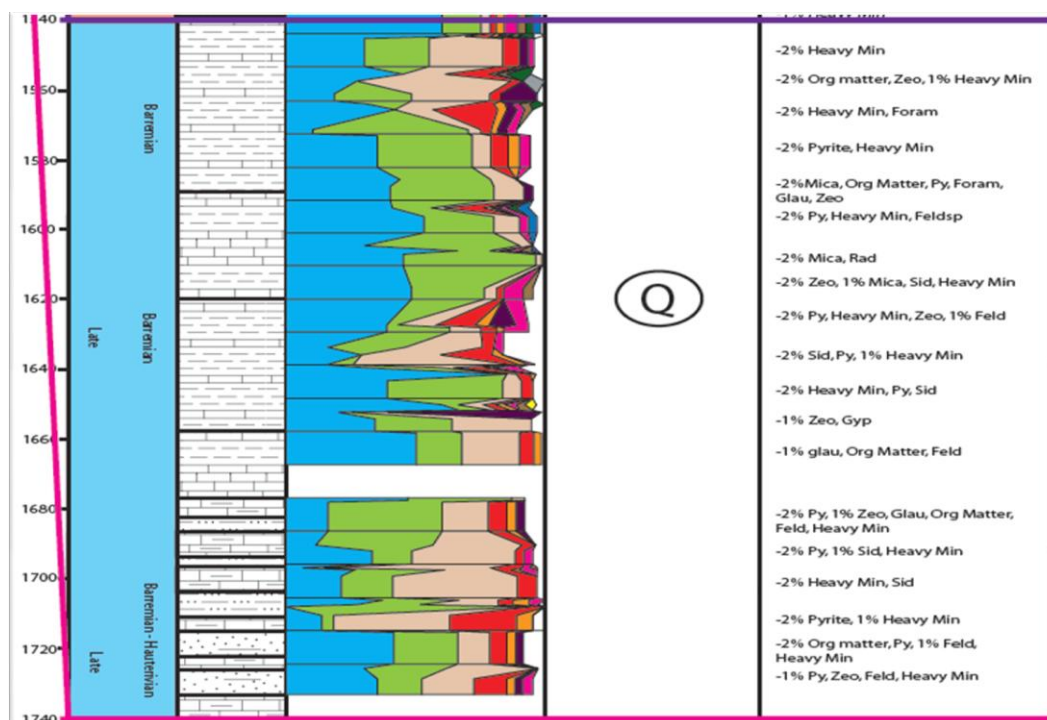


Figure 23; S398 event Q (see Appendix D)

5.1.2. Late Early Cretaceous

Barremian; S387 (Hatteras Abyssal Plain), S391 (Bahama), S367 (Cape Verde), S549 (Irish Basin), S398 (proximal Iberia), S105 (Hatteras), S641 (distal Iberia)

The Early Barremian in the northern Irish Basin (S549) consists primarily of quartz, accompanied by large positive (up to 50 %) grainsize excursions (Figure 2 & 21, Appendix D & F). The Late Barremian becomes more carbonaceous, in the early Late Barremian (720 mbsf) a large pyrite excursion is shown. The proximal Galician Barremian margin of S398 comprises of a large clay (30 – 50 %) and carbonate fraction (40 – 60 %) (Figure 2 & 21, Appendix D & F). The Latest Barremian in site S398 is characterized by a peak in clay (85 % at 1640 mbsf, referred to as Q Figure 21 & 23, Appendix D & F), event Q is succeeded by a strong increase in carbonates 75 % (predominantly nannofossils) and a large excursion of organic matter 10 %. Event Q is also recovered at 710 mbsf in site S549 (Figure 2, 21 & 24, Appendix D & F) and at 1040 mbsf in S391 (Figure 2, 18 & 25, Appendix A & E). Similar to the record in S549 site S398 contains a consistent fraction of quartz (5 -15 %) and mica (3 – 4 %) in the Lower Cretaceous. The transitions from Barremian to Aptian in S549, S398, S387, S391 and S105 are characterized by a strong increase in clay fraction (up to 70 - 80 %) (Figure 2 & 18 – 21, Appendix A – F). In all sites the carbonate fraction is dominant throughout the Late Barremian. S641 Contains strong mica peaks (60 – 70%) during the Early Aptian interval coinciding with nannofossils (20 %) and pyrite (5%) peaks (Figure 2 & 21, Appendix D). Late Barremian S641 (270 mbsf) contains a large grain size increase which coincides with a plant debris (3 %), large carbonate unspecified (50 %) and calcite (40 %) excursions, these excursion are related to a sandy silty lithology.

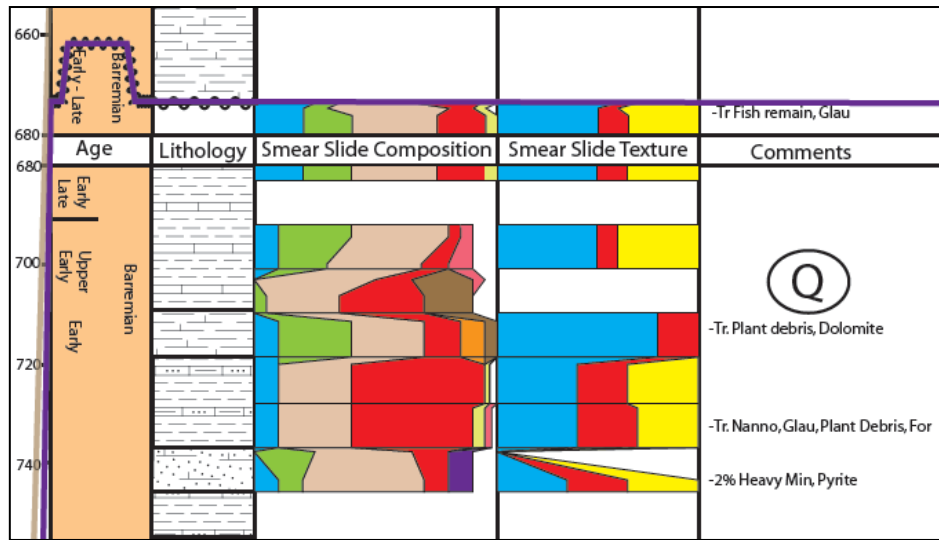


Figure 24; S549 (see Appendix D)

S367 Is mostly biogenic in the Lower Cretaceous, it contains a large (60 – 90 %) calcite fraction reported from X-ray measurements (Figure 2 & 18, Appendix A & F). Similar to S549 and S398 the clay fraction decreases during Barremian towards the Aptian as the carbonate fraction increases. Consistent throughout the Cape Verde site is a minor quartz fraction (3 %). This quartz fraction is present in all sites in the Eastern Atlantic but absent throughout the Western Atlantic sites S105 and S387 (Figure 2, 19 & 20, Appendix B, C & E).

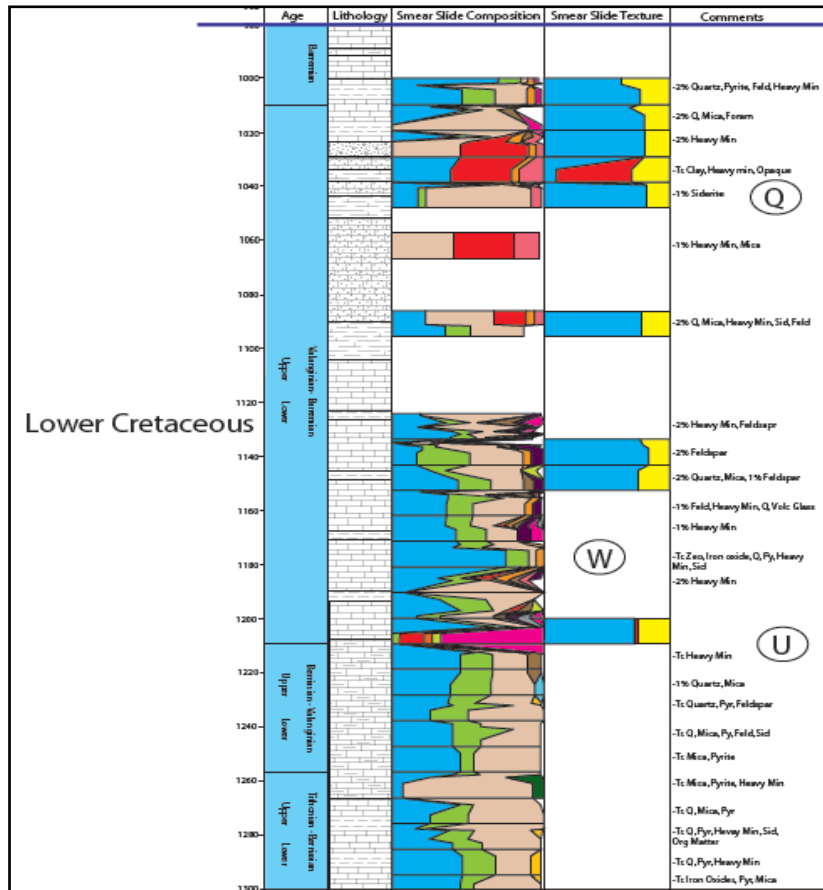


Figure 25; S391 events Q, W and U (see Appendix D)

S391 Bahama offshore contains large fluxes of quartz (1040 mbsf – 30 %, 1060 mbsf – 30 %) during the Lower Barremian, in combination with mica (3 %), feldspar (15 %) and an increased grain size (60 %) (Figure 2, 18 & 25, Appendix A & E). The Upper Barremian in sites S367, S549, S105, S398 and S391 all contain the same elements at the Barremian – Aptian boundary; clay, nannofossils, carbonate unspecified in large fractions and minor quartz, mica, preceded by an organic matter / pyrite (not in S367) flux (Figure 2, 18, 19 & 21, Appendix A, B, D, E & F). The Cape Verde sites show a slight fraction of smectite increasing from 2 % throughout the Barremian up to 4 %.

5.2. Mid Cretaceous

5.2.1. Earliest Mid Cretaceous

Aptian; S391 (Bahama), S367 (Cape Verde), S105 (Hatteras), S136 (Distal Morocco), S1276 (Grand Banks offshore), S641 (distal Iberia), S398 (proximal Iberia)

The Early Aptian S391 (Bahama) and S105 (Hatteras abyssal plain) commence with dominant clay (30 – 60 %) accompanied by a large portion of quartz (3 – 10 %), mica (5 %), feldspar (10 %) and pyrite (up to 10 %) (OAE1) (Figure 2, 18 & 19, Appendix A, B & E). Followed by a similar composition in Late Aptian (S391) containing a smaller pyrite (3 %) fraction. Early Aptian S398 consists largely of clay (60 – 80 %) with a mica (3 %) and organic matter (3 %) background signal (Figure 2 & 21, Appendix D & F). Site S398 is interfingered by large siderite peaks (40 – 70 %) which become larger to the top. The nannofossils fraction increases in size (from 5 to 10 %) towards the Late Aptian. S367

Early Aptian is biogenic (20 – 60 %) whilst the Late Aptian Cape Verde site comprises of mainly clay (60 – 80 %) with a small quartz (5 %) and smectite relict (4 %) (Figure 2 & 18, Appendix A & D). Late Aptian S136 consists primarily of clay (70 %) with nannofossils (25 %) (Figure 2 & 20, Appendix C & F). X-ray fractions show montmorillonite, quartz and mica and minor palygorskite. The Grand Banks site constitutes of dominantly clay (60 – 90 %) with a background infill of mica (10 %) and quartz (5 %), this site is strongly affected by allochthonous fluxes; large quartz abundances in combination with increased carbonate unspecified and a grain size increase (Figure 2 & 21, Appendix D & F). S641 is significantly different from the other sites, due to a large mica fraction (Figure 2 & 21, Appendix D & F). This is most likely related to an allochthonous influx inferred from; presence of plant material, lithological character and grain size up to conglomerate. S641 further contains calcareous elements and clay, it is important to note that the Late Aptian in this site is practically barren of quartz.

Summarizing the main elements; the western South Atlantic is mostly clayey S391, S105 and comprises of OAE1a (feldspar, mica, quartz and most importantly pyrite, S391) (Figure 2, 18 & 19, Appendix A, B & E). The south-eastern Atlantic is stronger calcareous in the early Aptian but becomes clay and smectite rich during Late Aptian. The northern North Atlantic Aptian is strongly dominated by clay (except S641 with large mica and nannofossils). Large incursion of quartz in S1276 are related to allochthonous influxes from the Grand Banks (Figure 2 & 21, Appendix D & F). Allochthonous fluxes in Iberia are much smaller of size and less quartzitic during the Aptian interval. Siderite inclusions only exist in the proximal Iberia site S398 (Figure 2 & 21, Appendix D & F).

5.2.2. Mid Cretaceous

Albian: S391 (Bahama), S1258 (Demerara), S367 (Cape Verde), S105 (Hatteras), S387, S415 (proximal Iberia), S137 (Western Sahara), S1276 (Grand Banks offshore), S549 (Irish basin), S641 (distal Iberia) S398 (proximal Iberia).

Site S391 demonstrates a dominantly clayey Albian (60 – 70 %), characterized by siderite incursions (30 – 40 %) (Lower and Uppermost Upper Albian) which coincides with prevalent quartz (5 – 10 %), mica (4 – 15 %), feldspar (3 – 8 %) and heavy minerals (3 – 5 %) fractions (Figure 2 & 18, Appendix A & E). Upper Albian Cape Verde site S367 comprises similarly to S391 primarily of clay (60 – 80 %) with an pyrite (10 %) and increased carbonaceous (5 – 10 %) composition (Figure 2 & 18, Appendix A & F). The X-ray fraction constitutes of minor smectite (5 %) and kaolinite (3 %). S105 is composed of zeolitic (5 – 25 %) clay (20 – 50 %) with a continuous background fraction of quartz (5 %), mica (3 %), pyrite (4 %) and heavy minerals (3 %). S387 comprises of pure clay (80 – 95 %) with a large fraction of radiolarians (2 – 15 %) (Figure 2 & 19, Appendix B). The Western Saharan offshore S137 is strongly calcareous with nannofossils (60 – 70 %), foraminifers (10 %) and contains a smaller kaolinite (5 %) and palygorskite (5 %) fraction (Figure 2 & 19, Appendix B & F). Throughout the Albian the Demerara rise dominantly calcareous (70 %) with a large organic matter component (15 %) and minor zeolitic-clay (15 %) (Figure 2 & 18, Appendix A & E). The signature of nannofossils and foraminifers within the calcareous fraction is similar to that of S137. S415 is strongly dolomitic (70 %) with minor pyrite (3 %) (Figure 2 & 20, Appendix C & F). The Albian part of S1276 is clayey (60 – 90 %) with incursions of terrigenous origin near the top Albian (quartz, mica and feldspar coincide with increased grain size) (Figure 2 & 21, Appendix D & E). Albian clay and calcareous intervals change pace, carbonate unspecified become more prevailing (up to 100%) towards the top (calcareous intervals are not always related to increased grain size and quartz). The Irish Basin site contains minor clay (10 – 20 %) with a large quartz fraction (70 – 80 %) (Figure 2 & 21, Appendix D & F). S641 is

dominated by clay with a mayor siderite inclusion (100 %) at 160 mbsf. Towards the Latest Albian S641 becomes more calcareous (30 % nannofossils). S398 Is dominated by clay (60 – 80 %) with a consistent background quartz (3 %) and mica (3 %) sedimentation. Major siderite inclusions (20 – 80 %) occur in lower Albian and towards the top site S398 becomes more calcareous (from 5 to 20 %).

Summarizing the previous paragraph, the Iberian offshore is dominated throughout the Albian by clay with large siderite occurrences, during the latest Albian the nannofossils fraction increases (Figure 2 & 21, Appendix D & F). The S1276 is composed dominantly of clay with turbidite incursions (Figure 2 & 21, Appendix D & E). Similarly the Bahama and Hatteras Plain are composed of dominant clay, with a consistent background signal of mica quartz and heavy minerals (Figure 2 & 18 – 20 , Appendix A – C, & E). The south eastern Atlantic, Western Sahara, Cape Verde, Demerara Rise and Moroccan offshore are calcareous throughout the Late Albian (Figure 2, 18 & 19, Appendix A, B, E & F). These sites also show a similar character (foraminifer and nannofossils in S415 and S1258), S415 and S367 contain organic matter in the form of pyrite. Significantly the Uppermost Albian in all three sites (apart from S1258) is terminated by an increasing clay fraction and decreasing biogenic segment.

Important is the difference between the eastern and western Atlantic (Appendix E & F). The western margin displays mica, quartz, heavy mineral and feldspar, while these elements are absent in the south east and only have a minor presence in the northern proximal sites. The minor presence in the north does not match the excursion size site S105 and S391 (Figure 2, 18 & 19, Appendix A, B & E). As such the influx of mica, quartz, heavy mineral and feldspar is bound to the two Hatteras locations and has not been retrieved in S387 (Figure 2 & 19, Appendix B & E), which consists of pure clay with radiolarians.

5.2.3. Latest Mid Cretaceous

Cenomanian - Turonian: S1258 (Demerara Rise), S367 (Cape Verde), S105 (Hatteras), S387 (Hatteras), S137 (Western Sahara), Ancona, S136 (distal Morocco), S415 (proximal Morocco), S1276 (Grand Banks), S549 (Irish Basin), S641 (distal Iberia), S398 (proximal Iberia)

The complicated North Atlantic sedimentation of the Cenomanian – Turonian is synthesised to Table 2, 3 and 4. The tables illustrate the detailed description of the different sites studied in the paragraph below.

The Cenomanian site S105 comprises of lower Cenomanian zeolitic (10 – 60 %) clay (50 – 70 %), followed by a strong quartz (5 – 15 %), mica (3 %), feldspar (5 %) and heavy mineral (5 %) occurrence (Figure 2 & 19, Appendix B & E). Site S387 has a dominant clay composition during the uppermost Cenomanian (65 %), with a large radiolarian fraction (30 %) and organic matter excursion (3 %) (OAE2) (Figure 2 & 20, Appendix C). S137 Is dominated by carbonates (20 – 70 %) during Cenomanian, with X-ray diffraction measured quartz (5 – 15 %) and calcite (20 %) (Figure 2 & 19, Appendix B & F). The Turonian comprises of zeolitic (15 %) clay (85 %) with montmorillonite (25 %) and heulandite (25 %). The Ancona site contains dominant clay (85 – 90 %) with a sand excursion (90 %) in late Cenomanian (1085 mbsf) (Figure 2 & 20, Appendix C). The Ancona core has a consistent background fraction of mica (3 – 10 %) and fine sand (3 – 10 %). S136 Is constructed of dominantly clay (40 – 90 %), kaolinite (10 %) and mica (10 %). The Turonian contains a large calcite (25 %) and volcanic glass (20 %) episode (Figure 2 & 20, Appendix C & F). The Cenomanian S415 is composed of clay (40 – 70 %), carbonate unspecified portion (20 – 40 %) and dolomite (5 – 30 %) (Figure 2 & 20,

Appendix C & F). The Mid Cenomanian is characterized by dolomite (30 %), pyrite (2 – 7 %) and a tiny quartz layer (3 %). Site S1276 contains a dominant clay (60 %) portion with changing carbonate fraction (up to 100 % at 1140 mbsf), large quartz peaks (up to 50 %) appear to the top Turonian (Figure 2 & 21, Appendix D & E). S549 is dominantly calcareous (80 % nannofossils) with minor quartz (4 %) and pyrite (4 %) (Figure 2 & 21, Appendix D & F). S641 consists chiefly of clay (95 %) with minor quartz (3 %) (Figure 2 & 21, Appendix D). S398 Consists primarily of zeolitic (10 – 12 %) clay (60 – 80 %) with the Lowest Cenomanian characterized by nannofossils (15 %), clay (60 %), mica (3 %) and organic matter (5 – 7 %) (Figure 2 & 21, Appendix D & F). The Demerara Rise Turonian consists of carbonate (60 %), zeolitic clay (20 %) and organic matter (15 %) the boundary to upper Cretaceous is characterized by a clay peak (60 %), siderite (5 %) and quartz (3 %) occurrence (Figure 2 & 18, Appendix A & E). During the Turonian Cape Verde is dominated by clay (80 – 90 %), zeolite peaks (20 %) and large smectite (5 – 30 %) and montmorillonite (3 – 40 %) black shale.

Site	Description – Cenomanian
S1258	Cenomanian carbonate rich with small zeolitic clay and organic matter
S105	Clay with only terrigenous components (quartz, mica, zeolitic clay, heavy and feldspar)
S387	Lower Cenomanian pure clay upper organic matter plus radiolarians large
S137	Carbonaceous dominated with in early zeolitic clay interfingering clay
Ancona	Clay with two quartz peaks (one in middle one in late Cenomanian)
S136	Clay pure with small quartz
S1276	Clay dominated with changing carbonate fraction (largest at 1140 mbsf) large quartz peaks top Turonian sideritic
S549	Dominantly nannofossils and carbonate unspecified
S641	Dominantly clay small quartz layer
S398	Early Cenomanian earliest part contains largest clay fraction with 25% nannofossils top no biogenic fraction left
S415	Half clay half calcite and carbonate unspecified top more clayey
S367	Clay with minor quartz and nannofossils

Table 2: General description Cenomanian

Site	Description – Turonian
S1258	Zeolitic clay with organic matter and pyrite
S137	Pure zeolitic clay
Ancona	Clay with small nannofossils and to top influx of 95% quartz
S136	Half calcite half clay 25% volcanic ash
S1276	Cay with two large peaks of nannofossils, quartz and foraminifer pyrite falls in clay peak Turonian towards end strong carbonate component
S367	Zeolitic clay

Table 3: General description Turonian

Dominantly Carbonate	Intermediate	Dominantly Clay
Cenomanian		
S1258	S387	S105
S137	Ancona	S136
S549	S1276	641
	s398	
	S415	
	S367	

<i>Turonian</i>		
	S136	S1258
	S1276	S137
		S367

Table 4: Summary of general descriptions

Cenomanian: Carbonate deposition is concentrated in the most southern part of the Atlantic, West Sahara offshore and in the Irish Basin (Table 2 & 4, Figure 2, 18, 19 & 21, Appendix A, B, D, E & F), intermediate (half clay half or 25% carbonate) is found in Hatteras Abyssal plain (S387) Grand Banks, proximal Iberia, proximal Morocco and Cape Verde (Table 2 & 4, Figure 2, 18 – 21, Appendix A – F). Pure clay with no biogenic components are found in the Hatteras Abyssal plain (S105), far offshore Morocco plus the far offshore Iberia (Table 2 & 4, Figure 2, 19 & 20, Appendix B, C, E & F).

Turonian: Intermediate carbonate composition was found in distal Morocco and New Foundland (Table 3 & 4, Figure 2, 19 & 21, Appendix B, D, E & F), pure zeolitic clay in Demerara rise, deep offshore Western Sahara and Cape Verde (Table 3 & 4, Figure 2, 18 & 19, Appendix A, B, & F).

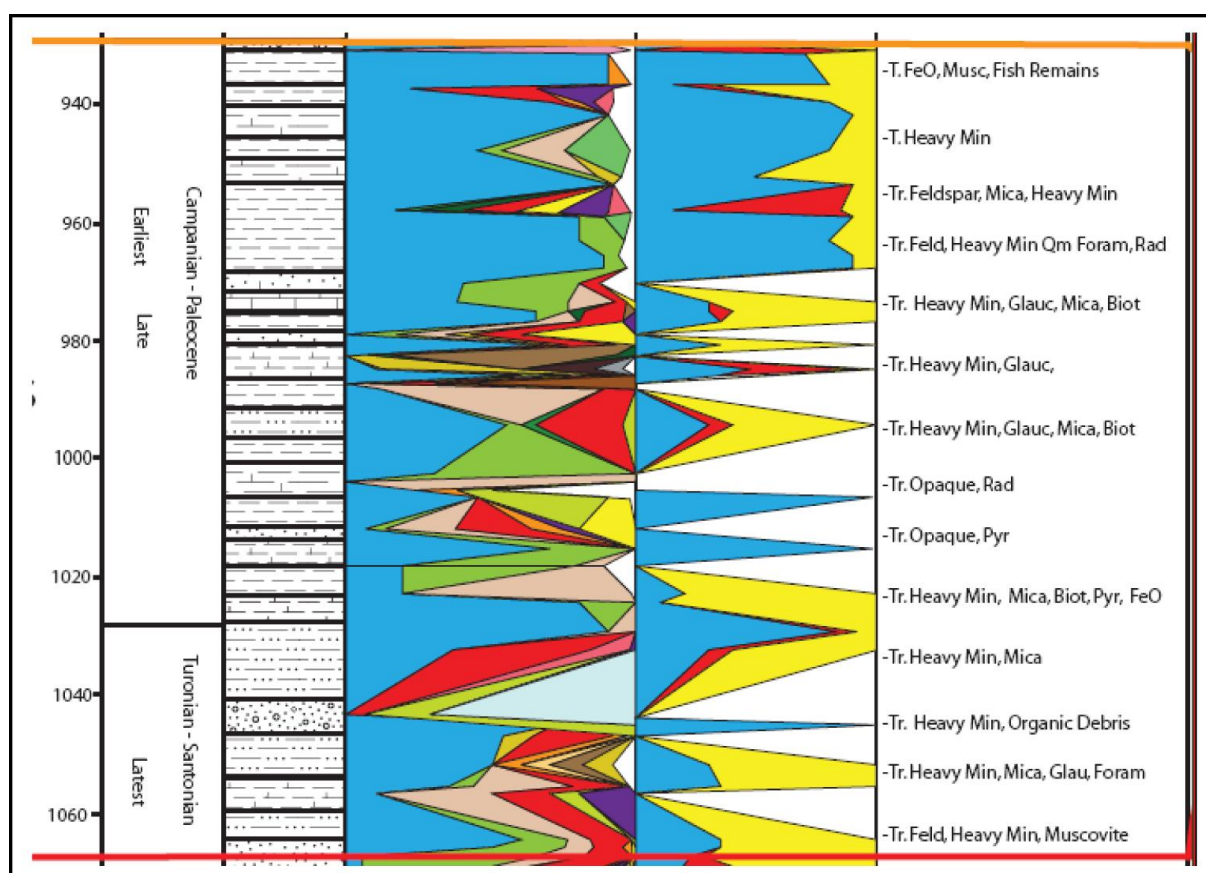


Figure 26; S1276 Upper Cretaceous (Appendix D)

5.4. Upper Cretaceous

Turonian / Coniacian boundary - Maastrichtian Palaeogene boundary: S1258 (Demerara Rise), S367 (Cape Verde), S387 (Hatteras), S137 (Western Sahara), Ancona (New Jersey shelf), S136 (distal Morocco), S1276 (Grand Banks), S398 (proximal Iberia), S641 (distal Iberia)

Site S1258 is strongly calcareous, containing nanofossils and foraminifers (5 – 50 %) and calcite (10 – 80 %) (Figure 2 & 18, Appendix A & E). The Cretaceous – Tertiary boundary at 250 mbsf is

identified by quartz (5 %) and radiolarian (20 %) occurrence and retreating clay fraction (from 15 % to 0 %). The Campanian is largely calcitic (80 %) the top is characterized by a clay (60 %) excursion, with a continuous background sedimentation of quartz (3 %) and pyrite (5 %). The Cape Verde site (S367) contains a large clay (60 – 90 %) fraction (Figure 2 & 18, Appendix A & F). The uppermost Cretaceous contains a strong quartz (5 – 15 %) peak as well as smectite (15 – 20 %) and kaolinite (5 – 10 %). S387 Has a strong clay (70 – 90 %) fraction with increasing biogenic (from 25 – 30 %) components to the top. The Campanian Western Sahara site S137 contains zeolitic (7 %) clay (93 %), the Maastrichtian is composed of clay with biotite (10 %) (Figure 2 & 19, Appendix B & F). The X-ray measurements found; montmorillonite (40 %), minor quartz (10 %), mica (10 %) and palygorskite (10 %). The Santonian Ancona site on the New Jersey shelf consists mainly of sand (70 %) with increasing glauconite (70 – 80 %) clay (15 %) towards the Campanian (Figure 2 & 20, Appendix C & E). The Mid Campanian increases the clay fraction to 90 % and by Late Campanian – Maastrichtian the glauconitic sandy (80 %) and clay (20 %) fraction are back to Lower Campanian values. S136 Comprises of clay (30 – 80 %) with zeolite, mica, feldspar, quartz (all between 3 – 5 %) and iron oxides (8 – 10 %) (Figure 2 & 20, Appendix C & F). The lower part of S1276 (Figure 26) is composed of clay (60 %) with large quartz peaks (20 – 30 %) and carbonate unspecified peaks (50 – 90 %) interfingering the sequence. S1276 Biogenic fraction becomes stronger to the top. S398 Biogenic event at 860 mbsf (Figure 21) can probably be related to same event at 1010 mbsf in site S1276. Both sites contain retreating clay fraction in combination with large carbonate unspecified, quartz (10 %) and mica (7 %) excursion. S398 Campanian – Maastrichtian period contains clay (30 – 70 %) with a continuous background sedimentation of quartz (5 – 20 %) and mica (5 %) (Figure 2, 21 & 27, Appendix D & F). The Maastrichtian period is strongly biogenic, nannofossils (60 %) become more abundant to the top. S641 contains a zeolite (7 %) and very large clay (90 %) fraction (Figure 2 & 21, Appendix D & F).

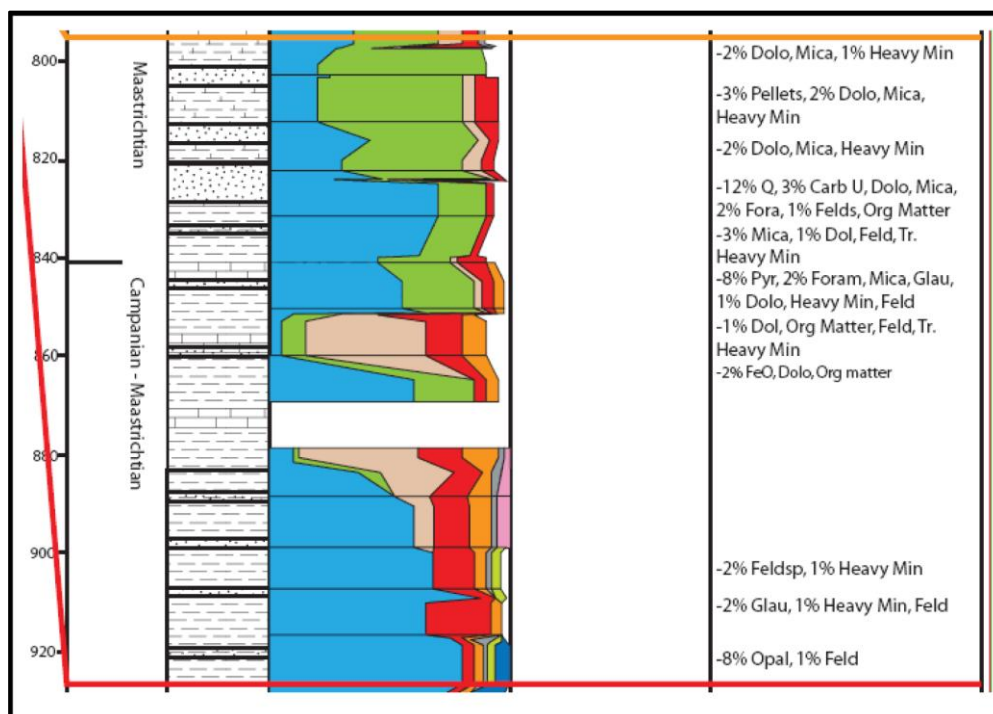


Figure 27; S398 Upper Cretaceous (Appendix D)

The Cretaceous – Tertiary boundary, in site S1276 at 980 mbsf, is indicated by a barite, pyrite, silica and dolomite occurrence (Figure 28). This peak is very distinct in both its composition and the

timing. The Cretaceous – Tertiary boundary of the Demerara Rise site S1258 (240-250 mbsf) comprises of a fading nannofossils record (Figure 29). This event is characterized by quartz, pyrite and manganese oxide and is very distinct from the rest of the sequence (Figure 26). The Campanian termination in site S1258 signals a distinct set back in clay in combination with a quartz and zeolite occurrence before the development of large-scale foraminifers and radiolarians (Figure 29).

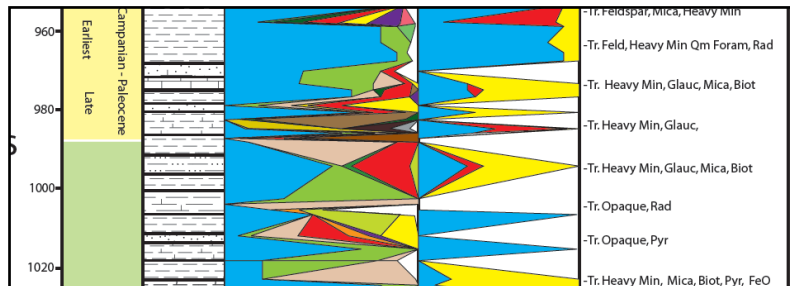


Figure 28; S1276, Grand Banks, Cretaceous – Tertiary boundary

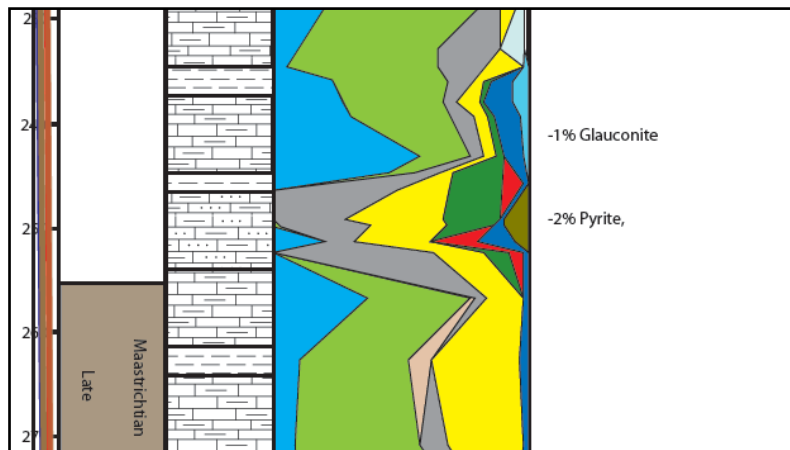


Figure 29; S1258, Demerara Rise, Cretaceous – Tertiary boundary

VI. Interpretation

This chapter summarizes the main elements from the chapter results and Appendix A – F. It interprets three important factors: 1) oceanic anoxic events (OAE's), 2) water depth and 3) eustatic sea level and CCD.

6.1. Oceanic Anoxic Events (OAE's)

This study correlates and identifies three oceanic anoxic events for the Cretaceous. These three events are the most prominent of the North Atlantic OAE's and are therefore most probable to be traceable in the cores. OAE1a the "Selli" event is found during the Early Aptian, OAE1b "Jacob, Paquier and Urbino" events are fixed as Late Aptian – Early Albian and OAE2 "Bonarelli" event is marked as Cenomanian – Turonian (Gradstein et al., 2004). Extrapolation of the anoxic events was based upon: 1) chronology, 2) microfossils data (planktonic foraminifera and calcareous nanoplankton), 3) presence of pyrite and / or organic matter, 4) low diversities, low abundances or even absence of benthic foraminifera (Kuhnt et al., 1992, Friedrich et al., 2009). The marking microfossils data per event are; OAE1a (Planktonic foraminifera *Leupoldina cabri*, Calcareous nanoplankton *Rotalipora angustus*), OAE1b (Planktonic foraminifera *Ticinella bejaouaensis*, *Hedbergella planispira*, *Ticinella primula*, Calcareous nanoplankton *Nannoconus steinmannii*, *P.*

columnata), OAE2 (Planktonic foraminifera *W. archaeocretacea*, Calcareous nannoplankton *Q. gartneri*) (Gradstein et al., 2004). The OAE's are depicted in appendixes A-F.

The interpretation of OAE's is troubled by the following two factors: 1) Continental margins, terrigenous material can obscure the OAE signal. This accounts for the OAE correlations of sites S415, Ancona and S398 as well as frequent turbidite incursions in site S1276. 2) Extrapolation of the OAE's was based on the data at hand. In some cases essential cores are missing e.g. site S549, in these cases no OAE was interpreted.

6.1.1. OAE interpretation per site

In this subchapter oceanic anoxic events are interpreted for the different sites of this study. OAE1b in site S391 is located above the *Hedbergella Trocoidea* zone (uppermost Aptian), OAE1b is located at the uppermost part of this zone (905 mbsf). OAE1a is located in the lower part of the *Perhabdolithus angustus* – *Chiastozygus litteranruus* zone at 934 mbsf (Benson et al., 1978, Gradstein et al., 2004). The two events are ascribed to the two pyrite excursions in this core respectively at 905 mbsf and 934 mbsf.

S1258 OAE1b is assigned to the interval 447 – 484 mbsf related to *Ticinella primula* occurrence. The interpreted position 446 mbsf is extrapolated from a decreasing nannofossils fraction in combination with an increasing clay fraction (Erbacher et al., 2004). OAE2 is located between the *Axopodorhabdus albianus* at 407,5 mbsf (late Albian) and the *Uniplanarius triffidum* zone at 392 mbsf (Campanian). The event is assigned to a depth of 394 mbsf based on the clay, organic matter and pyrite excursions. The absence of nannofossils and foraminifera is also a strong argument for anoxic conditions. Absence of calcareous material can be related to deposition below the CCD or in anoxic condition, in both cases planktonic foraminifers and calcareous nannoplankton are dissolved (Kuhnt et al., 1992, Friedrich et al., 2009). Uncertainty in the assignment of OAE1b in S1258 is related to absence of core coverage below OAE1b. The strongly enhanced organic matter and a continuous episode of organic matter deposition in site S1258 is different from sites in other basins. The strong organic signal is probably related to high organic production due to eutrophication (Hofmann et al., 2009).

The Cenomanian Turonian of site S367 is barren of planktonic foraminifera and calcareous nannoplankton. The only reference to the location of OAE2 are the *Ticinella primula* and *Hedbergella planispira* (latest Aptian – earliest Albian) zones, found in core 22 (720 – 730 mbsf). These two factors suggest that event OAE1b should be located at 730 mbsf (Lancelot et al., 1978). According to Lancelot et al., (1978) OAE2 should be assigned to the pyrite excursion in the Early Turonian black shales. Other locations within the stretch 640 – 700 mbsf have a strong nannofossil signal. A constant nannofossils signal is considered unlikely in an oceanic anoxic event, the OAE is inferred from a strong carbon isotope perturbation negative or positive. For S367 a 10 meter core section was recovered for the Early Aptian, in this section there is no trace of an anoxic event in the smear slides. The lithological description nominates it as black shale rich however this study focuses on the smear slide and X-ray studies. As the smear slide contains a nearly 90 % calcareous (nannofossils and carbonate unspecified) fraction denomination of OAE1a is highly controversial.

S105 OAE1a and OAE1b were correlated chronologically and on basis of the pyrite peaks. OAE1b is accentuated by a strong clay peak (Hollister et al., 1972). Based on the presence of *E. Turriseiffelli* 313 – 322 mbsf (Latest Albian – Early Cenomanian), OAE2 is located in a younger core. Deficiency of

nanno- and calcareous fossils in the interval 285 – 268 mbsf indicates anoxidity. This deficiency in combination with a pyrite excursion assigns OAE2 to 285 mbsf.

The Barremian – Cenomanian S387 has a strong deficiency in Mesozoic foraminifers probably due to reducing conditions (Tucholke et al., 1979). OAE2 and OAE1b (584 mbsf) are delineated based on pyrite excursions in combination with the chronology of Tucholke et al., (1979). The “Selli” OAE1a event is not contained in S387, considering there is barely an Aptian record and neither a pyrite or organic matter signal.

S137 The interval 256 – 265 mbsf is marked as *Rotalipori Cushmani* (Cenomanian), *Hedbergella planispira* (Albian – Cenomanian) and *S. sigali* (Turonian – Coniacian) as such this interval is interpreted as Coniacian – Cenomanian (Hayes et al., 1972). Core 8 (265 – 274 mbsf) composed of *Rotalipori Cushmani* and *Rotalipora appenninica* is identified as pure Cenomanian (Hayes et al., 1972). Since there is no pyrite to identify OAE2, the oceanic anoxic event was placed in the interval 256 – 265 mbsf following a the microfossil datum of Cenomanian – Turonian boundary (Gradstein et al., 2004).

The OAE2 in Ancona Site is most likely located in the *Whiteinella archeocretacea*, *Hedbergella planispira*, *Hedbergella simplex* and *W. Baltica* zone identified at the interval 1076 - 1075,2 feet (Miller et al., 1999, Gradstein et al., 2004). Absence of OAE1a in the Ancona site is explained by lack of Aptian – Albian sediments, no OAE1b was denominated in the Ancona site as Ancona does not cover the Aptian – Albian.

Site 136 OAE2 is located between core 7 (271 – 280 mbsf) and core 8 (280 – 289 mbsf) (Hayes et al, 1972). Core 7 is Santonian with a large portion of *Globotruncana* but also contains some *Hedbergella* (Turonian). Core 8 contains rare *Globotruncana* as well as Albian *Hedbergella*. As there is no strong perturbation indicating OAE2, the most plausible location for OAE2 is the boundary between the two cores at 280 mbsf. The condensed S136 Aptian Albian record corresponds to a highly uncertain delineation of OAE1b.

S415 (Lancelot et al., 1980) Core 8 (576 – 586 mbsf) to 12 (880 - 889,5 mbsf) consists of *Rotalipora cushmani* located directly below OAE2. The preservation of planktonic foraminifera in this location is poor and many are recrystallized. Core 14 (1032 – 1042 mbsf) to core 15 (1042 – 1080 mbsf) are dated Lower Cenomanian, consisting of *Rotalipora appenninica*. Hence the most plausible location of OAE2 is contained in core 8 coinciding with the high pyrite fraction at 576 mbsf.

S1276 Core 29 (1060 – 1070 mbsf) contains *Quadrum gartneri* and is located at the upper boundary of OAE2 and assigned to Lower Turonian. Core 31 contains the Cenomanian – Turonian boundary based on the calcareous nannoplankton *E. octopetalus* & *Quadrum intermedium* zones and *Rotalipora cushmani* & *W. archaeocretacea* planktonic foraminifera (Tucholke et al., 2004). The “Bonarelli” event is found in core 31 between 1089 and 1098 mbsf. OAE1b is probably located in core 94 as core 76 (1672 – 1681 mbsf) contains *Prediscosphaera columnata* and as such is assigned to middle Albian (lower boundary is Aptian / Albian boundary). The interval between core 76 and 94 is weakly represented by planktonic and calcareous nannoplankton, therefore the OAE1b was assigned to the first dated core and the perturbations and black shales of core 94 (Tucholke et al., 2004).

S549 Core 26 (427 – 436 mbsf) contains *Hedbergella* and *Globo truncana preaehelvetica* and is considered Turonian (Graciansky et al., 1985). Core 27 (436 – 446 mbsf) is excluded of nanofossils a probable Turonian - Cenomanian age was expected as core 28 (446 – 455 mbsf) contains *Rotalipora cushmani* and *Rotalipora appenninica*. Therefore OAE 2 was placed in core 27 (436 – 446 mbsf) at 446 meter in accordance with the pyrite excursion. The Albian and Aptian are recovered such that placement of OAE1b is impossible, there simply is a strong lack of core enabling a correlation.

S641 Between the poorly preserved core 5 (35 – 45 mbsf) (Coniacian – Maastrichtian) and core 6 (45 – 54 mbsf) (Albian), few age indicators were found (Boillot et al., 1987). Core 6 consists of traces *Hedbergella planispira* and *Rotalipora appenninica* affiliated to late Albian – Early Cenomanian (Boillot et al., 1987). Core 1 (151 – 161 mbsf) of S641C consists of *Podorhabdus albianus* exhibiting Mid Albian characteristics. Core 8 (218 – 228 mbsf) contains *Prediscosphaera columnata* characteristic for the start of the middle Albian OAE1b events (Boillot et al., 1987). Within core 12 (257 – 267 mbsf) *Nannoconus steinmanni* is retrieved, characteristic for the Aptian period (Boillot et al., 1987). Core 6 (199 – 209 mbsf) is supposedly located in the middle of OAE1b, however no characteristic lithological signature of an anoxic event is retrieved. Core 3 does show this signature with a large excursion of pyrite 170 – 180 mbsf. Consequently OAE1b stretches throughout the early Albian and is here chosen to represent OAE1b. OAE2 is not retrieved in this core contain an early Cenomanian section but no upper Cenomanian to Turonian core. Consequently OAE2 was not interpreted and is probably not present in this core.

In site S398 the Aptian was defined from core 127 (1630 – 1639 mbsf) up to core 98 (1354 – 1364 mbsf) on ground of *Chiastozygus litterarius*, *N. Colomi*, *P. asper*, *Z. crux* and *Cretarhabdus cenulatus* (Ryan et al., 1979). *Parhabdolithus angustus* was retrieved between 1449 – 1459 mbsf and is defining the Upper Aptian. According to Ryan et al., 1979 the lowermost *Prediscosphaera cretacea* zone and thus Aptian – Albian boundary was encountered first in core 92 (1307 – 1316 mbsf) by calcareous nannoplankton; *P. cretacea*, *C. litterarius* and *Corollithion achylosum*, while foraminifers identify the boundary between 1345 and 1364 mbsf. Taking the 1307 – 1364 mbsf interval as the bounding factor, OAE1b was placed at 1345 mbsf also based on the extensive excursion of pyrite and absence of nanofossils and foraminifers. The occurrence of *Rotalipora cushmani* in core 56 (947 – 956 mbsf) is proof of a Mid Cenomanian age, from this point onward the Cenomanian becomes poorly exposed due to anoxia (Ryan et al., 1979). Based on large organic matter excursion in combination with, black shale alterations and absence of nanofossils and green calcareous ooze, OAE2 was placed at 948 mbsf.

Site S391 has no retrieved OAE2 since site S391 is comprised of upper Albian and older sediments. OAE1a and OAE1b were appointed at pyrite excursions in accordance with nanofossils occurrences.

The OAE interpretation in sites S549, S136 and S137 is insecure. Oceanic Anoxic Events are determined in this research by means of the four factors named in the previous subchapter. However in these three sites carbon isotopes excursion correlations would generate a better constrained location of the OAE. Below Table 5, Figure 30 and 30a show the results of the OAE assessment for the three different OAE's.

Event	OAE1a	OAE1b	OAE2
Site	S391	S391	S1258

Site	S105	S1258 (uncertain)	S367
Site	S398	S367	S105
Site		S105	S387
Site		S387	S137 (uncertain)
Site		S1276	Ancona (uncertain)
Site		S641	S136 (uncertain)
Site		S398	S415
Site			S1276
Site			S549
Site			S398

Table 5; Oceanic Anoxic events and their occurrences (Appendixes A-F)

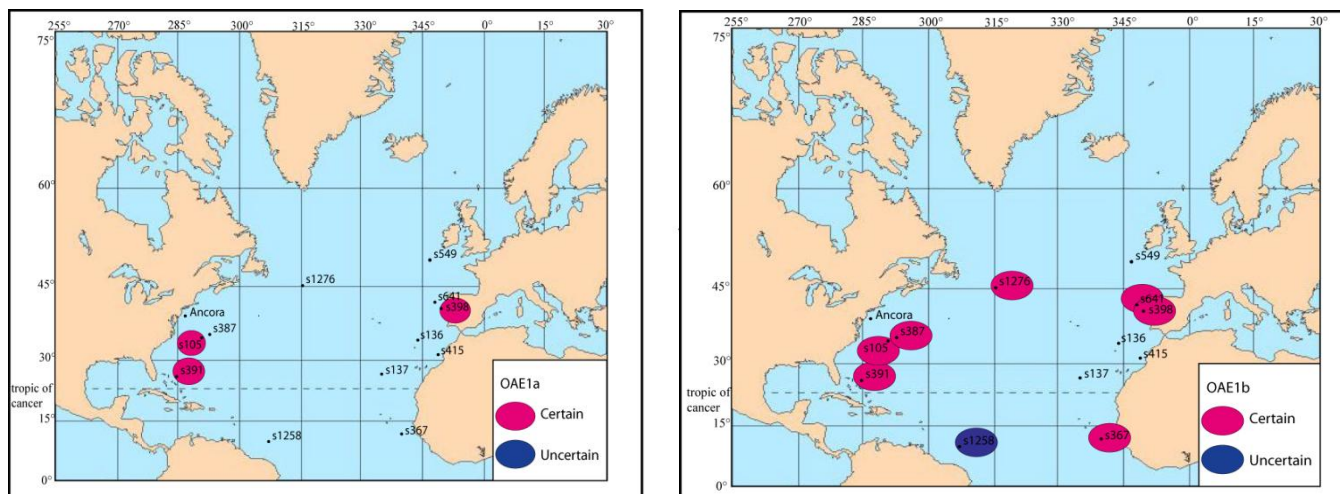


Figure 30 & 30a; Presence of anoxic event OAE1a, figure 30a presence of anoxic event OAE1b

General characterization of the OAE's.

The signal of OAE1b is generally weak, 3 % organic matter peas, often coinciding with an increasing mica fraction and nannofossil absence or low abundance. Sites S391 and S105 contain very similar signals characterized by a strong mica, feldspar, quartz and heavy mineral signal dominating 40 % of the smear slide. The strong enhancement of heavy minerals, mica and feldspar are probably related to volcanic activity in the region. The volcanic activity is also described in the chapter 3 Geological Setting. S398 is pointed out for its large organic matter and pyrite peak identified as OAE1b. This peak is related increased production due to eutrophication or upwelling similar to the upwelling zones on the Moroccan margin (Holbourn et al., 2001).

OAE2 is strongly distributed throughout the whole North Atlantic, it is characterized by a large organic matter peak as discussed earlier in this subchapter. World wide it is known to exhibit a strong carbon isotope excursion. This excursion, described in literature, has been used to verify the OAE position in the different sites. Regionally and locally this world wide event is characterized by distinct characteristics as is discussed in next paragraphs (Figure 17 – 21, Appendix A – F).

Comparison of different sites during the Bonarelli event (OAE2) shows similar signals in sites S105, S367 and S398 (Figure 2). These sites contain a strong zeolite presence ranging from 10 – 20 % in combination with feldspar 4 % and quartz fraction 3 – 10 % (Figure 17, 18 & 21). In the Demerara Rise and S136 zeolite is one of the more significant constituents. The other cores are mostly enriched in mica and feldspar coinciding with the expected signal for OAE. The question arises whether or not these zeolite occurrences are related. In the case of S367, S105 and Demerara Rise the premier

relation is the location on low tropical latitudes. Zeolite is mostly related to a volcanogenic or siliceous microfossil origin (Appendix G).

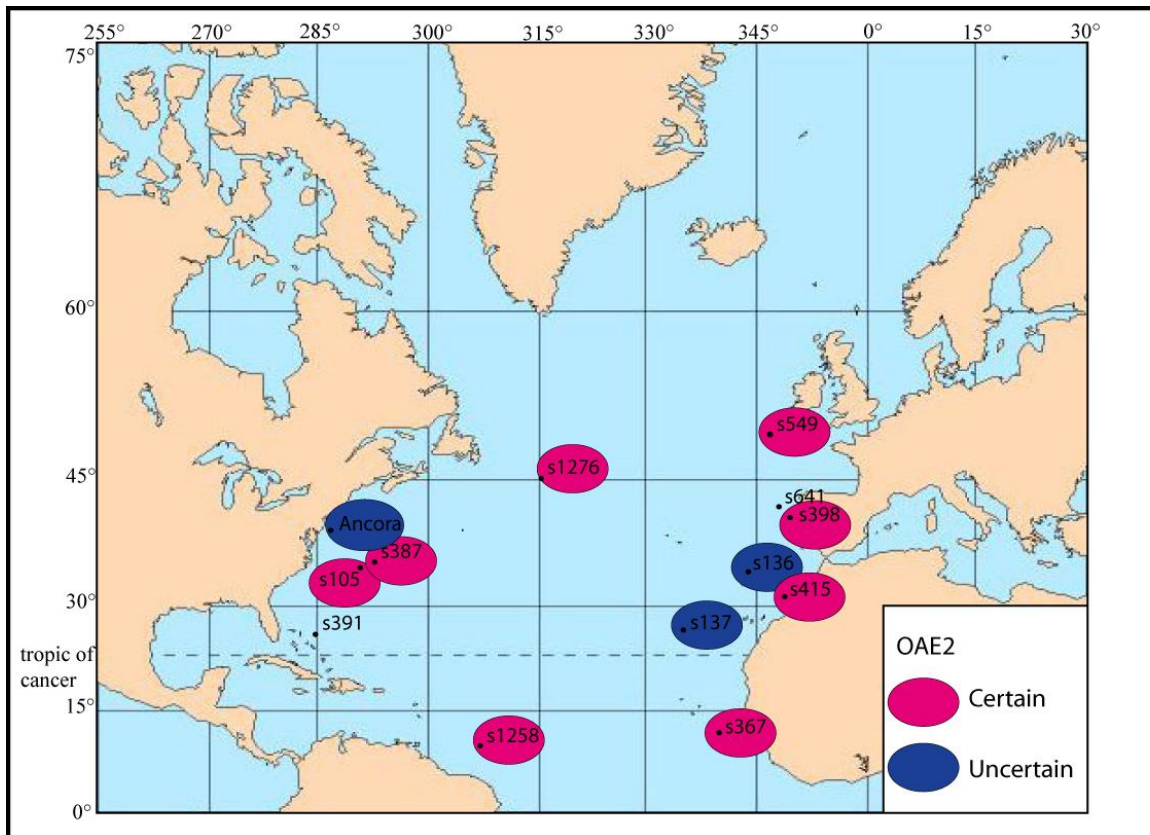


Figure 31; Presence of anoxic event OAE2

Especially the relation to radiolarians (siliceous microfossils) is of specific interest as S105 and S367 are related to radiolarian transition to zeolite. The strong peak of zeolites in site S105 can be correlated directly to a strong radiolarian abundance of site S387 (Figure 17 & 18). S105 exhibits a 30 % radiolarian peak coinciding with a 20 % zeolite excursion. Zeolite in S1258 also has a siliceous microfossil origin. The X-ray fraction in site S398 displays a strong presence of glauconite which in these shallower marine settings is related to slow deposition in presence of zeolite minerals. S137 contains the distinguished pyrite fraction in combination with heulandite and iron oxide also in the presence of zeolite also delineated to slow deposition.

Zeolite minerals can have numerous origins, related to volcanic, slow sedimentation, siliceous microfossils and radiolarians. Which of these four origins and can only be inferred from the character of other minerals. The main importance of the zeolite occurrences, is the fact that they occur synchronously. The co-excursion with OAE2 supports a hypothesis relating anoxidity to the alteration of microfossils. From the stratigraphic background there is nothing known of large volcanic activities during the Cenomanian Turonian boundary that could have caused zeolite excursion in the eastern Atlantic. But Ryan et al., (1979) interpret the zeolite concentration during the Cenomanian / Turonian oceanic anoxic event 2 as a condensed section-hiatus. The character of zeolite is thus of a different character in the named sites. A broad regional picture characterizes the Atlantic in: 1) western

Atlantic (siliceous microfossil origin) and 2) eastern and northern Atlantic (diagenetic origin through low sedimentation rates).

6.2. Water depth

The estimations and calculation of water depth is key to the understanding of sedimentation. The main importance of the paleodepth is the controlling factor it plays in carbonate sedimentation in relation to the CCD. The following subchapter estimates the water depth during the Cretaceous. This chapter use the simple cooling model constituted by Parsons and Sclater (1977), fauna documented in the IODP reports as well as lithological characteristics.

For the first interpretation of water depth the simple cooling model for oceanic crust was applied as constituted by Parsons & Sclater (1977). The model predicts a linear relation between depth, square root of ocean floor age, heat flow and 1 / square root of ocean floor age (Parsons & Sclater 1977). The relation is twofold, starting with an initial increase as the root of ocean floor age, up to 60 Ma. Between 60 and 80 Ma the ocean floor depth decays exponentially with age towards a constant asymptotic value. The constants used in this study are a plate thickness of 125 ± 10 km, bottom boundary temperature of $1350^\circ \pm 275^\circ\text{C}$, thermal expansion coefficient $(3.2 \pm 1.1) * 10^{-5}\text{C}^{-1}$. The following formula account for the following periods:

- 1) $0 < t < 70$ Ma: $d(t) = 2500 + 350 \sqrt{t}$
- 2) $t > 20$ Ma: $d(t) = 6400 - 3200 \exp(-t / 62,8)$

Core	Present Water Depth (PWD) (meter)	Age basement/crust (Ma)	Sort of basement	Subside nce by cooling (S)(meter)	PWD - S	Interpreted water depth at Earliest Cretaceous	Remarks
S391	4974	Tithonian	Basalt	6110	1136	4500 Albian	Large sedimentation (1700 m)
S1258	3192	Older then Albian (> 112 Ma)	??	5862	2670	2000 Late Cretaceous	
S367	4748	Middle Oxfordian	Basalt	6154	1406	3000 - 3500 Early Cretaceous	Magnetic anomaly
S105	5245	Older then Late Jurassic	Basalt	6254	909	4000 Valanginian	
S387	5117	Late Berriasian - Early Valanginian	Basalt	6066	949	2500 Late Berriasian	
S137	5361	Older then Late Albian (>106.6 Ma)	Basalt	5814	453	2500 Late Albian	
Ancona	0		??			200 - 600 Early Cenomanian	Continental margin
S136	4169	Older then Early Aptian (>125 Ma)	Basalt	5963	1794	2500 - 3000 Aptian - Albian	
S415	2794	Older then Late Albian (>106.6 Ma)	??	5814	3020	2500 - 3000 Late Albian	Tectonically active
S1276	4549	Older then Late	Basaltic	5814	1265	3500 m Late	Tectonically

S641	4640	Aptian (>115 Ma) Older then Late Jurassic	??	6154	1514	Aptian 2500 – 3500 Middle Cretaceous	active Tectonically active
S398	3910	Early Jurassic?	Basalt	6133	2223	2500 – 3500 Late Cretaceous	Tectonically active
S549	2515	Devonian	Micaceous foliated sandstone			1000 – 1500 Late Albian	Tectonically active

Table 6; Depth calculation following the simple cooling model of Parsons & Sclater 1977

All oceanic crust in this study is older than 70 Ma, therefore the second formula was used for calculating the original depth of the sea floor at the moment of formation. The second step involved matching the calculated sea floor depth to the present sea floor depth. In the situation of a match, between present and calculated sea floor depth, the assumption can be made that the sea floor behaved following Parsons & Sclater (1977) formulae since formation.

This follows from the fact that when formula 2 holds for the entire time span, formula 1 can be used to estimate the deepening since sea floor formation. The consequence is that formula 1 was only applied to calculate the depth since the start of sedimentation (crust in all sites is > 70 Ma). A near match is defined as a deviation of up to five hundred meters. Such a strong deviation can be reasoned by the poor control on the exact date of sea floor formation. From the moment of formation the sea floor is assumed to subside by means of cooling as depicted in Figure 32 (Formula 1). These calculations do not account for eustatic sea level variation. The eustatic sea level should be added to the water depth calculated above, this is explained further in this chapter.

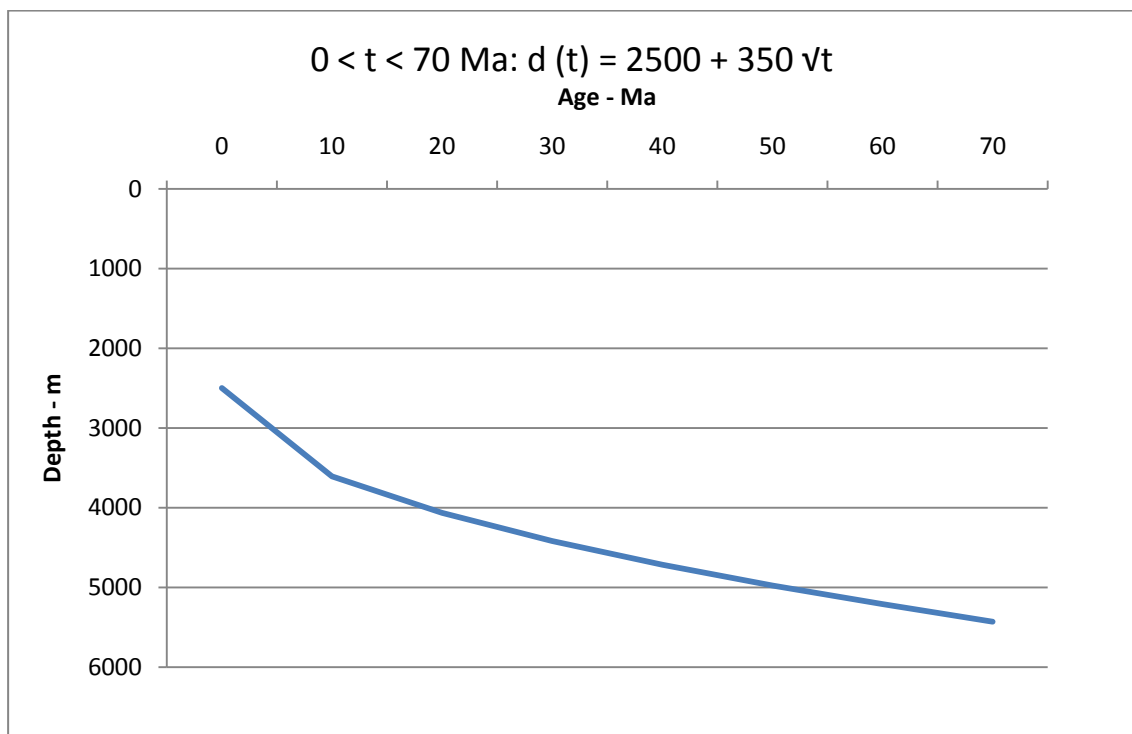


Figure 32; Formula 1 depth and time since formation (Parsons and Sclater 1977).

As is visible from the table 6 a correlation on the age for the sites used in this study is plausible only in a few situations. In the first place this is caused by the fact that sediment load was not added in the calculation, in second place due to the fact that many of the studied regions have been tectonically active and / or are influenced by magmatic anomalies. The sites located at the Bahama, Blake Nose and Cape Verde Basins are related to magmatic anomalies (Sclater et al., 1977). According to Sclater et al., (1977) the North Atlantic sea floor can be subdivided in three main divisions; 1) Normal ocean floor following formula 1 within ± 300 m, 2) Anomalous depth of more than local extent, excessive elevation of young sea floor and elevated regions of old sea floor, 3) Local features including fractures, islands arcs and aseismic ridges. As is visible from above and can also be concluded from the geological setting most sites are related the last two divisions. Only site S137 is probable to be located at a depth of 2500 m during Late Albian (date of formation of oceanic crust). For the other cores a faunal study in relation to a lithological interpretation had to be applied.

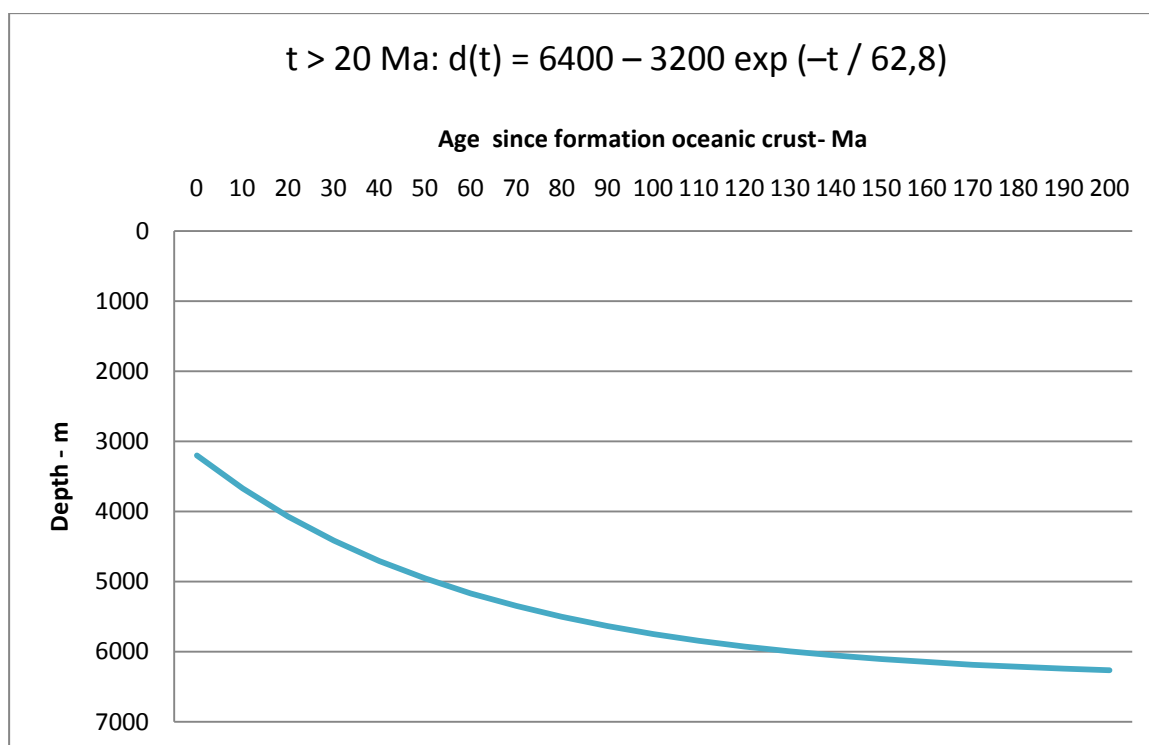


Figure 33; Formula 2 depth and time since formation (Parsons and Sclater 1977).

6.2.1. Water depth interpretation per site

S391 The Lower Cretaceous (Berriasian – Barremian) is interpreted to have been located near the CCD up to Aptian. This is determined from the constant presence of nannofossils (10 – 15 %). The oceanic crust beneath S391 was formed during Tithonian, the water depth without eustatic influence would be about 3600 m and by Albian around 4500 m (extrapolated from Figure 32 and 33). The Late Aptian – Late Albian interval is characterized by absence of biogenic calcareous materials and therefore must have dropped below the CCD ~3800 m. According to Benson et al., (1978) sediment input was coming from the Blake Plateau contributing to the biogenic fraction of the site. Apart from some nannofossils and carbonate unspecified peaks there are no large scale lithological peaks constituting evidence for this hypotheses. A correlation between an increasing grainsize and biogenic peaks would be the strongest evidence for such a relation to the Blake Plateau, in appendix A no such relation was found.

S1258 Contains a continuous fraction of nannofossils (60 %) and foraminifera (10 %) throughout the Mid and Late Cretaceous. This fractions suggests that this core must have been located above the CCD for both nannoplankton and foraminifera. No correlation can be made between S1258 and a Parsons and Sclater (1977) cooling model as the basement type is unknown and the possible calculated depth differentiates strongly from the present depth. The best indicators are the interpreted tempestite occurrence during Albian (Erbacher et al., 2004) related to depth up to 30 m. The Campanian – Maastrichtian relates to a open marine setting related to pelagic marls with glauconite deposition related to slow deposition and a depth of a few hundred meter.

S367 As underlined by Sclater et al., (1977) is associated with a broad swell under the Oxfordian oceanic crust. With no direct information on the timing of this uplift, identification of the water depth must be primarily based on lithology and biostratigraphy. The Earliest Cretaceous is marly with a 10 – 30 % nannofossils (nektonic) in combination with a mainly carbonate unspecified 80 % fraction in the Berriasian. Therefore S367 must have been located above the CCD during the Berriasian. The CCD was located around 4000 m during Berriasian (van Andel 1975). As such a depth assumption of 3000 – 3500 m was made for the Early Cretaceous. There is a obvious deepening during Aptian – Albian with a last nannofossils occurrence during Early Turonian. The Latest Cretaceous has little biogenic influence and as such is likely located below the CCD, coinciding with the presence of agglutinated foraminifera. A depth of 3500 – 4000 m was assumed for the Early Turonian related to the deposition below the CCD.

S105 Tithonian – Valanginian period is characterized by a strong foraminifer (10 – 50 %) and calcite fraction (10 – 50 %). A relation to Parsons & Sclater 1977 can be considered (not in detail), the difference between the calculated and present depth is to large (probably due to strong sedimentation related to the proximal location of the continental shelf). On the basis of an Oxfordian age a depth of about 4000 m is inferred during Valanginian (using Parsons & Sclater 1977). From Barremian – Cenomanian the site becomes progressively deeper and is excluded from calcareous sedimentation, agglutinated foraminifer *Glomospira diffundens* suggests deposition below the CCD. As such site S105 is interpreted to have subsided below 4000 m to up to 4500 m by Barremian (Kuhnt et al, 1992, Van Andel 1975).

S387 Earliest Cretaceous, Berriasian – Valanginian, marl is characterized by a strong carbonate unspecified fraction (40 – 90 %) with a small nannofossils fraction (5 – 10 %). The carbonate dominance from Berriasian – Lower Barremian points to deposition above the CCD. According to Tucholke et al., (1979) Berriasian – Valanginian nannofossils are baked in the basalt therefore a water depth of 2500 m can be interpreted during the same period (Figure 33).

A strong change occurs during the Upper Albian where strong clay (80 – 90 %) with a minor radiolarian fraction (3 – 10 %) prevails. This points to a progressive deepening up to Cenomanian or a shoaling CCD. Using the cooling model by Parsons & Sclater (1977) a water depth of 4200 m can be assigned for middle Albian. The prevailing background radiolarian supply suggests either allochthonous radiolarian input or a deeper CCD for radiolarians than nannofossils. Tucholke et al., (1979) suggests turbidites related to the increased terrigenous influx (mica fraction in Upper Albian – Cenomanian). Although the size of terrigenous influence in S387 is much smaller, the strong terrigenous influence in Cenomanian in S105 (located near S387) shows the influence of redeposition. On the basis of this last argument and the fact that between 470 and 480 mbsf (Maastrichtian) agglutinated formaminifera were found, deposition below CCD is accepted (Kuhnt et

al., 1992, Tucholke et al., 1979). The calcareous fraction greatly increases during the uppermost Maastrichtian (20 % calcareous). As such a strong deepening of the CCD for Upper Albian – Cenomanian in relation to a falling eustatic level can explain the increasing carbonate fraction.

S137 As claimed earlier site S137 has a Late Albian water depth of 2500 m and as such is located above the CCD. This is obvious from the strong (30 – 60 %) nannofossils fraction and minor fraction of foraminifers 10 % from Late Albian – Late Cenomanian. Towards the Late Cretaceous the clay content becomes stronger and dominant from the Turonian - Maastrichtian (90 – 95 %). Cooling of oceanic crust, led to a depth of around 3900 m by Early Turonian. Which by interpretation of the lithological record must have been located below the CCD. Deposition below the CCD is underlined by the presence of agglutinated foraminifera throughout the Late Cenomanian – Maastrichtian (Kuhnt et al., 1992).

For the Ancona site no use can be made of the cooling model as the basement is comprised of continental crust. From Early Cenomanian up to Early Turonian the site is dominated by clay with three minor peaks of nannofossils. The Ancona site is located on the continental margin well above the CCD, the Cenomanian – Turonian was most probably related to a transgressional event with a upper bathyal 200 – 600 water depth (Miller et al., 1999, Haq et al., 1987). From Turonian – Santonian a strong sandstone influx (95 %) was related to the strong late Turonian regression (Miller et al., 1999, Haq et al., 1987). The glauconite rich Santonian is assigned to a depth of 125 – 500 m (Chamley 1989). The Lower Campanian comprises dominantly clay, related to the Campanian transgression. Latest Campanian – Maastrichtian becomes dominantly siliciclastic (70 – 80 %) with a minor production of nannofossils (5 %). The depth range of this site was between 600 and 0 m, to more accurately indicate paleodepth sedimentary structures (e.g. cross bedding, storm bed deposits) should be observed in relation to habitats of marine fauna.

Site S136 is strongly condensed and has a poorly preserved Cretaceous biostratigraphic record. This poor preservation was related to deposition below CCD and volcanism according to Hayes et al., (1972). The Aptian – Albian interval has a strong nannofossil fraction (25 %), which totally retreats during Cenomanian, probably related to anoxia. The Turonian – Santonian exhibits a strong calcite fraction, volcanic pollution lead to diagenesis such that the record is unreadable (Hayes et al., 1972). The Coniacian – Santonian period contains primarily clay, with a 5 % fraction of carbonate unspecified. The Late Cretaceous shows an obvious deepening and deposition below CCD related to the absence of nannofossils. From the data above a deposition above the CCD, between 2500 – 3000 m was assumed for the Aptian – Albian period. The Coniacian – Santonian water depth was interpreted as ~ 3500 m related to (Van Andel 1975). No relation could be made to the cooling model, the difference between present depth and calculated depth is too large.

Site S415 contains an extremely strong deviation from the cooling models calculated depth. This is probably caused by uplift from Atlas orogeny. The Upper Albian – Middle Cenomanian is dominated by dolomite (90 – 25 %), carbonate unspecified (10 – 15 %) and the other main constituent is clay. As such the sea floor must have been located above the CCD; the carbonaceous fraction is prevalent and not incident. Depositional depth was probably 2500 – 3000 m as Lancelot et al., (1980) proposes a Albian – Cenomanian depth of outerslope to upper slope. The dolomite fraction contracts towards the Mid Cenomanian containing dominant clay, carbonate unspecified (20 – 50 %), pyrite (4 %) and nannofossils (3 %). Which infers a location near or below the CCD. Lancelot et al.,

(1980) interprets the Albian – Middle Cenomanian marlstone with dolomite limestone as an indicator of a deep water environment (3000 – 4000 m). Agglutinated foraminifera *Recruvoides nonioninoides* (Upper Albian – Cenomanian), *Gaudryina pyramidata* (Campanian – Maastrichtian), *Hyperammina elongatea* (Turonian – Maastrichtian), *Ammodiscus infimus* (Upper Albian – Cenomanian) are found from 510 – 1080 mbsf indicating deposition below the CCD (Kuhnt et al., 1992). Therefore a depth 3500 – 4000 meter is inferred on the basis that the Cenomanian sea floor must have been located beneath the CCD.

S1276 The Late Aptian – Albian period is dominated by clay and interfingering by quartz rich turbidites which in the upper part become carbonate rich. These layers are the effect of redeposition of more proximal facies. A tiny fraction (10 %) is calcareous background sedimentation, consisting of: micrite, nannoplankton and organic debris (Late Aptian – Lower Cenomanian). This suggests either little carbonate production or deposition near the CCD boundary. The Albian – Cenomanian period is characterized by a very clayey 60 – 90 % lower part and more calcareous upper part. The formation has regular biogenic and quartz excursions caused by turbidites. These turbidites form the only calcareous input during Cenomanian. The background sedimentation is barren from a calcareous fraction suggesting deposition below the CCD. The Turonian - Santonian period is characterized by a strong terrigenous fraction with a large carbonate excursion at 1040 mbsf. The concentration of terrigenous materials is correlated by Tucholke et al., (2004) to a slow sedimentation rate. The Campanian – Paleocene episode constitutes mainly claystone (60 – 80 %) influenced by carbonaceous incursions. The incursions are allochthonous probably transported from the continental margin to the deep sea, Tucholke et al., (2004) identified them as kaolinite rich. At 960 mbsf a background sedimentation of nannofossils is retrieved. This indicates deposition above the CCD during Latest Cretaceous. Maastrichtian – Campanian agglutinated foraminifera are characteristic for a range of 200 – 2000 m. They are not related to normal sedimentation but probable to be transported from bathyal environments. The Campanian – Albian interval is characterized by *Glomospira diffundens* (Latest Campanian – Maastrichtian), *Ammodiscus infimus* (Upper Albian – Cenomanian), *Trochammina papillata* (Turonian – Maastrichtian) from 1012 – 1710 mbsf. Occurrence of these agglutinated foraminifera suggest a abyssal deposition, well below the CCD (deeper than 3500 m) however strong presence of mass flows could suggest transportation.

The interpretation of S1276 is the most troubled one, due to the large influence of allochthonous deposits. In the previous paragraph this study tried to establish the allochthonous deposits versus the true deposition related to depositional depth (background sedimentation). As such the Campanian – Paleocene was interpreted as deposited below the CCD during (below 3500 m), related to the agglutinated foraminifera and absence of other carbonate sediment. Tucholke et al., (2004) is determined in assigning site S1276 to abyssal depth beneath the CCD. However from the smear slide interpretation column a small nannofossils fraction was derived for the Aptian – Lowermost Cenomanian suggesting deposition during this interval near the CCD boundary (3500 m). The same depth is related to CCD during the Cenomanian – Turonian. For the Upper Cretaceous Campanian – Maastrichtian period it is questioned whether the nannofossils fraction is indeed a nannofossils fraction from above the CCD or from agglutinated foraminifera. The latter is assigned to deposition below the CCD (deeper than 3500 m) the first to deposition above 3500 m. Last should be noted the physiographic situation of the New Foundland margin which might have been prone to a large

surface production, and a related deposition of calcareous material lower than the CCD predicted by Van Andel (1975).

S641 Barremian consists of claystone and calcite with a background sedimentation of nannofossils (10 %), quartz and mica. The Aptian – Albian consists of 60 – 70 % clay with 5 – 30 % nannofossils and calcite 20 – 40 % decreasing to the top. The site is strongly influenced by turbidite and slump deposits from Barremian – Early Albian. With only the deposition of carbonate as a reference, a depth of 2500 – 3500 m was interpreted for the Mid Cretaceous period. The Cenomanian – Maastrichtian is barren of biogenic influence and therefore concluded to have been deposited below the CCD (3500 – 4000 m). This interpretation is underlined by section 45 – 54 mbsf consisting of significant portions of calcareous material, these becoming scarcer towards 45 mbsf where agglutinated foraminifers dominate up to 15 mbsf. These Santonian – Maastrichtian foraminifers include *Hormosina ovulum*, *Hormosina ovulum crassa*, *Gaudryina pyramidata* are a clear indicator of deposition below the CCD (Boillot et al., 1987, Kuhnt et al., 1992).

Site S398 contains a strongly calcareous Hauterivian / Barremian – Early Aptian section nannofossils (20 – 30 %), carbonate unspecified (15 – 20 %) and minor radiolarians. Barremian deposition must have been located above the CCD. Allochthonous flows import carbonate unspecified and siderite as well as benthic calcareous foraminifers associated with epicontinental seas (Ryan et al., 1979). The consistent terrigenous background sedimentation of quartz, mica and organic matter suggests a continental slope / prodeltaic setting (Ryan et al., 1979). The Mid – Late Aptian is strongly clayey with a background sedimentation of quartz, carbonate unspecified, mica and in some instances nannofossils. Ryan et al., (1979) suggests that the absence of calcareous plankton could be related to deposition depth below the CCD or by restrictive circulation. However nanoplankton remains an important constituent throughout the Lower – Mid Aptian and even in Late Aptian is a profound component. Indeed by the deepening of the basin the clay fraction increases relative to the carbonate fraction. But the influx of the nannofossils seems more likely to be related to a shoaling and deepening CCD. During Late Albian – Maastrichtian (apart from Campanian) calcareous components strongly increase with a large up to 70 % nanoplankton fraction during uppermost Maastrichtian. From 882 – 920 mbsf Kuhnt et al., (1992) found traces of *Uvigerinamina jankoi*, an agglutinated foraminifer known as the indicator for deposition below the CCD. From 860 – 882 mbsf the *Goesella rugosa* zone indicates a deposition above the CCD, as a absolute high stand can only be formed above the CCD (Kuhnt et al., 1992). A depth between 2500 and 3500 meter is implied for the Latest Cretaceous.

Site S549 has a non marine basement (Devonian micaceous sandstone). The Early Barremian contains obvious terrigenous character with quartz (60 – 80 %) with a minor clay fraction (10 – 30 %). Plant debris and coalified wood are common. The Latest Barremian constitutes of an increasing carbonaceous fraction (predominantly carbonate unspecified) of 30 % with nannofossils (15 %). This unit is a coastal deposit, it deepens towards the Barremian. The Barremian is characterized by open marine conditions (De Graciansky et al., 1985). The 112 Ma sea level drop and its related unconformity, are succeeded by open marine conditions to coastal marine environment. This sequence is terminated by the Middle Albian – Cenomanian unconformity, which is related to another sea level drop. The Cenomanian – Maastrichtian core contains 80 % nannofossils and 20 % carbonate unspecified. The strong nannofossil deposition during the Late Cretaceous sealevel high

stand was related to primary production. De Graciansky et al., (1985) relate the large nannofossil deposition to a rapid subsidence to 1000 – 2000 m within 12 Ma and from there to a present seabottom depth of 2000 – 3000 m. This seems too fast for such a short period of time. The subsidence from a possible depth of 100 – 200 m to a sudden 1000 – 2000 would mean a faster subsidence rate than that of oceanic crust. This is not considered logical for a non marine basement where strong subsidence is related to burial. The sedimentary load in this sites only consists of an proximate 2 km of sediment. Rather a deeper marine setting is interpreted for Middle Albian – Cenomanian. This setting is followed by an unconformity related to nondeposition and superseded by a progressive deepening to a bathyal water depth up to 2000 m.

The main conclusions on the interpretation of water depth are listed in Table 7. Table 7 specifies the most certain water depth interpretation for a specific margin. These interpretations can be extrapolated to an earlier or later interval using the eustatic sea level (Figure 34) and the 2D cooling model. This water depths are applied in chapter discussion to Figures 38 & 40 – 44.

Summarizing the main elements, sites S1276 and S387, with strongly complex sedimentary record, were problematic for water depth interpretation (Figure 3). This study used the relation of carbonate precipitation relative to the CCD, which implied splitting the background / normal sedimentation from the turbidites sedimentation. Another problematic site is S136 which is such condensed that estimating the paleo depth is highly precarious. Less complicated were the calcareous rich sites which suddenly changed to calcareous barren (S391, S367, S136 & S641), in these sites this relation was used to interpret the water depth in relation to the CCD (Figure 3). Sites S105, S415 & S398 used agglutinated foraminifers, which are a strong indicated of sedimentation below the CCD (Figure 3). In most cases a combination of carbonate deposition in relation to the CCD and agglutinated foraminifera was used. The 2 cooling model was only used to determine the water depth of Site S137 (Figure 3). S1258, S549 and Ancona were not located on oceanic crust as such their water depth was interpreted using sedimentary characteristics such as tempestites (Figure 3).

Site	Time	Water Depth	Method
S391	Late Aptian – Late Albian	3800 – 4500 m	Absence calcareous material & 2D cooling model
S1258	Albian	30 m	Tempestite (Erbacher et al., 2004)
S367	Early Turonian	3500 – 4000 m	Agglutinated foraminifers
S105	Valanginian	4000 m	2D cooling model and agglutinated foraminifers
S387	Berriasian – Valanginian	2500 m	Nannofossils in basalt (Tucholke et al., 1979)
S137	Albian	2500 m	2D cooling model
Ancona	Cenomanian – Turonian	200 – 600 m	Marine fauna (Miller et al., 1999)
S136	Aptian – Albian	2500 – 3000 m	Change in carbonate fraction relative to CCD
S415	Albian – Mid Cenomanian	3500 – 4000 m	Agglutinated foraminifers (Kuhnt et al., 1992)
S1276	Albian – Lower Cenomanian	3500 m	Change in carbonate fraction relative to CCD
S641	Cenomanian – Maastrichtian	3500 – 4000 m	Absence calcareous material & agglutinated foraminifers
S398	Latest Cretaceous	2500 – 3500 m	Calcareous material & agglutinated

				foraminifers
S549	Early Barremian	Above level	sea	Terrigenous material

Table 7; Summarizing water depth interpretation

6.3. Eustatic Sea Level and CCD

This subchapter aims to describe the behaviour of the eustatic sea level and the CCD during the Cretaceous. As well as correlate the two to get a better grip on sedimentation within the different sites of this research.

For the interpretation of eustatic sea level and CCD, the study of Haq et al., (1987) was used (Figure 34). The Haq et al., (1987) study follows from the heavily debated study on sea level chronology by Vail et al., (1977). Haq constructed an accurate time scale in which depositional sequences were integrated (Figure 34). This study makes use of the eustatic sea level as a consequence of the North Atlantic connection to the Pacific and Tethys during the Cretaceous (see chapter Geological Setting).

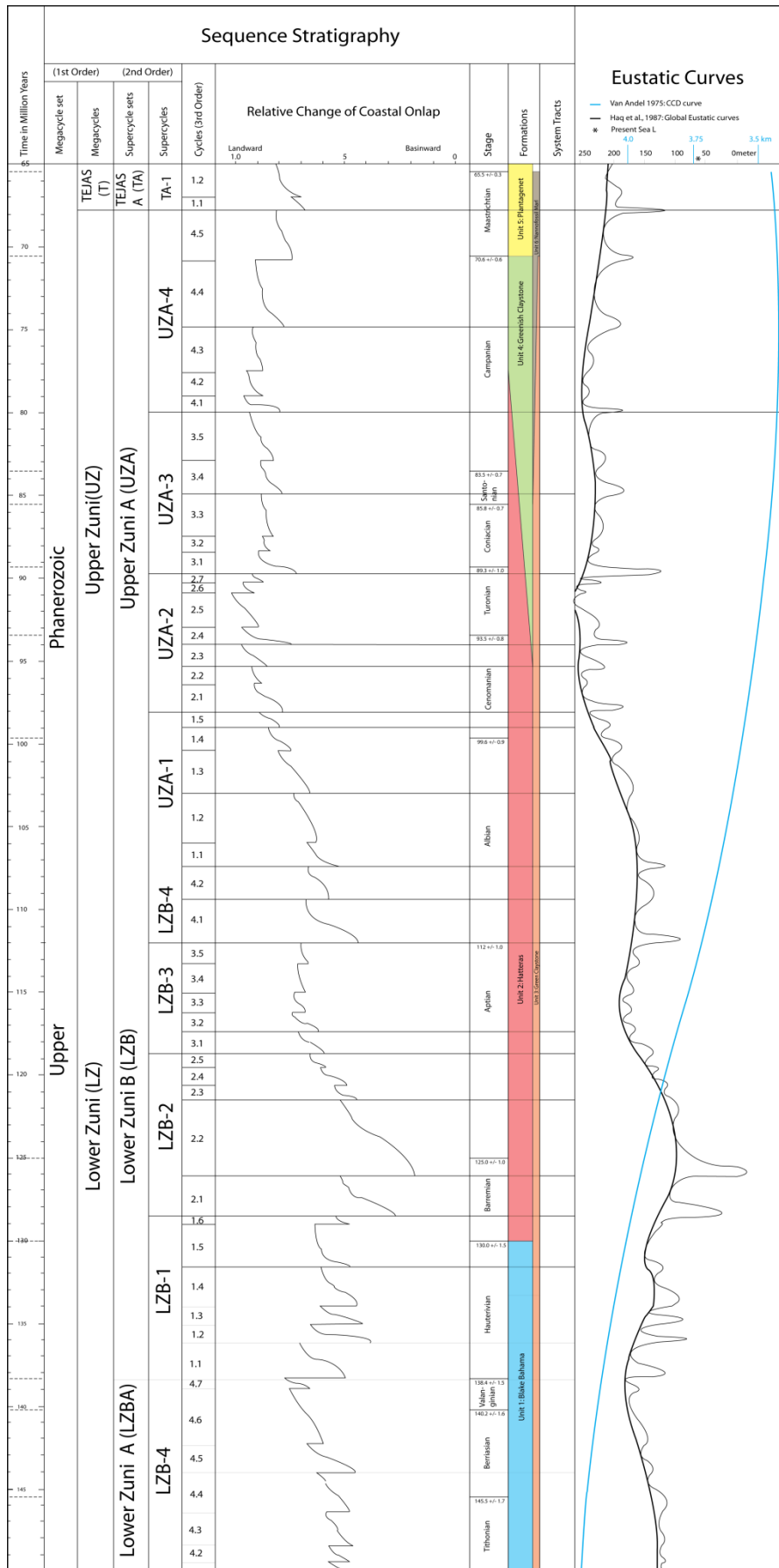


Figure 34; Eustatic Sea level Curve and CCD curve (compiled using data from Haq et al., 1987, Van Andel 1975)

Figure 34 shows that eustatic sea level change (Haq et al., 1987) never exceeds 250 m of relative change during the Cretaceous. The change of eustatic sea level has two main effects. Firstly it controls the amount of shelf exposed to weathering. Secondly it determines the distance terrigenous sediment has to travel in order to reach the deep ocean basins (abyssal plain). As such the eustatic sea level change strongly contributes / dominates the supply of terrigenous material. During a sea level lowstand (Early Cretaceous) the supply of terrigenous material (quartz, mica, heavy minerals, plant debris, kaolinite) to the deep sea is strongly increased. The continental margin is now exposed to denudation, secondly rivers and canyons directly supply the sediment to the deep ocean. During a transgression and sea level highstand the continental shelf, previously exposed to weathering and direct sediment supply to the deep ocean, is now blanketed by shallow seas. This strongly reduces the terrigenous supply to the deep ocean and thus the deep marine sites in the Atlantic ocean, as these shallow seas serve as terrigenous reservoir.

The CCD curve of Van Andel 1975 (Figure 34) illustrates one important relation. The CCD curve contains double the amplitude of the eustatic sea level change (Figure 24). High sea level relates to high production of marine lithosphere by submarine volcanism (mid oceanic ridge formation). This lithosphere production is correlated to a shoaling CCD, as a consequence of an increased production of CO₂ and the related acidification of the ocean. During episodes of lower submarine volcanism, during a relatively low eustatic sea level less CO₂ is discharged inherently leading to a deeper CCD. Hence the larger amplitude of the CCD, compared to that of the eustatic sea level curve results has to be strongly observed in describing carbonate sedimentation. Since the publication by Van Andel 1975 is a relatively old one, it is treated as an illustration of the relative CCD rather than applied as an exact representation.

6.3.1. Eustatic sea level and CCD per site

This subparagraph interprets large-scale relations described in the previous two paragraphs for North Atlantic sites. It observes large scale relations between the eustatic sea level and CCD in two periods: 1) Early Cretaceous (low eustatic sea level) and 2) Mid – Late Cretaceous (high eustatic sea level) (Figure 34).

One of the large scale effects of eustatic sea level, is the increased supply of terrigenous material to the abyssal plain from the Berriasian to Barremian (a period of relative lower sea level) (Figure 34). This is especially clear for the eastern Atlantic sites S549, S398 and S641 (Figure 3). S549 Consists of a dominantly continental terrigenous input, which was interpreted in the subparagraph water depth as shelf area. S398 And S641 show a rather constant terrigenous background sedimentation with plant debris in S641, indicating terrigenous input.

As stated in the previous subchapter a low eustatic sea level would lead to an intensification of the CCD and increased calcareous deposition. The relation holds, there is indeed large scale deposition of Unit 1 (Blake Bahama formation) in sites S391, S367, S105, S387 and S398. However as concluded in the chapter waterdepth some sites are located in a relatively bathyal setting (S391 and S398), approximately 2500 – 3000 m and as such are located well above the CCD. A deepening of the CCD would therefore not have influenced deposition of carbonates in these sites, carbonate preservation would have prevailed anyhow. In sites S105, S367 and S391 the CCD depth is of major importance to carbonate deposition. These three sites contain an interpreted (subchapter water depth) paleodepth of 3500 – 4500 m. With CCD depth of 4000 – 4200 m the eustatic sea level and

CCD are of major importance in controlling the sedimentation character. For the western Atlantic lower Cretaceous the relation between low eustatic sea level and CCD holds.

However the western Atlantic does not entirely behave according to the relation described above. During Early Cretaceous the North American coast forms a large marginal sea separating the abyssal plain from a terrigenous influx. The American coast consists of a carbonate reef system trapping terrigenous sediments amidst. Therefore terrigenous input in the western North Atlantic US offshore is largely absent.

The correlation between eustatic sea level rise and a shoaling of the CCD, has is also applicable for Middle to Late Cretaceous period. During the Aptian to Turonian the eustatic sea level rises to an absolute high stand, from the Turonian the sea level slowly falls up to Maastrichtian but the eustatic sea level still remains considerably higher than the pre Albian eustatic sea level (Figure 34). During entire time span the CCD continuously shoals.

Sedimentation is dominated by bituminous shale during the Mid Cretaceous. Which is an obvious representation of a deepening carbonate barren oceanography. The progressive deepening trend is found in cores S391, S367, S105, S387, S1276, S641, S398 (Figure 3). Especially in sites S105 and S641 the consequence of a relative deepening by eustatic sea level rise and shoaling effect of the CCD are visible with an increasingly carbonaceous barren Upper Cretaceous. The cooling of the ocean lithosphere is a major contribution to the disappearing carbonaceous fraction in the primary deposition, as the sea floor becomes relatively deeper. In some abyssal sites (S1276), primary deposition is strongly influenced by turbidite and debris flow fluxes of carbonate rich material from the continental margin, in a principally carbonate barren environment.

The importance of the eustatic sea level and a shoaling CCD for carbonate sedimentation, is underlined by the Campanian – Maastrichtian increase of carbonaceous deposition in site S398 (Figure 3). S398 is considered as an abyssal setting with an interpreted water depth of 2500 – 3000 m (subparagraph water depth). Site S398 contains a strong nannofossils (70 %) fraction, whilst strongly being influenced by the Iberian continental margin. Preceding this strong nannofossils fraction is a period of no carbonate preservation (Figure 35). The return of carbonate deposition is related to the Late Cretaceous regression in combination with a CCD at its shallowest level. Site S398 illustrates that CCD in this site must have been deeper than the ocean floor leading to strong carbonate deposition. Site S398 underlines the importance in marginal setting to the combined effect of CCD and eustatic sea level. Where the combined effect led to carbonate deposition after a Late Cenomanian – Early Maastrichtian period barren of carbonates (Figure 35).

Influence of climate and oceanography on Cretaceous sedimentation in the North Atlantic

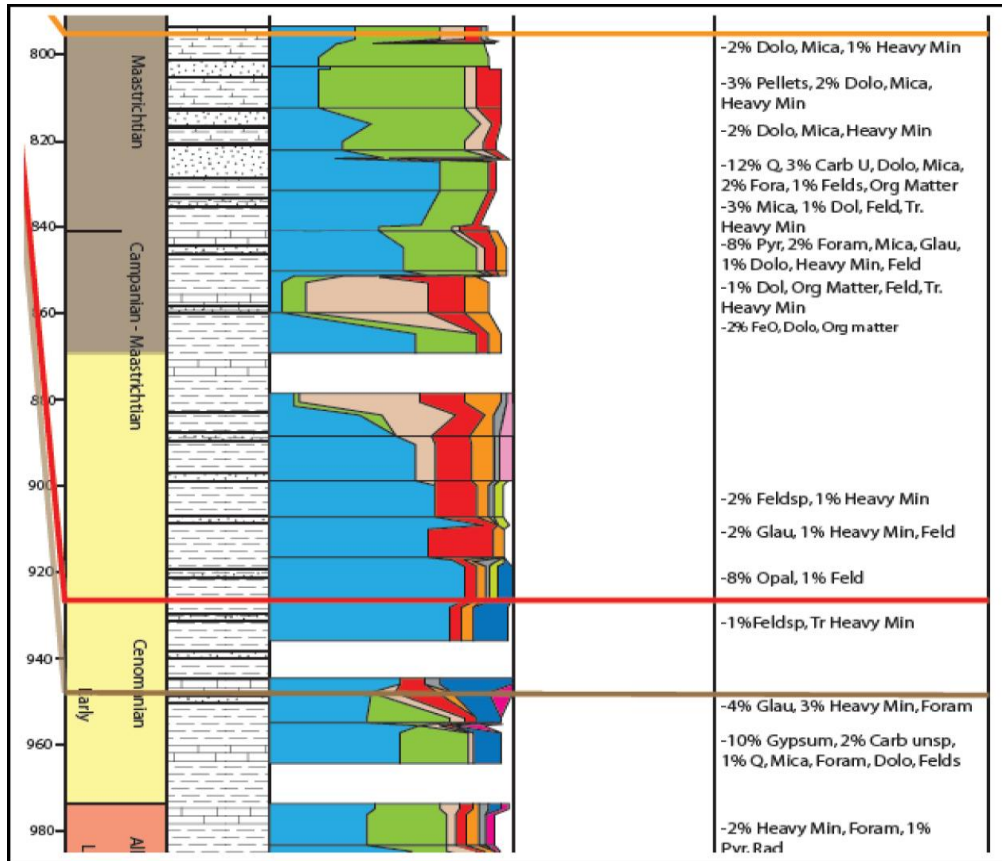


Figure 35; Combined effect in site S398 of CCD and Eustatic Sea Level shoaling CCD during Early Cenomanian – Early Campanian (Appendix D)

Another important example of this effect is S137, interpreted in subchapter water depth as the best match to the Parsons and Sclater (1977) cooling model. With a proposed depth of 2500 m during Albian and a constant subsidence away from any magmatic or tectonic anomalies, it is the perfect site in determining the point of deposition below the CCD: the point where carbonaceous sedimentation stops and clay dominated deposits progress. The termination of carbonate deposition is reached Earliest Turonian ~ 94 Ma estimated at ~ 3600 m. The composition changes to totally carbonate barren at 220 mbsf (Figure 36). The absence of carbonates infers that the CCD, during the earliest Turonian, must have been located shallower than ~3600 m which is a near to exact match to the Van Andel curve (Figure 34 and Figure 36). This result also confirms the correlation between shallowing of the CCD and rising eustatic sea levels.

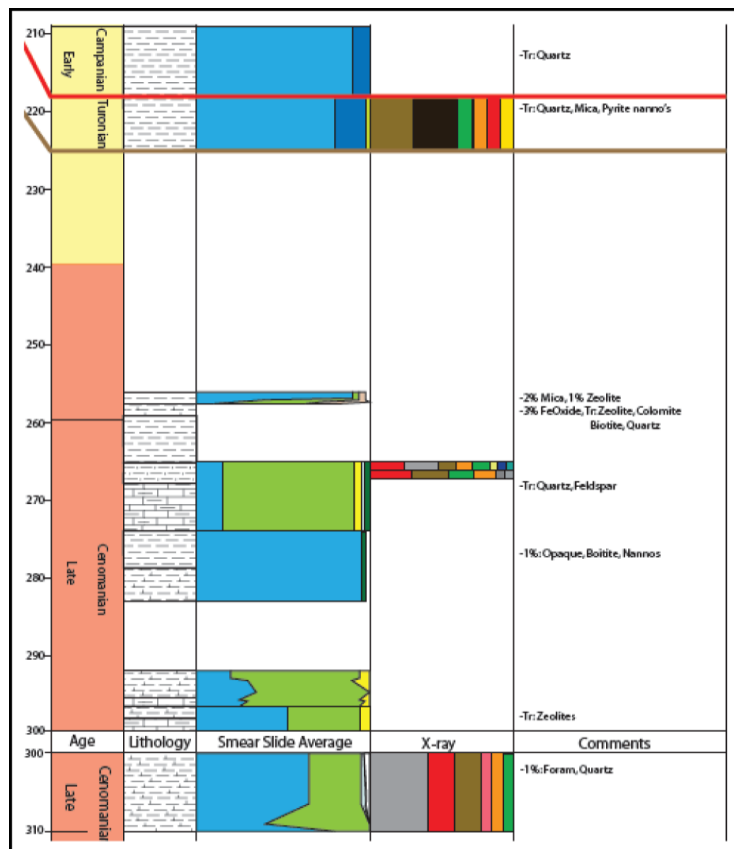


Figure 36; Site 137 linear mantle cooling in relation to shoaling CCD falling deposition of carbonaceous sediments (Appendix B)

VII. Discussion

7.1. Limitations

7.1.1. Limitations on the interpretation of core data

This subchapter will discuss limitations within the IODP data, the processing and representation of the data influencing the reliability of the results.

In the first place it needs to be pointed out that smear slide and X-ray figures are a representation of the IODP data (appendix A – G). The appendixes do not include the full IODP data set (as stated in Chapter 2, Methods). There are four factors within the IODP data that affect the

quality of results: 1) Inconsistent measurements by the IODP, 2) Smear slide density in the core, 3) Smear slide and X-ray samples do not always report 100 % of the sample, 4) X-ray diffraction studies are rare.

The first factor, results from the fact that IODP smear slide studies often sample only a specific interval in a core. Consequently smear slides do not always represent the entire stretch of a Cretaceous site; they leave gaps. The second factor, involves the measurement density of smear slides. A smear slide measurement is a measurement of 1 cm, often only one or two measurements represent a 10 meter core. In most situations this is considered a viable representation, however in cases of rapid lithological change, a lack of smear slide density will obscure essential detail and not record the lithological change. The third factor is the measurement and reporting of smear slides. In many cases 90 to 95 % of the smear slide is reported in the ODP and DSDP reports. The exact reason why in some cases the IODP reports do not record the full 100 % is unknown. The final factor is the lack of X-ray diffraction studies of the IODP cores. X-ray diffraction studies the clay mineralogy of a core. As clay mineralogy presents a record of both climate and oceanography, it would enhance the ability and precision of this study in interpreting climate and oceanography. However few sites have been studied by X-ray diffraction in the IODP reports. The problem lies in the fact that the ones that have been studied cannot be correlated to the ones that have not been X-ray sampled.

The processing of the IODP data contains one major limitation. As was stressed in the previous paragraph, smear slide and X-ray fraction measurement density is key to report strong and fast lithological change in a core. In the processing of IODP data in some situations the exact opposite occurs to the problem in the previous paragraph; very high smear slide or X-ray densities. Measurements in these cases were processed as follows (Chapter Methods): "Transferred smear slide and X-ray fractions are represented by a maximum detail of 1 measurement per 3 meter." Consequently, in extreme cases, where cores contain a higher density of data and lithological change, data is condensed. The study has chosen in these few extreme cases to summarize and record large lithological changes (e.g. S1276) to 1 measurement per 3 meter (Figure 37). The main argument is that large lithological changes need to be recorded, they might represent key climatic or oceanographic changes. Opposing this argument is the fact that sites as S1276, become very complicated to study, as the density of data becomes enormous (Figure 37).

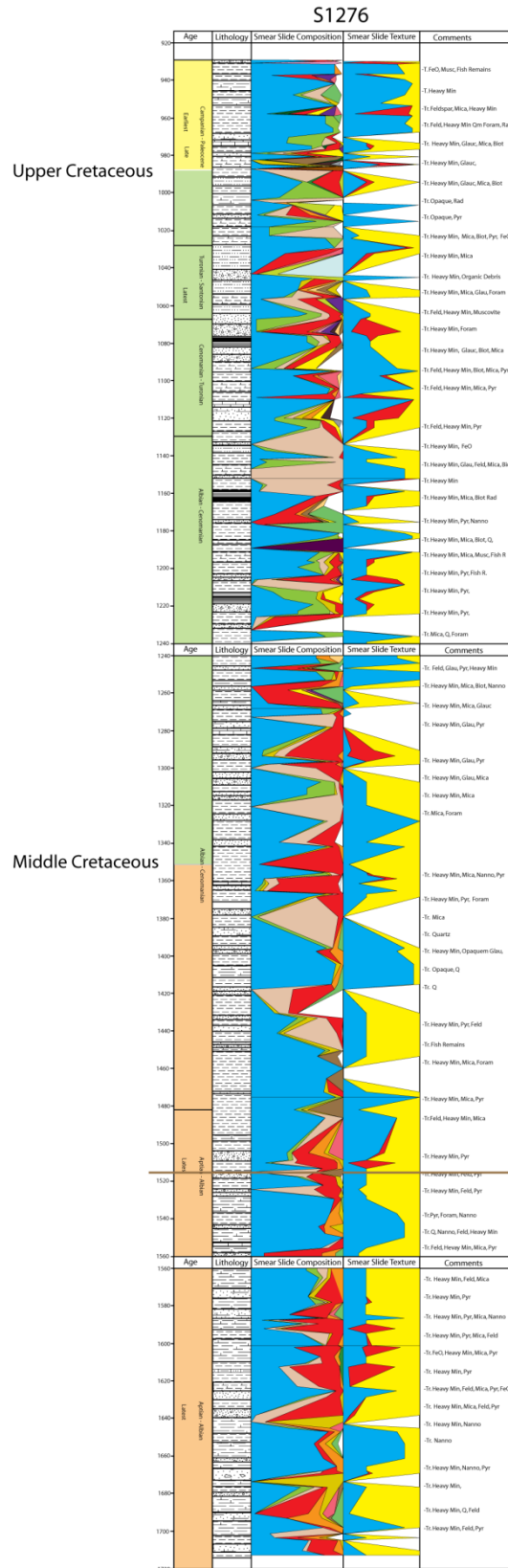


Figure 37: Complexity of high data density S1276 (Appendix D & F)

Representation of results, the thirteen IODP sites, located on the different margins of the North Atlantic, present a good Cretaceous coverage from ODP and DSDP cores (Figure 2 & 3). The excel study of all North Atlantic ODP and DSDP core, allows a grounded choice for the sites used in this

study. The choice was based on the longest possible Cretaceous succession at a specific location and the ability of the core to represent a specific part of the North Atlantic margin. The structuration into six different transects (Figure 18 – 21, Appendixes A – F) allows a systematic analyses of the different margins, western and eastern and the four different latitudinal zones. The question whether thirteen cores can give a good representation of the North Atlantic sedimentation is grounded. However time did not allow a much larger study using a larger number of cores. Studying similarities and differences between the different sites and transect allows a systematic insight in the large-scale sedimentary development of the North Atlantic Ocean. It is key to stress that in observing the sites and transects we have to pay attention to the broader scale sedimentation rather than focus on the detail also present in the data.

7.1.2. Limitations on the interpretation of OAE's

Interpretation of oceanic anoxic events is limited as this study did not study carbon and oxygen isotopes to identify OAE's. Instead the interpretation of OAE's in this study was based on: 1) chronology, 2) microfossils data (planktonic foraminifera and calcareous nannoplankton), 3) presence of pyrite and or organic matter, 4) low diversities, low abundances or even absence of benthic foraminifera (Chapter 6 Interpretation).

Since the selection of oceanic anoxic events is obscured by large terrigenous input in continental margins or absence of essential core data, OAE identification on based on the factors in the paragraph above is precarious. Especially since interpretation of OAE's in academia is interpreted with much greater precision based on carbon and oxygen isotopes. However this study did not chose the carbon and oxygen method since it was to elaborate and did not serve the large-scale interpretation purpose of this study.

7.1.3. Limitations on the interpretation of water depth

The identification and extrapolation of paleo water depth as conducted in the Chapter Interpretation is speculative. In this study three variables are used to get an indication of the water depth. In the first place the cooling model by Parsons and Sclater (1977), second the relative absence or presence of calcareous material and third agglutinated foraminifers serve as a basis to the interpretation of water depth of deposition below or just above the CCD (Figure 32 & 33).

The calculation and direct correlation of the ocean floor depth is strongly anomalous (Table 6). Tectonic changes are often difficult to scale to water depth. A second problem is the often highly uncertain age control of the time of ocean crust formation. Thirdly agglutinated foraminifers only suggest deposition below the CCD (not all, some do) and therefore only give an indication of depositional depth. Two of the three factors used to reconstruct the water depth refer to the CCD. It is important to notice that the CCD is strongly dependent on surface production, local topographic and local tectonic influences. Consequently the interpretation is relatively limited in some cases.

Sites which are considered relatively uncertain are S367, S136 and S1276 (Table 7). S367 Is hard to interpret for its strongly anomalous relation to the cooling model which probably is related to a later Tertiary event. S136 Poor control is directly related to a strongly condensed core and poor biostratigraphic control. S1276 Presence of many turbidites and debris flows makes it precarious to relate to deposition relative to the CCD and distinguish the presence of nannofossils. The current interpretation is largely based on appendix D and E and as such deviates to from the initial interpretation by Tucholke et al., (2004).

7.2 Cretaceous climate and oceanography

This subchapter will focus on the three Cretaceous periods; Lower Cretaceous, Mid Cretaceous and Upper Cretaceous. It will discuss the main sedimentary trends, characteristic events (Chapter 5 Results) and the OAE's (Chapter 6 Interpretation). These factors will be linked to climatic and oceanographic conditions prevailing in the different regions during the selected intervals

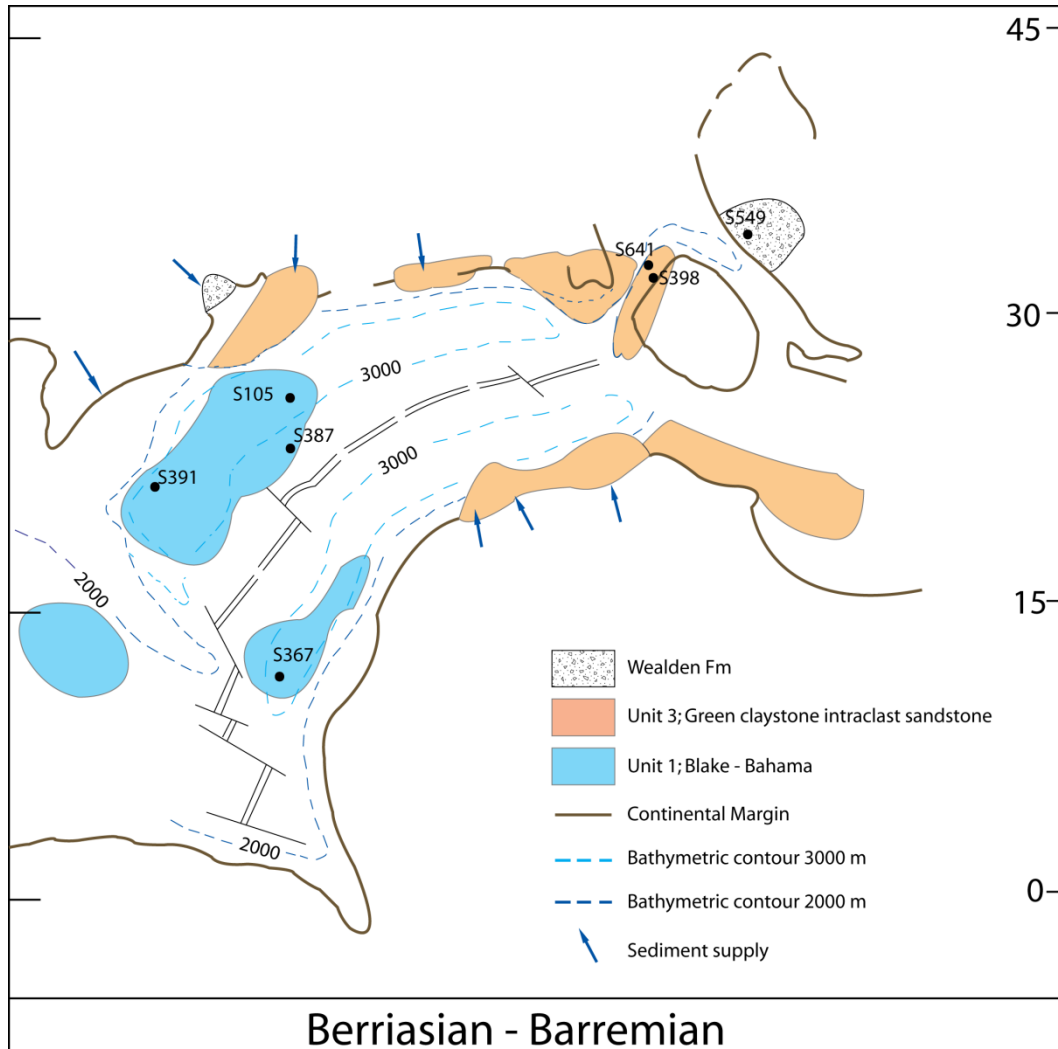


Figure 38; Berriasian – Barremian interpretation adapted from Von Rad & Sarti 1986.

7.2.1 Lower Cretaceous

Figure 38 summarizes the sedimentary interpretation of the Lower Cretaceous interval based on the units created by Jansa et al., (1979) (Figure 1). This interpretation delineates two main sedimentary provinces: 1) The Blake – Bahama formation in the southeastern and southwestern North Atlantic (Figure 11), 2) The Hatteras grayish green claystone intraclast sandstone member in the northwestern and northeastern North Atlantic (Figure 13).

The first province is characterized by the organic rich marls of the Blake – Bahama Formation. The formation is composed of strong terrigenous influxes of coarse and fine grained turbidites during the Valanginian – Lower Barremian period (S105 & S391) (Figure 1 & 11). This is in accordance with the description of Jansa et al., (1979) in the Chapter 4 (Stratigraphy). These influxes are identified as event U, W and Q in the Chapter 5 Observations (1120 – 1210 mbsf) (Figure 22 – 25). Event W (S105

and S387) is limited to the Western Atlantic (Figure 19), event W decreases in size from S391 to S387, suggesting that the origin of the sediment must have come from S391 (Figure 25). This is underlined by strong quartz excursions in S391 pointing to a siliciclastic source in the proximity of S391. Event W is interpreted as a turbidite, Sheridan et al., (1977) also claimed Bouma sequences during the same period and claim they are sourced by the North America continental shelf (Figure 9). This study confirms these sporadic influxes of terrigenous sediments during the Earliest Cretaceous, the North American continental shelf is considered the source for these terrigenous sediments (Figure 18).

Figure 39 shows that the western North Atlantic composition is characterized by large smectite fractions. In comparison, the eastern North Atlantic is composed of calcite in the south, kaolinite throughout the northern margins and only a minor presence of smectite (Figure 39). The strong abundance of smectite, absence of kaolinite and other terrigenous materials points to low sedimentation rates in the western North Atlantic. Consequently the smectite of the western Atlantic is believed to have formed by transformation and recrystallization of detrital materials (Thiry and Jacquin 1993).

The second Lower Cretaceous province, northern North Atlantic (Unit 3; S549, S641 and to lesser extent S398), is characterized by a strong siliciclastic input (Figure 21). The author in accordance with Jansa et al., (1979) believes that the composition of siltstone, sandstone, sapropel and conglomerate are related to reworked shelf slope sediments. The Iberian shelf siliciclastics are linked to the onshore Wealden formations. The terrigenous Wealden formation formed on the European and Iberian craton the formation consisted of red fluvial sediments related to rifting (Pinheiro et al., 1996) (Chapter 4 Stratigraphy).

The Hatteras green claystone intraclast sandstone member has been extrapolated to the North Moroccan margin (S370) (Figure 1 & 13). This link is based on the observation of kaolinite and palygorskite in site S370 by Von Rad & Sarti (1986) and a strong similarity of the mineral composition described by Thiry and Jacquin (1991) (Figure 39), mineral composition of S370 is similar to site S398 and S549 Figure 39. Another extrapolation are the Iberian proximal margin (S398) and S1276 of the Grand Banks continental margin. Both locations contain a high concentration of turbidites with similar compositions (Appendix D & E). The high turbidite concentration points to a high terrigenous supply (Wealden clastics) whilst the similar composition points to a similar type of weathering (climate). A third argument is the proximity of the two location to each other, since the opening of Grand Banks – Iberia is placed during Mid Cretaceous Early Aptian (Chapter 3, Geological Setting), the two margin lie adjacent to each other (Figure 5).

Hallam (1984) linked the presence of plant debris (S641) and pyrite (S398 and S1276) in the northern North Atlantic to a warm climate and continental humidity (Figure 21). Other evidence for warm climate and continental humidity is the paleotropical location and the presence of kaolinite (S370, S398 & S549, Figure 39). Consequently the northern North Atlantic climate is interpreted as warm and humid.

Climatic conditions were very different in the southern part of the North Atlantic Ocean. As stated earlier the smectite underlines a slow deposition, and the absence of kaolinite points to a non humid climate in the western North Atlantic margin. The fact that the southwestern North Atlantic contains a much lower concentration of turbidites is another argument for a non humid climate. Since non humid climate would have produced and transported less terrigenous material. Other

factors contributing to the western Atlantic deposition are the high eustatic sea level (Haq et al., 1987, Figure 34), flooding the shelf and acting as a sediment trap to the abyssal plain (Chapter Stratigraphy).

The dominance of illite, illite – smectite and chlorite illustrated by figure 39, during the Early Cretaceous, is related to the progressive spreading of the North Atlantic margins. Figure 39 observes a systematic decrease of these three minerals in the deep sea cores with time, highest concentrations are generally found at site in proximity of the spreading ridge. Deposition and formation of these minerals is related to the contribution of volcanoclastics and proximity to the sea-floor spreading axis. Consequently occurrences diminish as sites are drawn away from these sources as is clearly pointed by the lowest composition in the Cenomanian (Thiry and Jacquin 1993).

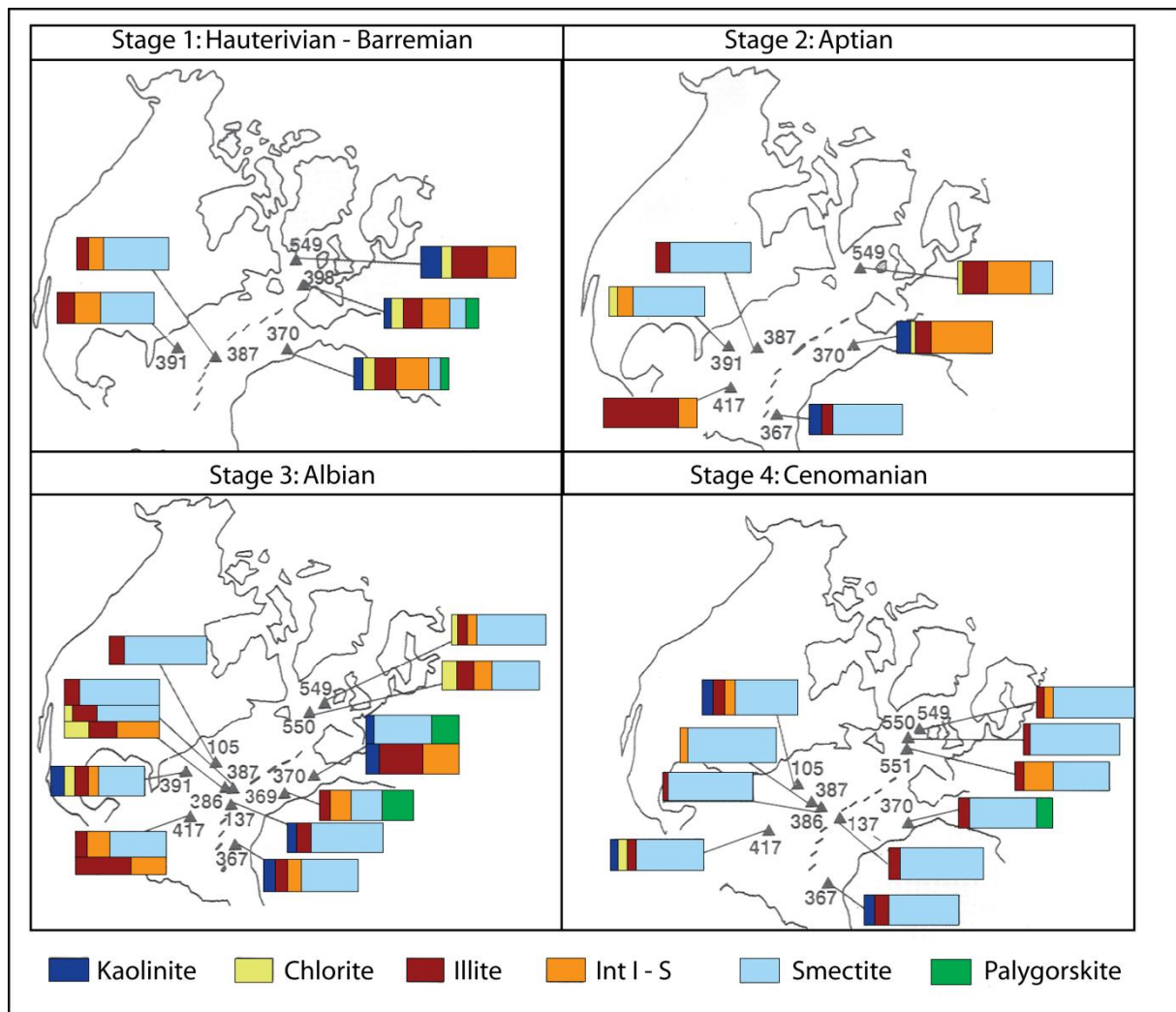


Figure 39; Mineral interpretation adapted from Thiry & Jacquin 1993.

7.2.2. Mid Cretaceous

The Mid Cretaceous (Aptian – Turonian) discussion is separated into three different intervals; 1) Aptian, 2) Albian, 3) Cenomanian – Turonian. The Mid Cretaceous contains five sedimentary units (Chapter 4 Stratigraphy): 1) The Hatteras black bituminous shale unit (Figure 12), 2) The Hatteras grayish green claystone member (Figure 13), 3) The Hatteras greenish claystone member (Figure 14), 4) Plantagenet zeolitic clay unit (Figure 15), 5) Cresnet Peak member (nannofossils marl) (Figure 16).

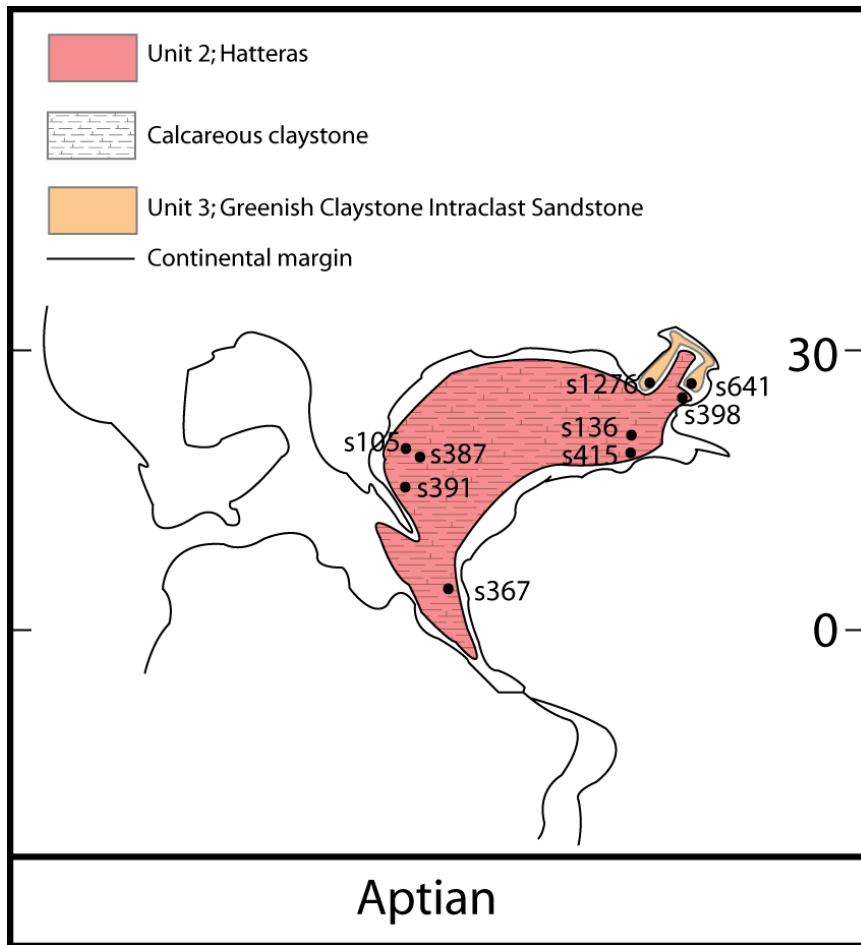


Figure 40; Aptian interpretation adapted from Li et al., (2008)

Earliest Mid Cretaceous: Aptian

The Aptian interval is characterized by deposition of the Hatteras black bituminous shale unit (Figure 12). Deposition of this formation took place in the western and southeastern North Atlantic and is characterized by an increasing clay fraction towards the Late Aptian. Clay deposition dominated throughout the Aptian North Atlantic the Cape Verde site was prone to a very strong calcareous deposition (90 %) in Early Aptian (Figure 17). The Aptian is characterized by a eustatic sea level rise (Haq et al., 1987) and shoaling CCD (Figure 34) (Van Andel 1977), these two have been related to the heating of the Cretaceous climate into the Upper Cretaceous (Aptian – Cenomanian) (Donnadieu et al., 2008). The Early to Late Aptian increasing clay fraction and shoaling CCD are related a biogenic crises (Burla et al., 2008) (Figure 34). The cause for this large perturbation of the carbonate cycle has been related to the Late Barremian – Late Aptian enhanced volcanism of the Ontong Java Plateau and Kerguelen Plateau (Larson & Erba 1999). Enhanced volcanism is related to a higher oceanic pCO_2 levels, which led to a stronger dissolution of $CaCO_3$ (shoaling of the CCD) as well as a carbonate growth crisis. The effect of the increased pCO_2 levels and carbonate growth crisis, is a decrease of oceanic carbonate precipitation, as we observe in the Aptian deposition of the Hatteras shale unit.

The chapter observations shows that the southern North American offshore Hatteras unit is comprised of clay with a background signal of mica, quartz and heavy minerals. Figure 38 by Thiry and Jacquin (1991) shows an increasing smectite and increasing chlorite fraction. Increased smectite,

chlorite and volcanic glass (S387), MgO (S105) and background signal are related to volcanic deposits identified by Lancelot et al., (1972) and Thiry & Jacquin (1993). This is in line with the observation made in the previous subchapter, relating the occurrence of chlorite to a volcanogenic origin, the increased smectite fraction is related to low sedimentation rates.

The northern North Atlantic is dominated by terrigenous supply (S641, S549, S391 and S1276) (Figure 3); with large quartz, mica excursions (S641) as well illite and illite – smectite rich X-ray fractions (S549) (Figure 21). This dominant terrigenous supply to the deep ocean is related to the still narrow and elongated nature of the northern North Atlantic (Figure 40). Increased illite and illite – smectite are related to the Early Aptian break-up of the northernmost Atlantic and the related volcanogenic mineral production. Chapter 5 Observations and Tucholke et al., (2004) show a strong continued similarity between the Grand Banks on the western margin and Iberian margin on the eastern margin during the early Cretaceous (Figure 21 & 40). Aptian – Turonian deposits in the Iberian margin (S398) are comprised of clay with major siderite incursions related to a sulphate reduction in an iron rich environment (S641 and S391) (Figure 21). Whilst the western margin (S1276) is comprised of clay with strong allochthonous excursion. The similarity between the Grand Banks and Iberia is found in the turbidites consisting of siliciclastics and contemporaneous pelagic carbonate (Appendix D) (Tucholke et al., 2004) (Figure 21). Tucholke et al., (2004) stated; “The overall patterns of changing sedimentation rates at Site 1276 are strikingly similar to that of DSDP Site 398 on the conjugate margin of the Iberia Peninsula.” Since the break up between Iberia and Grand Banks commenced during Early Aptian (114 - 125 Ma) (Blakey 2007, Wilson et al., 1989, Boillot et al., 1989, Pinheiro et al., 1996), the northernmost North Atlantic still contained a narrow elongated shape (Figure 40). Therefore oceanographic and climatic conditions would have been similar on both sides of the basin, underlined by the similar patterns of changing sedimentation.

The terrigenous turbidite character of the northernmost North Atlantic differentiates from the biogenic dominated turbidites / mass flows of the south western North Atlantic (Figure 18 – 21). The difference can be related to the still narrow Atlantic Ocean in the North and the much wider Ocean to the south as well as the character of margin sedimentation (Figure 40). The width of the basin allows turbidites to transport terrigenous material to the deep ocean floor in a narrow basin setting, whilst in a wide basin terrigenous sediment would have already been settled before reaching the deep ocean. However this is strongly dependent on the character of the sedimentation of the margins. The northernmost margins are characterised by terrigenous sediment (Chapter 4 Stratigraphy) and produce terrigenous comprised turbidites (Figure 40). Similarly the character of the sites on the US continental margin underlines that the south western North Atlantic continental margin is characterized by carbonate production (Chapter 4 Stratigraphy) (Figure 18 – 21, Appendix B, C, D, E).

The Moroccan margin is comprised of a continued supply of kaolinite in sites S370 and S367 of the West African continental margin (Figure 17). The continued rise of the eustatic sea level (Haq et al., 1977) is related to the decreased terrigenous input (Figure 34). Humid conditions still prevailed on the continental margin related to the maintained kaolinite supply Figure 39 (Thiry and Jacquin 1993, Hallam 1984).

The other important observation of the Aptian is OAE1a which was only retrieved in sites S391, S398 and S105 Figure 30. OAE1a is the least studied OAE of the three and its triggering mechanisms

are not well constrained. However the relation of this first oceanic anoxic event to the onset of the northern most rifting of the Atlantic (Grand Banks and Iberia) and start of the Mid Cretaceous greenhouse, is speculated to be related to the occurrence of the first OAE (Li et al., 2008). It is key to acknowledge that the Mid Cretaceous warming and the related eustatic sea level rise and shoaling CCD set the stage for an entirely different sedimentary setting then the Early Cretaceous Blake Bahama unit (Figure 34).

The main elements characterizing the Aptian are firstly the change from the Blake Bahama carbonates to Hatteras black bituminous shale with a strong calcareous fraction in the southern North Atlantic (Figure 38 & 40). This change was correlated to the eustatic sea level rise and shoaling CCD. Secondly the northern North Atlantic still narrow and elongated remains dominated by a strong terrigenous supply. Climate in the Aptian was hot and humid in the south eastern North Atlantic.

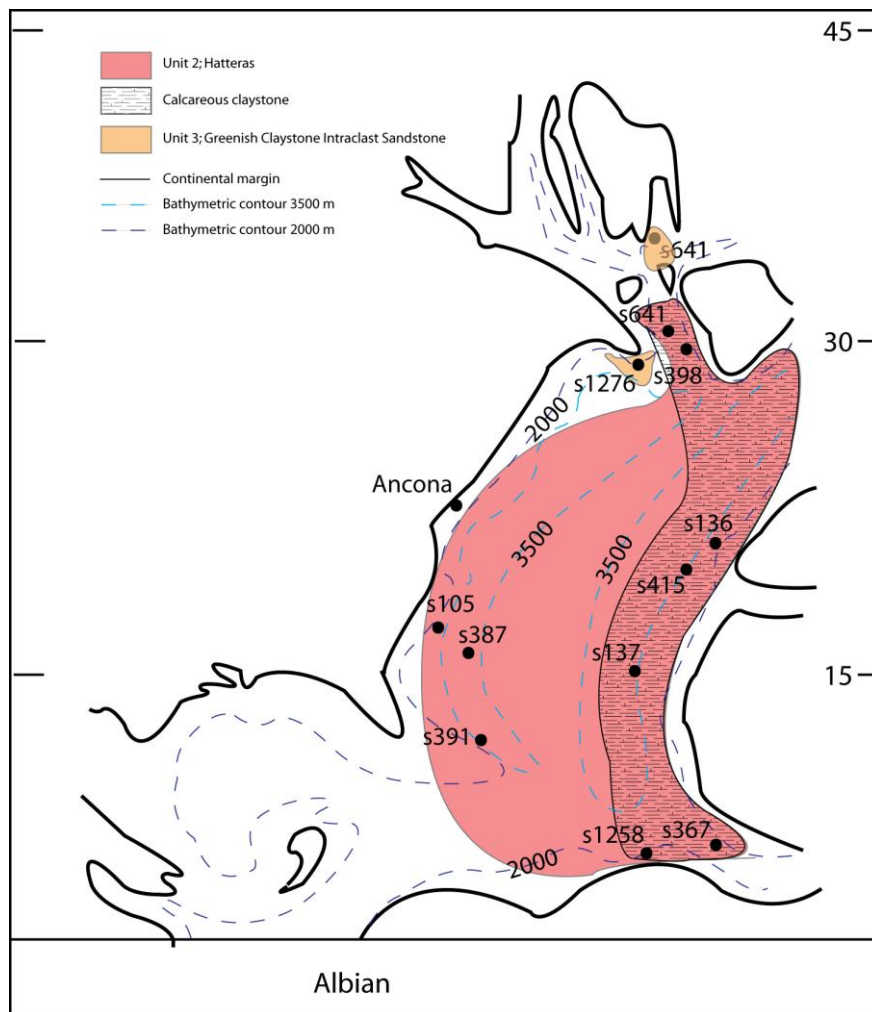


Figure 41; Albian (~115 Ma) interpretation adapted from Blackey 2007

Mid Cretaceous: Albian

During the Albian southwestern North Atlantic was prone to deposition of the Hatteras black bituminous shale unit (Figure 41), which is characterized by strong clay deposition (S391, S105 and S387) with a constant sedimentation of quartz, mica and siderite (S391). S391 Is contains turbidite incursions of terrigenous origin. In the northernmost western North Atlantic margin Hatteras black

bituminous shale is also deposited, clay deposition of this site is frequently interrupted by turbidites (Figure 21). Carbonate input in this site increases towards the Cenomanian, the increase has been related to a higher carbonate production as will be discussed later.

The eastern North Atlantic Iberian margin (30 - 37° N (Sclater et al., 1977)) is comprised of the Hatteras black bituminous shale unit with strong siderite incursions and a characterizing increased carbonate input during Late Albian (Chapter 5 Interpretation) (Figure 20 & 41). The Moroccan, Demerara and Cape Verde margins (15 – 30° N (Sclater et al., 1977)) are imposed to a strong biogenic sedimentation of dolomite and nannofossils, these three margins behave asymmetrically from the Iberian margin and the western North Atlantic (Figure 17 – 20 & 41). The large siliciclastic composition of the northernmost part of the North Atlantic (S549) was interpreted as green claystone intraclast sandstone member (Figure 21 & 41).

From the previous two recaps of the Chapter 5 Results and Chapter 6 Interpretations we can delineate three main types of deposition for the Albian: 1) Hatteras black bituminous shale (western North Atlantic and Iberia) (Figure 12 & 41), 2) Hatteras black bituminous shale prone to strong biogenic sedimentation (Moroccan, Demerara and Cape Verde margins) (Figure 41), 3) Green claystone intraclast sandstone (Goban Spur) (Figure 13 & 41). Deposition of the Hatteras shale is considered a consequence of the Early to Late Albian sea level rise, up to 100 m (Haq et al., 1987), and even stronger (+/- 200 m) shoaling of the CCD (Van Andel 1977) (Figure 34). These two effects have been related to heating of the Cretaceous climate from the Aptian – Cenomanian (Donnadieu et al., 2008), this heating is not a directly proven but is widely attributed to high levels of atmospheric greenhouse gases (Wilson and Norris 2001).

The Albian mineralogy is characterized by large-scale smectite deposition throughout the North Atlantic (Figure 39). The strong presence of illite and illite – smectite in the western North Atlantic, is related to the close proximity of the mid ocean ridge and the supply of volcanogenic material. Other characteristics of the Albian interval is kaolinite deposition in the Moroccan North Atlantic margin and S391 on the western North Atlantic margin (Figure 17). The continued presence of kaolinite in the southeastern North Atlantic points to a continuation of the warm humid climate of the Early Cretaceous and Aptian (Figure 39).

However presence of palygorskite in Figure 39 on the eastern North Atlantic margin points to semi-arid condition. Pletsch et al., (1996) pointed out that the lower Albian West African margin contains onshore evaporite deposition and interpret the Lower Albian as semi – arid (Hofmann et al., 2008). Palygorskite in perimarine environments is seen as an indicator of semi arid or seasonally arid environments (Singer and Galan 1984). Following the insight by both Thiry & Jacquin (1993) and Pletsch et al., (1996) palygorskite in Albian – Cenomanian/Turonian sediments, is interpreted to be transported by mass flow brines to deep marine sediments. Palygorskite mainly was formed through coastal evaporation in North Africa (Figure 6). No palygorskite was deposited in the Western North Atlantic since conditions were adverse; rapid sedimentation and no large restricted coastal basins (Chamley & Debrabant 1984). It seems that the presence of both kaolinite and palygorskite in one site during the same contradict each other, however the detail on the Albian interval presented by Thiry & Jacquin (1993) is insufficient. Hofmann et al., (2008) interpret the Late Albian as humid and warm whilst the Early Cretaceous is interpreted as semi-arid for the West African margin, as interpreted by Thiry and Jacquin (1993) who leap the whole period together. This study proves both

hypothesis but feels that a definite conclusion on the palygorskite issue needs further study, the humid warm climate is accepted based on the widely spread kaolinite deposition.

The largest OAE of the Albian, OAE1b Figure 30a is clearly much stronger expressed than the Aptian OAE1a (Figure 30), OAE1b is retrieved throughout the entire western North Atlantic, Iberia, Cape Verde and Demerara Rise (Figure 4). The OAE1b is similarly to OAE1a deposited during a eustatic sea level rise (Figure 34). The specific changes in the mineralogical composition during this event (quartz and clay) resulted from major-element chemistry and reflect cyclic climatic changes (Hofmann et al., 2001). Erbacher et al., (1996) interpreted the change in mineralogy to result from leaching of nutrients from coastal lowlands. Leaching led to increased fertilization and a productivity rise in the ocean, resulting in increased preservation of marine organic matter. The shift in mineralogy can be observed in the OAE's reported in Figure 17 – 21 (Appendix A – F). Hofmann et al., (2001) relates the OAE1b changes to North African climate change and the eustatic sea level rise flooding the coastal region of the US continental margin (Figure 40 & 41). North African climate change is retrieved in the change from Aptian clay deposition to the Albian biogenic influence. Other evidence for the Hofmann theory is the supply of kaolinite in both the West African and western Atlantic, supporting his thoughts on nutrients transport from the continental margin to the deep sea (Figure 17, 18 & 39).

The observed asymmetry between the western (dominantly clay) and eastern margin (Moroccan, Demerara and Cape Verde contain a strong carbonate fraction) was also reported by Holbourn et al., (2001) (Figure 17, 18 & 41). The enhanced carbonate preservation of the eastern margins can be explained by an increased production. Increased production can be the result of: 1) increased fertilization from the supply of nutrients from the continent 2) increased fertilization due to upwelling. The presence of kaolinite throughout the entire West African margin increases the likelihood of the first option. Holbourn et al., (2001) study of benthic foraminifers points to coastal upwelling, the author thinks that a combination of the two seems the most likely.

As such the main element characterizing the Albian is the change to a carbonate barren Hatteras Formation in the western North Atlantic. The author assumes that this is caused by the continued eustatic sea level rise and shoaling on the CCD. The asymmetry of the continued deposition of carbonaceous mudstone on the eastern margin carbon is claimed to be the consequence of increased fertilization on the eastern margin (related to a warm humid climate) and the subsequent increased carbonate production.

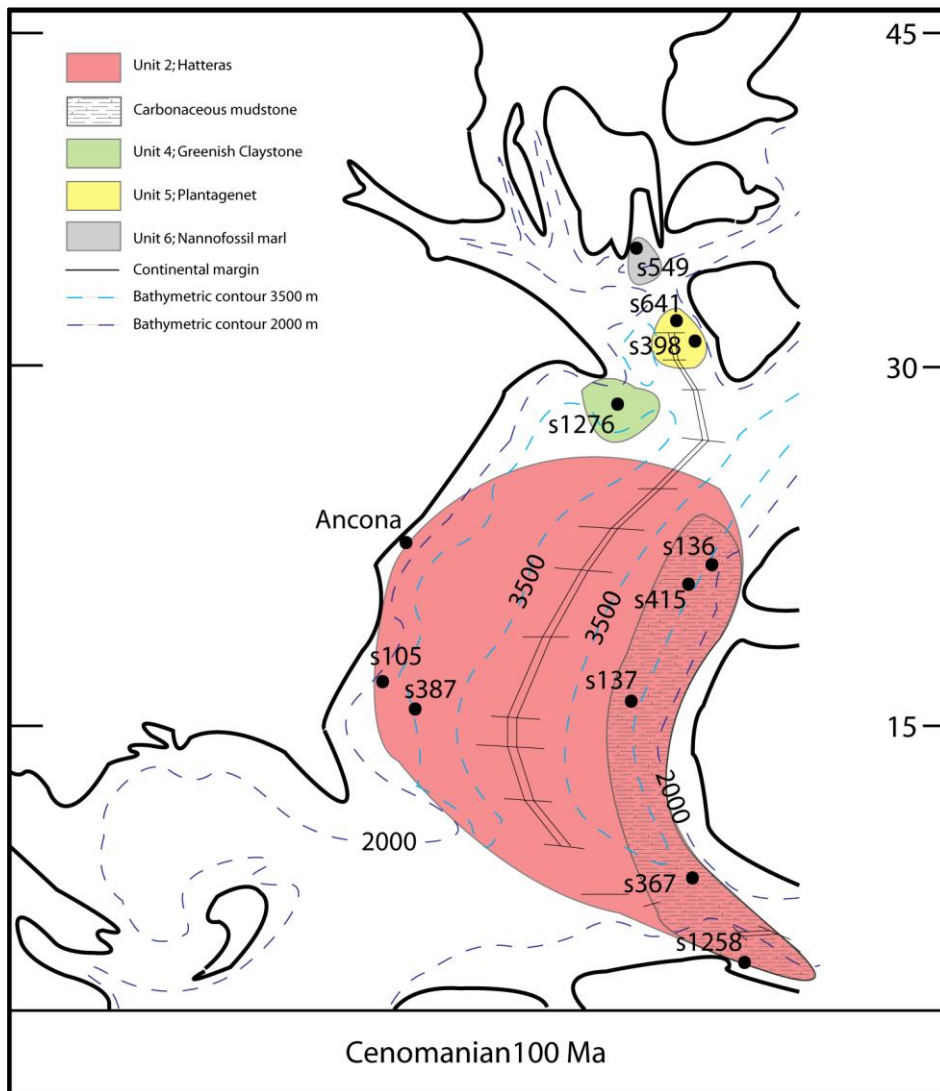


Figure 42; Cenomanian interpretation adapted from Blackey 2007

Latest Mid Cretaceous; Cenomanian – Turonian

Figure 43 summarizes the sedimentary interpretation of the Cenomanian – Turonian interval based on the units created by Jansa et al., (1979). This interval is characterized by four different stratigraphic units: 1) Hatteras bituminous shale unit (Figure 12), 2) Greenish claystone intraclast sandstone member (Figure 13), 3) Plantagenet varicolored zeolitic clay unit (Figure 14), 4) Nannofossil marl member (Figure 15).

The western Atlantic North American margin is comprised of a continued deposition of the Hatteras black bituminous shale unit (Figure 17 – 20 & 43). Similar to the late Albian organic matter and radiolarian fractions continued to rise during the Cenomanian in S387 (Chapter Results). The northwestern North Atlantic Grand Banks, is characterized by deposition of the greenish claystone intraclast sandstone, based on the high portion of siliciclastic material (Chapter Results) (Figure 21 & 43).

The eastern North Atlantic Iberian margin is also prone to deposition of the Hatteras bituminous shale unit (Figure 21 & 43). Similar to the western North Atlantic the Hatteras black bituminous shale

unit contains an increasing biogenic fraction (Chapter Results, S398) (Figure 21). The lithologically diverse Cenomanian Moroccan margin contains two types of Hatteras shale, most sites are dominated by the Hatteras black bituminous shale unit, two exceptions are sites S137 and S1258 which contain a very high carbonate fraction (Figure 17 & 18). During the Turonian sites S137, S367 and Demerara Rise change to the pure zeolitic clay Plantagenet unit (Chapter 5 Observations) (Figure 44).

The primary cause for the complex Cenomanian – Turonian sedimentation is the intricate sedimentary reaction to the CCD, eustatic sea level rise, oceanography and climate, the following paragraphs delineate and explain these different factors.

The Cenomanian is opposed to the last strong eustatic sea level rise up to the Turonian high stand (Figure 34). Lack of a dominant Cenomanian lithology (carbonate or clay) in the different margins (Table 4, Figure 43) suggests that the sedimentary character is strongly determined by the water depth in relation to CCD and eustatic sea level. Different from the strong Albian clay distribution, the stronger Cenomanian carbonate supply under a eustatic sea level rise and shoaling CCD (Van Andel 1978, Figure 34) suggests: 1) Increased production leading to increased burial or 2) Increased preservation e.g. euxinic conditions. Sites located below the CCD were prone to clay deposition this has in detail been described in the Chapter 6 Interpretation.

The Cenomanian organic matter and pyrite excursions surrounding the OAE2 are stronger expressed than the excursions bounding OAE1a and OAE1b (Figure 17 – 21, 30, 30a & 31). The mechanisms responsible for strong organic carbon sedimentation were defined by Stein et al., (1989) as: 1) Terrigenous organic matter supply, 2) Increased paleoproductivity, 3) Preservation due to anoxic marine environments and 4) Preservation due to rapid burial (Stein et al., 1989). The mechanisms described above are under intense debate over the past four decades since Schlanger and Jenkyns (1976). It is not the intent of this research to collaborate on the complicated mechanisms of OAE formation and identify the different situations in the specific locations. The aim of this study is to link large scale lithology and mineralogy to the North Atlantic climate and paleoceanography. The general interpretation for the cause of the southeastern North Atlantic increased deposition was increased production (upwelling) (Kuypers et al., 2002), the western North Atlantic margin is generally related to increased preservation (Kuypers et al., 2002).

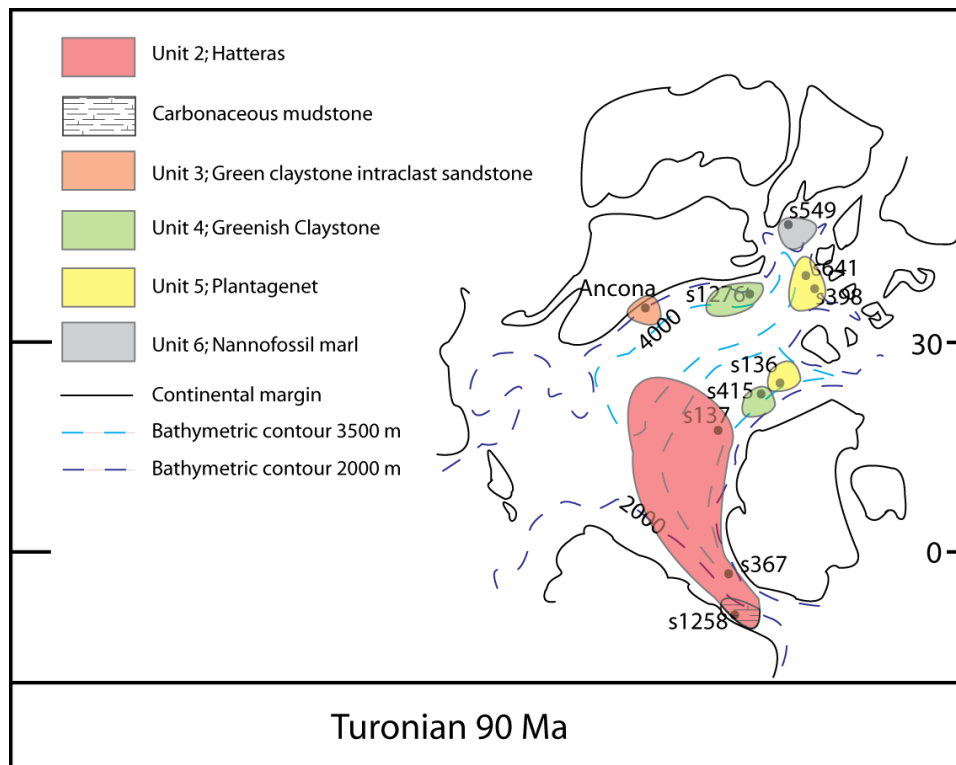


Figure 43; Late Turonian interpretation adapted from Blackey 2007

The Cenomanian in the northern S398 and S1276 exhibits an increase in the turbidites (S1276 from 1380 – 1080 msbf and S398 880 – 849 mbsf) (Figure 21). Tucholke et al., (2004) relates this to an increased continental weathering related to stronger humid conditions in the Grand Banks region. Humid conditions are underlined and extrapolated, by an increased kaolinite fraction in S105 and S417 (Figure 27), to the entire US eastern continental terrain. Climate on the eastern margin was less humid related to absence of kaolinite and less terrigenous supply to the deep sea.

The main factors determining the depositional character of the Cenomanian – Turonian period are the eustatic sea level rise and the warm Mid Cretaceous climate (Figure 34). Sea surface temperatures were interpreted by Norris et al., (2001) based on the benthic and planktonic $\delta^{18}\text{O}$ isotopes. For the Middle Cretaceous (Albian – Cenomanian) middle bathyal water temperatures were determined at 20°C. The Middle Cretaceous climatic optimum coincides with the absolute sea level high, base Turonian Figure 21 (Haq et al., 1987), and high middle bathyal water temperatures coincide with the wide deposition of black shales. In subchapter 6.3.1. a correlation was proposed between the rising eustatic sea level and a strongly decreased terrigenous influence to the deep sea. This is applicable to the eastern North Atlantic reduced terrigenous influence, the high carbonaceous and organic production are correlated to upwelling (Figure 43 & 44). However on the western North Atlantic an increased terrigenous input was reported (Figure 17 – 21). The increasing carbonate fraction during the Cenomanian are therefore also related to an increased eutrophication.

The last important difference noted in Chapter 5 Observations is the difference in character between the western North Atlantic margin (including the Iberian margin) and the eastern margin during the Cenomanian – Late Turonian (Figure 43 & 44). In the Figures 17 – 20 (Appendix A, B, C) a strong change was observed in the southeastern North Atlantic sites; the carbonate Cenomanian changed to a dominant clay composition during the Late Turonian (Table 4, Figure 44). This is

correlated to the abrupt ending of the Cenomanian – Turonian black shale event, which is related by Norris et al., (2001) to deep water ventilation by the opening of the Southern Atlantic (Figure 44). This ventilation was probably also related to the cooling commencing in Coniacian reaching its maximum during mid-Maastrichtian. The changed oceanography had an especially profound effect of the eastern margin where the sedimentation changed from carbonaceous mudstone to zeolitic clay (carbonate barren) by the Late Turonian (Figure 43 & 44).

The main element characterizing the Cenomanian – Early Turonian is the increased carbonaceous fraction of the Hatteras shale unit in the southern North Atlantic (Figure 17, 18 & 19). The increased production was interpreted by the author as increased production in the southeastern margin and to increased preservation in the western North Atlantic, which compensate the effects of the eustatic sea level rise and shoaling CCD on carbonate deposition. Western production was aided by the increased nutrient supply from the warm and humid continental margin.

The Late Turonian sedimentary change from the carbonaceous Hatteras Unit to zeolitic clays of the Plantagenet Formation and Greenish Claystone Unit is interpreted as a consequence of changed oceanography. The change from a stagnant basin to a ventilated basin due to the opening of the South Atlantic is thought to be the cause of the sedimentary change.

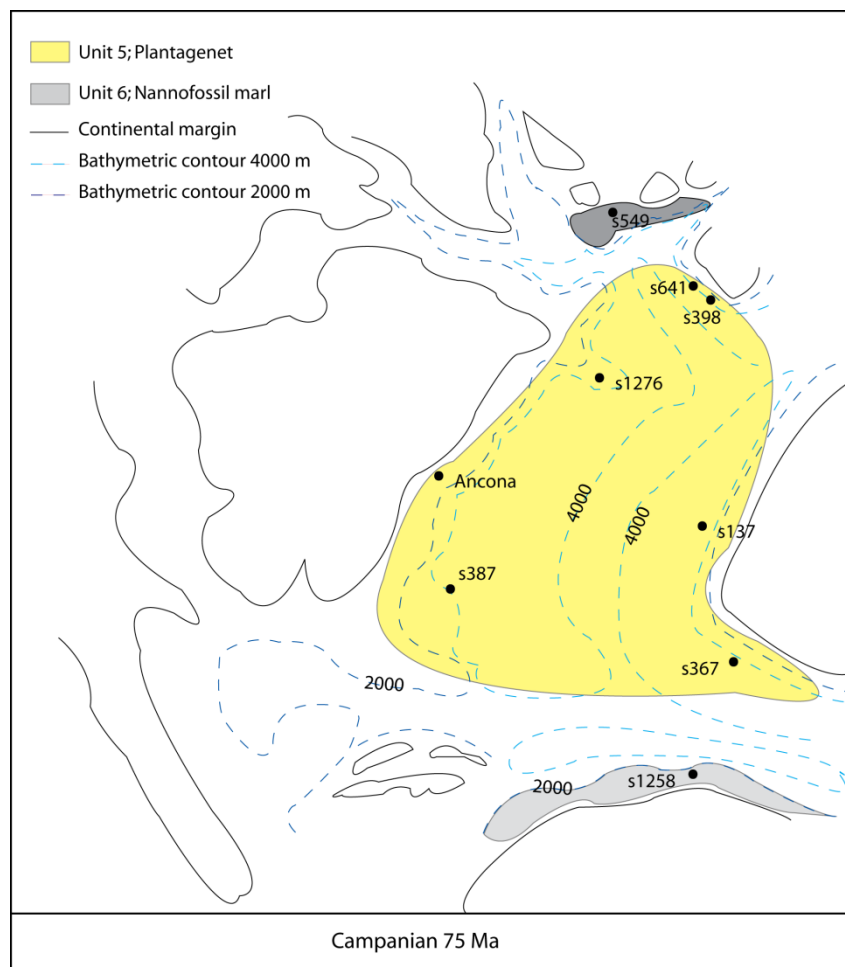


Figure 44; Campanian interpretation adapted from Blackey 2007

7.2.3. Upper Cretaceous

The Upper Cretaceous (Turonian – Maastrichtian) is characterized by deposition of: 1) Hatteras greenish claystone member (Figure 14), 2) Plantagenet varicolored zeolitic clay unit (Figure 15), 3) Crescent Peaks Member (nannofossil marl) (Figure 16).

The eastern North American margin is characterized by deposition of the Plantagenet Formation succeeded by the Crescent Peaks member (Figure 44). The proximal part of the US offshore region is undergoing increased deposition of terrigenous sediments (Figure 18 – 20 & 45). Similarly the Grand Banks is comprised of an increased supply of carbonate material and turbidites (Figure 21).

Different from the western North Atlantic the Moroccan and Iberian margins (S641) are dominated by zeolitic clay with carbonate excursions (Figure 19, 20 & 44). During Maastrichtian the proximal Iberian margin is prone to nannofossil marl deposition (Figure 19 & 20). The southernmost North Atlantic Demerara Rise is characterized by a large continuous supply of nannofossils (Figure 17 & 45). The Moroccan margin is the only margin studied by X-ray diffraction, for the Late Cretaceous it consists of large portions of montmorillonite, palygorskite as well as mica and quartz (Figure 18). The high portion of palygorskite is also described by Singer and Galán (1984) and was interpreted to be of a oceanic origin (Appendix G).

The Latest Cretaceous Coniacian – Maastrichtian is subject to a falling eustatic sea level, cooling Cretaceous climate (Santonian – Maastrichtian) and a deepening of the CCD (Figure 34) (Norris et al., 2004, Haq et al., 1987, Van Andel 1987). In the Western Atlantic the formation is strongly enriched in heavy metals, sphalerite, pyrite, goethite, hematite and zeolites (Sheridan et al., 1977), in some cases these are attributed to a volcanic origin (Figure 17 – 20) (Jansa et al., 1978). The Grand Banks and the Iberian margin are interpreted as slow sedimentation in an oxygenated basin during latest Cretaceous (Turonian – Latest Santonian and Campanian – Latest Maastrichtian). Nannofossil marl deposition is widespread in the northern and western North Atlantic sites during the Santonian – Maastrichtian S549, S398, S387 and S1258 (Figure Figure 17, 18 & 21). The strong carbonate deposition during the Latest Cretaceous is probably caused by a deeper CCD and increased carbonate production in the northern North Atlantic.

The eastern North Atlantic behaves totally asymmetrical to its western and northern counterparts. The large-scale deposition of clay during the Upper Cretaceous is caused by two main events: 1) Open circulation causing a stronger dissolution of carbonate (colder bottom waters increase dissolution), 2) Climate induced environmental stress lead to adverse carbonate precipitation conditions. The first factor is strongly contributed by the opening of a deep water connection between the Northern and Southern Atlantic placed at 80 Ma, as well the contribution of a deep water spillway between Iberia and Africa at 95 Ma (Latest Campanian) (Sclater et al., 1977). It is important to note that after the Aptian the similarity between the western North Atlantic and eastern North Atlantic disappeared. This is largely the consequence of different oceanic conditions and circulation patterns as well as different continental conditions. Scarcity of turbidites in the eastern margin points to less sediment transported to the margin this is probably related to the colder climate and decreased nutrient supply in the southeastern North Atlantic.

VIII. Conclusions

The investigation of IODP smear slide, X-Ray and grainsize analyses led to the following conclusions on the climatic and oceanographic development of the North Atlantic Basin.

1) The Lower Cretaceous was characterized by organic rich marls in the southern North Atlantic and a strongly siliciclastic northern North Atlantic. The strongly carbonaceous western margin was prone to low sedimentation rates while the still narrow elongated northern North Atlantic was influenced by strong siliciclastic turbidite input under a warm and humid climate.

2) Bituminous clay was deposited in southwestern North Atlantic during the Aptian, southeastern deposits contained a large carbonate fraction, the northern North Atlantic remained dominantly siliciclastic. The change from the Lower Cretaceous marls to Aptian bituminous clay was caused by biogenic crises related to heating climate, eustatic sea level rise and shoaling CCD. This worldwide change resulted from large production of oceanic crust and volcanic activity. The strong climatic and oceanographic changes led to OAE's (Aptian – Turonian), from the Aptian onward the western and southeastern margins behave asymmetrically.

3) The Albian was prone to black shale deposition and OAE's are recognized throughout the entire western and northern North Atlantic. The southeastern margin was influenced by carbonate deposition. The continued warming climate, eustatic sea level rise and shoaling CCD were responsible for the continued shale deposition. Carbonate deposition in the southeastern margin was related to increased nutrient supply from a humid and warm continental margin as well as upwelling.

4) The bituminous Cenomanian – Early Turonian shale is characterized by increased carbonate sedimentation in the southern North Atlantic. This is caused by increased production in the southeastern margin related to increased nutrient supply from the warm and humid continental margin, and increased preservation in the western North Atlantic. Deposition changed entirely in Late Turonian; a carbonate enriched western North Atlantic and a zeolitic clay dominated southeastern North Atlantic. The Late Turonian change from the bituminous clay unit to zeolitic clays is interpreted as a consequence of changed oceanography. The change from a stagnant basin to a ventilated basin due to the opening of the South Atlantic and cooling climate are the cause of the sedimentary change.

5) The Latest Cretaceous was prone to marl deposition in the western margin and clay deposition in the southeastern margin. Changed oceanography and climate on the southeastern margin led to adverse carbonate production conditions related to a decreasing continental nutrient supply and a shallower CCD. The western and northern continental humidity, increased continental weathering and high temperatures created an increased nutrient supply and thus optimum surface water conditions for the growth of micro organisms.

IX. Acknowledgements

The author is grateful to Prof. P. de Boer (University of Utrecht) who systematically contributed to this study by advising on structure and for his comments on this manuscript and English editing. As well as J. Trabucho MSc (University of Utrecht) for his consultation concerning Microsoft Illustrator and help in the herculean task of describing and interpreting the data. Further I like to thank Drs. M.

Zeylmans for his help with discussing the task of creating a systematic database as well an introductory class to ARCGIS. Last I would like to thank R. van Gilst BSc for his contribution in discussing trends and sharing our progress on Cretaceous sedimentation.

X. References

Andel van, T.H., 1975. *Mesozoic / Cenozoic Calcite Compensation Depth and the Global Distribution of Calcareous sediments*, Earth and Planetary Science Letters, Vol: 26, Pag: 187 – 194.

Balkwill, H.R., Legall, F.D., 1989. *Whale Basin, Offshore Newfoundland Extension and Salt Diapirism*, American Association of Petroleum Geologists Memoir, Vol: 46, Pag: 233-245.

Barron, E.J., 1985. *Warm Cretaceous Climates: High Atmospheric CO₂ as a Plausible Mechanism*, AGU, Washington D.C.

Benson, W.E., Sheridan, R.E., Enos, P., Freeman, T., Gradstein, F.M., Murdmaa, I.O., Pastouret, L., Schmidt, R.R., Stuermer, D.H., Weaver, F.M., Worstell, P., 1978. *Site 391: Blake Bahama Basin*, International Ocean Drilling Program, http://www.deepseadrilling.org/44/dsdp_toc.htm.

Blakey, R., 2007. *Paleogeographic maps of the Cretaceous*, <http://jan.ucc.nau.edu/~rcb7>.

Boillot, G., Winterer, E.L., Meyer, A.W., Applegate, J., Baltuck, M., Bergen, J.A., Comas, M.C., Davies, T.A., Dunham, K., Evans, C.A., Girardeau, J., Haggerty, J., Jansa, L.F., Johnson, J.A., Kasahara, Loreau, J.-P., Luna, E., Moullade, M., Valrose, P., Ogg, J., Lafayette, W., Sarti, M., Thurow, J., Williamson, M.A., 1987. *Site 641*, International Ocean Drilling Program, http://www-odp.tamu.edu/publications/103_IR/103TOC.HTM.

Bula, S., Heimhofer, U., Hochuli, P.A., Weissert, H., Skelton, P., 2008. *Changes in sedimentary patterns of coastal and deep-sea succession from the North Atlantic (Portugal) linked to Early Cretaceous environmental Change*, Palaeogeography, Palaeoclimatology, Palaeoecology, Vol: 257, Pag: 38 – 57.

Chamley, H., 1989. *Clay Sedimentology*, Springer-Verlag, ISBN: 3-540-50889-9.

De Boer, P., and Trabucho 2009

Donnadieu, Y., Pierrehumbert, R., Jacob, R., Fluteau, F., 2006. *Modelling the primary control of paleogeography on Cretaceous climate*, Earth and Planetary Science Letters, Vol: 248, Pag: 426 – 437.

Erbacher, J., Mosher, D.C., Malone, M.J., et al., 2004. *Site 1258*, Proceedings of the Ocean Drilling Program, Initial Reports, Vol: 207, Pag: 1-117.

Ellwood, B.B., Chrzanowski, T.H., Hrouda, F., Long, G.J., Buhl, M.L., 1988. *Siderite formation in anoxic deep-sea sediments: A synergetic bacteria controlled process with important implications in paleomagnetism*, Geology, Vol: 16, Pag: 980 – 982.

Graciansky, de, P.C., Poag, C.W., Cunningham, R., LoubereMasson, D., Mazzullo, J.M., Montadert, L., Müller, C., Otsuka, K., Reynolds, L., Sigal, J., Sneyder, S., Townsend, H. A., Vaos, P., Waples, D., 1985. *Site 549*, International Ocean Drilling Program, http://www.deepseadrilling.org/80/dsdp_toc.htm.

Graciansky de, P.C., Wylie Poag, C., Hailwood, E.A., O'B.Knox, R.W., Masson, D.G., Montadert, L., Ravenne, C., Müller, C., Sibuet, J.C., Sigal, J., Snyder, S.W., Waples, D.W., Cunningham, R., 1986. *Evidence for changes in Mesozoic and Cenozoic oceanic circulation on the south-western continental margin of Ireland DSDP/IPOC Leg 80*, Geological Society Special Publication, Vol: 21, Pag: 17-33.

Gradstein, F., Ogg, J., Smith, A., 2004. *A Geologic Time Scale*, Cambridge University Press, ISBN 0521786738, Pag: 355 - 357.

Grant, A.C., Jansa, L.F., McAlpine, K.D., Edwards, A., 1988. *Mesozoic-Cenozoic geology of the eastern margin of the Grand Banks and its relation to Galicia Bank*, Proceedings of the Ocean Drilling Program, Scientific Results, Boillot, G., Winterer, E.L. et al., Vol: 103.

Hafid, M., Tari, G., Bouhadioui, D., El Moussaid, E., Echarfaoui, H., Aït Salem, A., Nahim, M., Dakki, M., 2008. *Atlantic basins*, in Michard, A., Saddiqi, O., Chalouan, A., Frizon de Lamotte, D., Continental Evolution: The Geology of Morocco, Pag: 303-329, Springer-Verlag.

Hayes, D.E., Pimm, A.C., Beckmann, J.P., Benson, W.E., Berger, W.H., Roth, P.H., Supko, P.R., von Rad, U., 1972. *Site: 137*, International Ocean Drilling Program, http://www.deepseadrilling.org/14/dsdp_toc.htm.

Hayes, D.E., Pimm, A.C., Beckmann, J.P., Benson, W.E., Berger, W.H., Roth, P.H., Supko, P.R., von Rad, 1972. *Site: 136*, International Ocean Drilling Program, http://www.deepseadrilling.org/14/dsdp_toc.htm.

Haq, B.U., Hardenbol, J., Vail, P.R., 1987. *Chronology of Fluctuating Sea Levels Since the Triassic*, Science, Vol: 235, Pag: 1256 – 1167.

Hofmann, P., Ricken, W., Schwark, L., Leythaeuser, D., 2001. *Geochemical signature and related climatic-oceanographic processes for early Albian black shales: Site 417D, North Atlantic Ocean*, Cretaceous Research, Vol: 22, Pag: 243 – 257.

Hofmann, P., Stüsser, I., Wagner, T., Schouten, S., Sinninghe Damsté, J.S., 2008. *Climate-ocean coupling off North-West Africa during the Lower Albian: The Oceanic Anoxic Event 1b*, Palaeogeography, Palaeoclimatology, Palaeoecology, Vol: 262, Pag: 157 – 165.

Hollister, C.D., Ewing, J.I., Habib, D., Hatahway, J.C., Lancelot, Y., Luterbacher, H., Paulus, F.J., Poag, W.C., Wilcoxon, J.A., Worstell, P., 1972. *Site 105 – Lower Continental Rise Hills*, International Ocean Drilling Program, http://www.deepseadrilling.org/11/dsdp_toc.htm.

Holbourn, A., Kuhnt, W., Soeding, E., 2001. *Atlantic paleobathymetry, paleoproductivity and paleocirculation in the late Albian: the benthic foraminiferal record*, Palaeogeography, Palaeoclimatology, Palaeoecology, Vol: 170, Pag: 171 – 196.

Johannes, W., 1968. *Experimentelle Sideritbildung aus Calcite + FeCl₂*, Contr. Mineral. And Petrol., Vol: 17, Pag: 155 – 164.

Kuhnt, W., Geroch, S., Kaminski, M.A., Moullade, M., Neagum, T., 1992. *Upper Cretaceous abyssal claystones in the North Atlantic and Western Tethys: current status of biostratigraphical correlation using agglutinated foraminifers and palaeoceanographic events*, *Cretaceous Research*, Vol: 13, Pag: 467 – 478.

Lancelot, Y., Winterer, L., Bosellini, A., Boutefeu, G.A., Boyce, R.E., Cepek, P., Fritz, D., Galimov, E.M., Melguen, M., Price, I., Schlager, W., Sliter, W., Taguchi, K., Vincent, E., Westerberg, J., 1980. *Site 415, Agadir Canyon, Deep Sea Drilling Project LEG 50*, http://www.deepseadrilling.org/50/dsdp_toc.htm.
Lancelot, Y., Seibold, E., Cepek, P., Dean, W.E., Eremeev, V., Gardner, J., Jansa, L.F., Johnson, D., Krasheninnikov, V., Pflaumann, U., Rankin, J.G., Trabant, P., 1980. *Site 367: Cape Verde Basin, International Ocean Drilling Program*, http://www.deepseadrilling.org/41/dsdp_toc.htm.

Kuypers, M.M.M., Pancost, R.D., Nijenhuis, I.A., Sinningh Damsté, J.S., 2002. *Enhanced productivity led to increased organic carbon burial in the euxinic North Atlantic basin during the late Cenomanian oceanic anoxic event*, *Paleoceanography*, Vol: 17, Pag: 1051.

Lawver, L.A., Dalziel, I.W.D., Gahagan, L.M., Martin, J.M., Campbell, D., 2002. *Plates 2002 Atlas of Plate Reconstructions, (750 Ma – present day)*, <http://www.vanmaerlant.sghetplein.nl/pdf/Plates.pdf>.

Larson, R.L., Erba, E., 1999. *Onset of the Mid-Cretaceous greenhouse in the Barremian – Aptian; igneous events and the biological, sedimentary, and geochemical responses*, *Palaeogeography, Palaeoclimatology, Palaeoecology*, Vol: 14, Pag: 663 – 679.

Li, Y.-X., Bralower, T.J., Montañez, I.P., Osleger, D.A., Arthur, M.A., Bice, D.M., Herbert, T.D., Erba, E., Silva, I.P., 2008. *Toward an orbital chronology for the early Aptian Oceanic Anoxic Event (OAE1a, ~120 Ma)*, *Earth and Planetary Science Letters*, Vol: 271, Pag: 88 – 100.

Miller, K.G., Sugarman, P.J., Browning, J.V., Cramer, B.S., Olsson, R.K., de Romero, L., Aubry, M-P., Pekar, S.F., Georgescu, M.D., Metzger, K.T., Monteverde, D.H., Skinner, E.S., Uptegrove, J., Mullikin, L.G., Muller, F.L., Feigenson, M.D., Reilly, T.J., Brenner, G.J., Queen, D., 1999. *Ancona Site*, *Proceeding of the Ocean Drilling Program, Initial Reports, Volume 174AX*, <http://www-odp.tamu.edu/publications/174AXSIR/74AXSTOC.HTM>.

Norris, R.D., Kroon, D., Huber, B.T., Erbacher, J., 2001. *Cretaceous-Palaeogene ocean and climate change in the subtropical North Atlantic*, *Geological Society, London, Special Publications*, Vol: 183, Pag: 1-22.

Parsons, B., Sclater, J.G., 1977. *An Analysis of the variation of ocean floor bathymetry and heat flow with age*, *Journal of geophysical research*, Vol: 82, No: 5, Pag: 803 – 827.

Pinheiro, L.M., Wilson, R.C.L., Pena dos Reis, R., Whitmarsh, R.B., Riberio, A., 1996. *The Western Iberia Margin: A geophysical and geological overview*, *Proceedings of the Ocean Drilling Program*, Vol: 149, Pag: 1-23.

Pletsch, T., Daoudi, L., Chamley, H., Deconinck, J.F., Charroud, M., 1996. *Palaeogeographic controls on palygorskite occurrence in Mid-Cretaceous sediments of Morocco and adjacent basins*, *Clay Minerals*, Vol: 31, Pag: 403-416.

- Posamentier, H.W., Allen, G.P. 1993. *Variability of the sequence stratigraphic model: effects of local basin factors*, Sedimentary Geology, Vol: 86, Pag: 91-109
- Postma, D., 1982. *Pyrite and Siderite formation in brackish and freshwater swamp sediments*, American Journal of Science, Vol: 282, Pag: 1151 – 1183.
- Rad von, U., Sarti, M., 1986. *Early Cretaceous »events« in the evolution of the eastern and western North Atlantic continental margins*, Geologische Rundschau, Vol: 75, Is: 1, Pag: 139-158.
- Robertson, A.H.F., Ogg, J.G., 1986. *Palaeoceanographic setting of the Callovian North Atlantic*, Geological Society Special Publication, Vol: 21, Pag: 283-320.
- Rothe, P., Tucholke, B.E., 1981. *Mineralogy of Sedimentary Formations in the Western North Atlantic Ocean: Preliminary Results*, Geologische Rundschau, Vol: 70, Pag: 327 – 343.
- Rothe, P.H., 1986. *Mesozoic palaeoceanography of the North Atlantic and Tethys Oceans*, Geological Society Special Publication, Vol: 21, Pag: 299-320.
- Ryan, W.B.F., Sibuet, J.-C., Arthur, M.A., Lopatin, B.G., Moore, D.G., Rehault, J.-P., Iaccarino, S., Sigal, J., Morga, G.E., Blechschmidt, G., Williams, C.A., Johnson, D., Bames, R.O., Habib, D., 1979. *Site 398*, , International Ocean Drilling Program, http://www.deepseadrilling.org/47_2/dsdp_toc.htm.
- Sclater, J.G., Hellinger, S. and Tapscott, C., 1977. *The paleobathymetry of the Atlantic ocean from the Jurassic to present*, The Journal of Geology, Vol: 85, Pag: 509-552.
- Sheridan, R.E., Crosby, J.T., 1981. *Stratigraphy and Structure of Southern Blake Plateau, Northern Florida Straits, and Northern Bahama Platform from Multichannel Seismic Reflection Data*, American Association for Petroleum Geologists, Vol: 65.
- Singer, A., Galan, E., 1984. *Palygorskite – Sepiolite, Occurrences, Genesis and Uses*, Developments in Sedimentology, Vol: 37, <http://books.google.nl/books?hl=nl&lr=&id=-AwxuM2VJU0C&oi=fnd&pg=PR5&dq=palygorskite&ots=ajZCgWBTUy&sig=j1z7IU7J6fMPhix3kB3gn9KzJw#v=onepage&q=&f=false>.
- Stein, R.G., Rullkötter, J., Welte, J.D.H., 1989. *Changes in paleoenvironments in the Atlantic Ocean during Cretaceous times: results from black shales studies*, Geologische Rundschau, Vol: 78, Is: 3, Pag: 883-901.
- Tankard, A.J., Balkwill, H.R., 1989. *Extensional tectonics and Stratigraphy of the North Atlantic Margins: Introduction*, American Association of Petroleum Geologists Memoir, Vol: 46, Pag: 1-6.
- Tankard, A.J., Welsink, H.J., 1989. *Mesozoic Extension and Styles of Basin Formation in Atlantic Canada*, American Association of Petroleum Geologists Memoir, Vol: 46, Pag: 175-195.
- Thiede, J., Ehrmann, W.U., 1986. *Late Mesozoic and Cenozoic sediment flux to the central North Atlantic Ocean*, Geological Society Special Publication, Vol: 21, Pag: 3-15.
- Thiry, M., Jacquin, T., 1993. *Clay mineral distribution related to rift activity, sea-level changes and paleoceanography in the Cretaceous of the Atlantic Ocean*, Clay Minerals, Vol: 28, Pag: 61-84.
- Tucholke, B.E., Sibuet, J.-C., Klaus, A., et al., 2004. *Site 1276*, Proceedings of the Ocean Drilling Program, Initial Reports, Volume 210.

Tucholke, B.E., Vogt, P.R., Demars, K.R., Galehouse, J.S., Houghton, R.L., Kaneps, A., Kendrick, J.W., McCave, I.N., McNulty, C.L., Murdmaa, I.O., Okada, H., Rothe, P., 1979. *Site 387: Cretaceous to recent sedimentary evolution of the Western Bermuda Rise*, International Ocean Drilling Program, http://www.deepseadrilling.org/43/dsdp_toc.htm.

Vail, P.R., Mitchum, R.M., Thompson, S. 1977. *Seismic Stratigraphy and Global Changes of Sea Level, Part 1-3*, American Association of Petroleum Geologists Memoir, Vol: 26, Pag: 51 – 98.

Velde, B., 1995. *Origin and Mineralogy of Clays; Clays and the Environment*, Springer – Verlag, ISBN: 3-540-58012-3, Pag: 1-329.

Verhoef, J., Srivastava, S.P., 1989. *Correlation of Sedimentary Basins Across the North Atlantic as Overlain from Gravity and Magnetic Data, and Its Relation to the Early Evolution of the North Atlantic*, American Association of Petroleum Geologists Memoir, Vol: 46, Pag: 131-147.

Wenk, H.R., Bulakh, A., 2004. *Minerals, Their Constitution and Origin*, Cambridge University Press, ISBN 052152958.

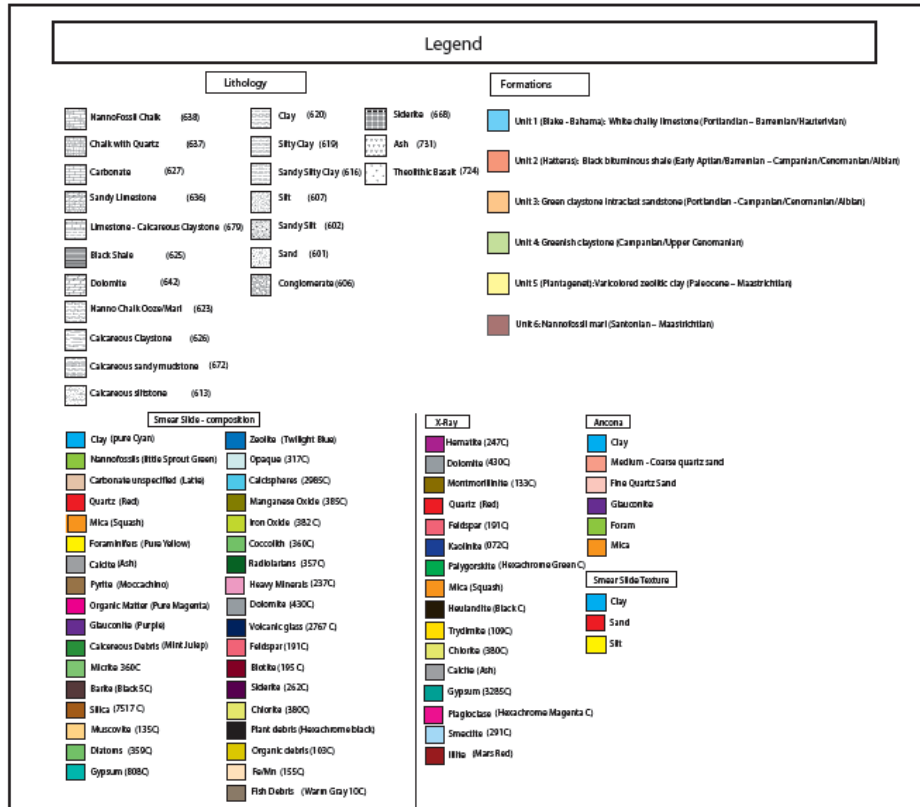
Wilson, P.A., Norris, R.D., 2001. *Warm tropical ocean surface and global anoxia during mid-Cretaceous period*, Nature, Vol: 412, Pag: 425 – 429.

Wilson, R.C.L., 1975. *Atlantic opening and Mesozoic continental margin basins of Iberia*, Earth and Planetary Science Letters, Vol: 25, Pag: 33-43.

Ziegler, P.A., 1989. *Evolution of the North Atlantic – An overview*, American Association of Petroleum Geologists Memoir, Vol: 46, Pag: 111-129.

XI. Appendixes

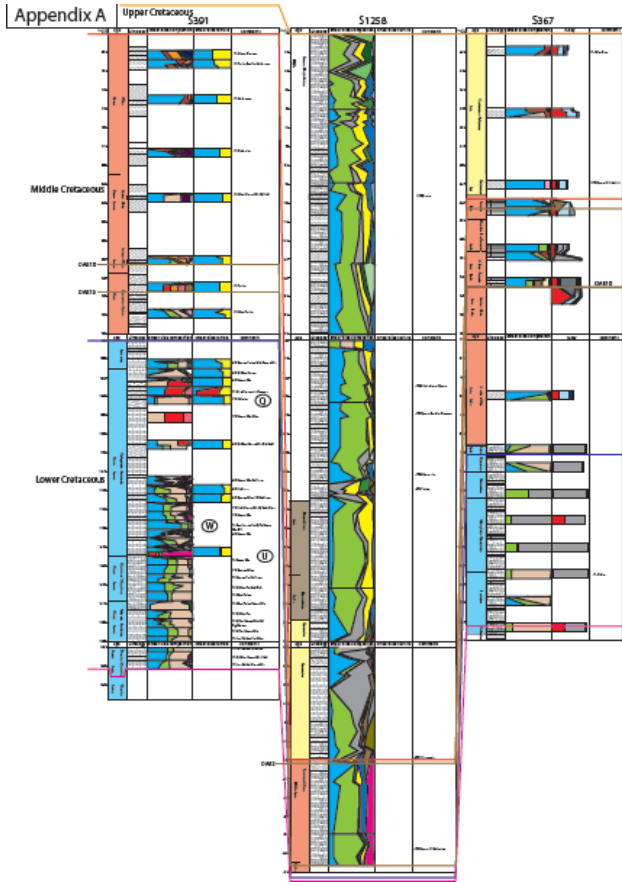
11.1. Legend



11.2. Appendix A

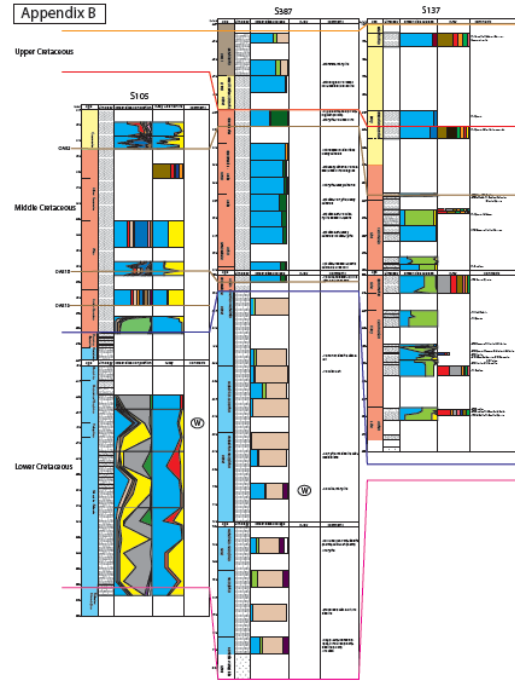
Southernmost Transect S391, S1258, S367

Appendix A.pdf



11.3. Appendix B
 Southern Transect S105, S387, S137

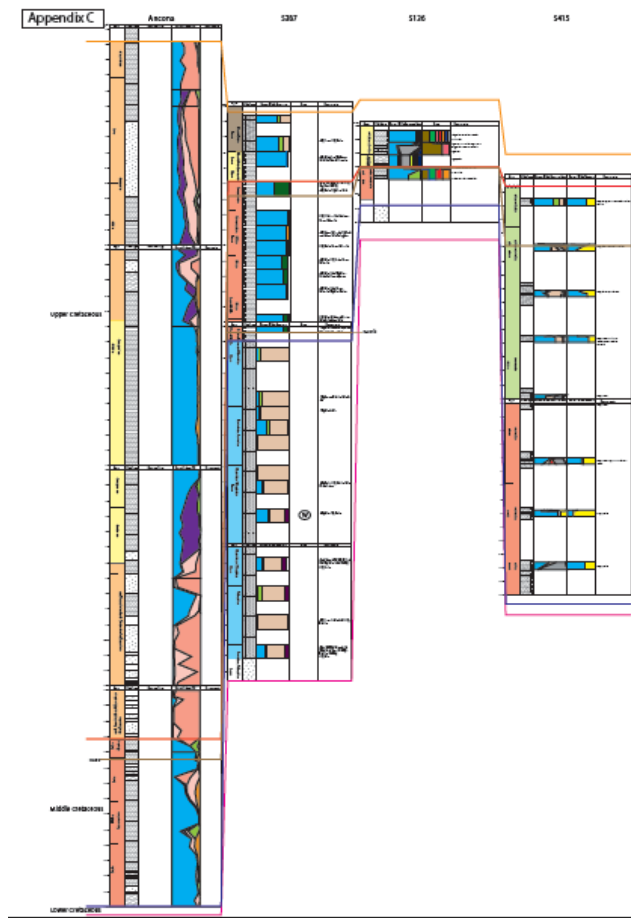
Appendix B.pdf



11.4. Appendix C

Northern Transect Ancona, S387, S136, S415

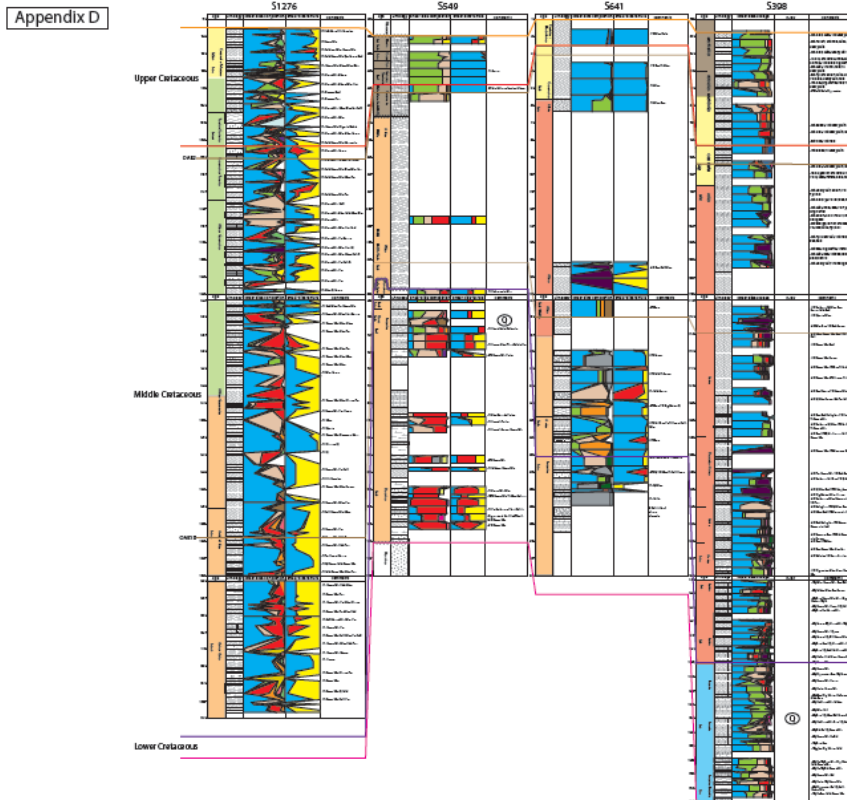
Appendix C.pdf



11.5. Appendix D

Northernmost Transect S1276, S549, S641, S398

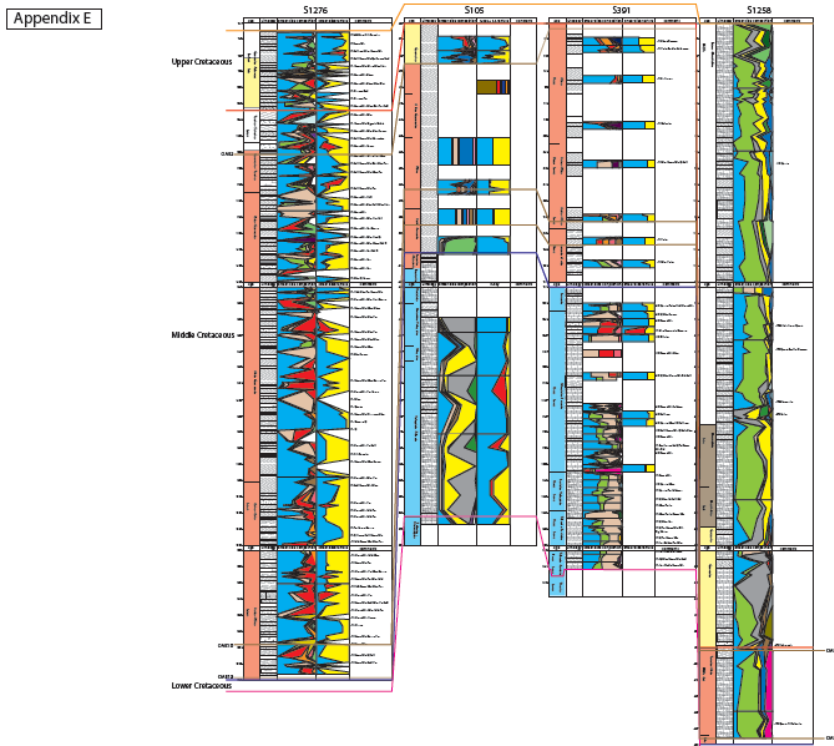
Appendix D.pdf



11.6. Appendix E

Western Transect: S1276, S387, S105, S391, S1258

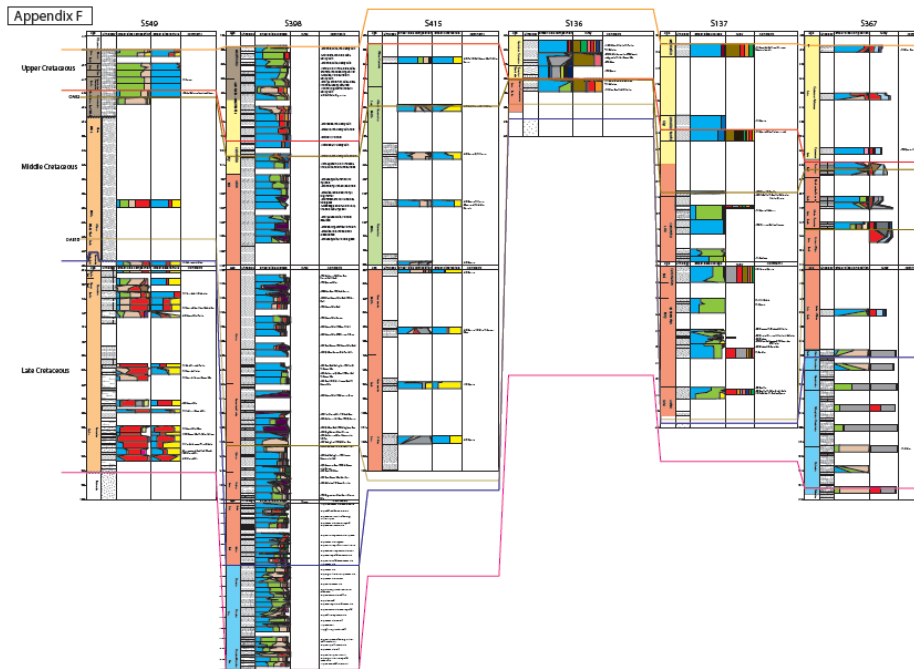
Appendix E.pdf



11.7. Appendix F

Eastern Transect: S549, S398, S415, S136, S137, S367

Appendix F.pdf



11.8. Appendix G

11.9.1. Clay mineralogy

Anhydrite: is a typical evaporate deposit is also found in medium temperature hydrothermal sulfide ore deposits.

Biotite is a mica, part of the Mica group, and is very common and precipitates at temperature >310 °C.

Calcite: Known as calcium carbonate (often contains minor amounts of magnesium, iron and manganese) can have both a chemical as well as a biological origin. Calcite can precipitate in warm seawater (Wenk & Bulakh 2004)

Chlorite: Chlorite is a mostly magnesium mineral, part of the Chlorite group. Chlorite is a physical denudation product of predominantly crystalline igneous and metamorphic rocks. The physical weathering limits chlorite as a denudation product to mostly high latitudes. Chlorite is therefore considered the antipodal to kaolinite which is predominantly concentrated at lower latitudes (Chamley 1989). Chlorite being an aluminum mineral it has a strong correlation to igneous and metamorphic rocks which makes it susceptible to clay generation by deep sea volcanics. Hydrothermal metamorphism has been recorded for chlorite. It also forms a diagenetic product in deep burial of smectite in a magnesian environment and from kaolinite under basic conditions (Chamley 1989).

Dolomite: is a salt consisting of both magnesium and calcium. Dolomite forms in hydrothermal deposits as well as highly saline waters.

Glaucinite: Glaucinite is a ferriferous clay granule, part of the Mica group it is characterized by its occurrence in clayey, silty and sandy fractions of sedimentary rocks, glauconite can occur both in terrigenous/lacustrine settings as well as marine environments (Chamley 1989). Marine glauconite is most commonly formed between 125-500 m. Glaucinite is formed as a subrounded pellet near the water sediment interface by alteration of biogenic components but can also be a minor fraction in mineral and rock debris (Chamley 1989, Velde 1995). Glaucinite formation is restricted between 50°N and 50°S, in tropical regimes it is replaced by verdine between 50-80 meters of depth. Glaucinite formation in deep sea environments is incircumstantial and most probably related to reworked shelf material. Glaucinite is related to slow sedimentation rates, distal zones with low terrigenous input and slow sedimentary are essential to the glaucony process. Glaucony is repeatedly related to hiatuses or very slow sedimentation and therefore strongly but not exclusively related to transgressive sequences for the reduction in terrigenous input hence slow sedimentation Chamley 1989.

Gypsum is part of the sulfate group and forms as a low-temperature hydrothermal mineral. Gypsum mainly forms in evaporitic deposits but can form in sands and clay from meteoric water (Wenk & Bulakh 2004).

Kaolinite: Kaolinite is a aluminum rich clay mineral part of the kaolin – serpentine group, it is formed by pedogenetic processes in a surficial environment (Chamley 1989). The mineral is related to tropical lateritic moist regimes with strong chemical denudation. The parent material varies from igneous, metamorphic to sedimentary rocks. Kaolinite deposition in marine sediments is directly

dependent on the intensity of continental hydrolysis and is considered a low latitudinal mineral, marine kaolinite is hence associated with abundant iron oxides (Chamley 1989).

Montmorillonite: Montmorillonite is part of the smectite group. Montmorillonite forms mostly chemically on surficial soils or sediments, it is part of the second denudation step in the formation of pedogenic clays in temperate conditions on volcanic parent rock. Hot and humid climate do not endure montmorillonite formation. Montmorillonite can also grow diagenetically in silicic acidic glass during burial where glass is altered to montmorillonite at a burial between 1700 and 3500 m equivalent to 84 - 91 °C (Iijima 1984; Chamley 1989).



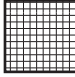



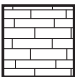
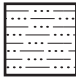
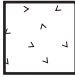

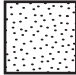

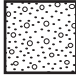

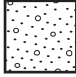
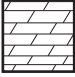

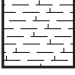


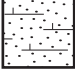
Palygorskite: Palygorskite is a magnesium rich clay mineral of the palygorskite – sepiolite group. Palygorskite is not easily destroyed by transportation (Pletsch et al., 1996) in contrast to the claims of Chamley 1989. Its main occurrence are sites of authigenic formation, Cretaceous formation mainly took place in shallow marine and terrestrial environments. Although palygorskite is only a minor component of the investigated cores in this research it is important to understand its origin and development for where it occurs. To understand Cretaceous palygorskite occurrences the interpretation by Pletsch et al., 1996 for the Mid Cretaceous was used and extrapolated to the entire Cretaceous. Palygorskite consists of two types of 1) long fibers related to shallow marine carbonate and evaporation origins 2) short fibers in deep marine mass flow deposits indicated by reworked shallower parts. Currently type one is identified as the source of type 2, palygorskite can be transported along long transects by aeolian processes. However other mechanisms: diagenesis, hydrothermal activity, halmyrolysis of magnesium magmatic rocks, smectite transition and precipitation from hypersaline brines are possible causes for palygorskite formation (Thiry & Jacquin 1993). Following the insight by both Thiry & Jacquin 1993 and Pletsch et al., 1996 palygorskite in at least Albian – Cenomanian/Turonian sediments must either be authigenic in peri marine sediments transported by mass flow to deep marine sediments. Palygorskite mainly was formed through coastal evaporation in North Africa, conditions in Western Atlantic were adverse, rapid sedimentation and no large restricted coastal basins (Chamley & Debrabant 1984).

Siderite is part of the non clay species and a diagenetic product of the carbonates FeCO_3 . It forms chemically in sedimentary rocks as late stage of hydrothermal alteration (Wenk & Bulakh 2004). Siderite in limestones is a very important indicator of the depositional environment and appears to be relict to the original sedimentation. The formation of siderite may be directly related to metabolic activities of bacteria (Ellwood et al., 1988). Siderite may be formed as a freshwater swamp deposit as well as in brackish marine environments below a sulphate reduction zone when sufficient iron is present (Postma 1982). Siderite forms a diagenetic product from calcite at temperatures > 300°C which is not the case in the sites investigated here (Johannes 1968).







Zeolites are a non clay species. It can form from volcanic glass, ash, precipitates in alkaline ground water as well as precipitate in saline lakes. Zeolite minerals are mainly related to a volcanic origin in marine sediments. Heulandite is one of its subspecies specifically linked to hydrous precipitation. Zeolite is also related to diagenetic alteration of radiolarians and as a dissolution product of siliceous microfossils (Erbacher et al., 2004). Zeolites indicate a slow sedimentation (Hayes et al., 1972).

Legend




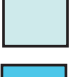
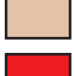



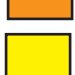

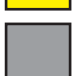















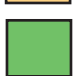


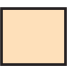





Lithology

 NannoFossil Chalk (638)	 Clay (620)	 Siderite (668)
 Chalk with Quartz (637)	 Silty Clay (619)	 Ash (731)
 Carbonate (627)	 Sandy Silty Clay (616)	 Theolitic Basalt (724)
 Sandy Limestone (636)	 Silt (607)	
 Limestone - Calcareous Claystone (679)	 Sandy Silt (602)	
 Black Shale (625)	 Sand (601)	
 Dolomite (642)	 Conglomerate (606)	
 Nanno Chalk Ooze/Marl (623)		
 Calcareous Claystone (626)		
 Calcareous sandy mudstone (672)		
 Calcareous siltstone (613)		

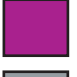


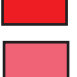




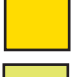



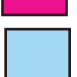



Formations

 Unit 1 (Blake - Bahama): White chalky limestone (Portlandian – Barremian/Hauterivian)
 Unit 2 (Hatteras): Black bituminous shale (Early Aptian/Barremian – Campanian/Cenomanian/Albian)
 Unit 3: Green claystone intraclast sandstone (Portlandian - Campanian/Cenomanian/Albian)
 Unit 4: Greenish claystone (Campanian/Upper Cenomanian)
 Unit 5 (Plantagenet): Varicolored zeolitic clay (Paleocene – Maastrichtian)
 Unit 6: Nannofossil marl (Santonian – Maastrichtian)


Smear Slide - composition

 Clay (pure Cyan)	 Zeolite (Twilight Blue)
 Nannofossils (little Sprout Green)	 Opaque (317C)
 Carbonate unspecified (Latte)	 Calcispheres (2985C)
 Quartz (Red)	 Manganese Oxide (385C)
 Mica (Squash)	 Iron Oxide (382 C)
 Foraminifers (Pure Yellow)	 Coccolith (360C)
 Calcite (Ash)	 Radiolarians (357C)
 Pyrite (Moccachino)	 Heavy Minerals (237C)
 Organic Matter (Pure Magenta)	 Dolomite (430C)
 Glauconite (Purple)	 Volcanic glass (2767 C)
 Calcareous Debris (Mint Julep)	 Feldspar (191C)
 Micrite 360C	 Biotite (195 C)
 Barite (Black 5C)	 Siderite (262C)
 Silica (7517 C)	 Chlorite (380C)
 Muscovite (135C)	 Plant debris (Hexachrome black)
 Diatoms (359C)	 Organic debris (103C)
 Gypsum (808C)	 Fe/Mn (155C)
	 Fish Debris (Warm Gray 10C)

X-Ray

 Hematite (247C)
 Dolomite (430C)
 Montmorillinite (133C)
 Quartz (Red)
 Feldspar (191C)
 Kaolinite (072C)
 Palygorskite (Hexachrome Green C)
 Mica (Squash)
 Heulandite (Black C)
 Trydimite (109C)
 Chlorite (380C)
 Calcite (Ash)
 Gypsum (3285C)
 Plagioclase (Hexachrome Magenta C)
 Smectite (291C)
 Illite (Mars Red)

Ancona

 Clay
 Medium - Coarse quartz sand
 Fine Quartz Sand
 Glauconite
 Foram
 Mica

Smear Slide Texture

 Clay
 Sand
 Silt

Appendix A

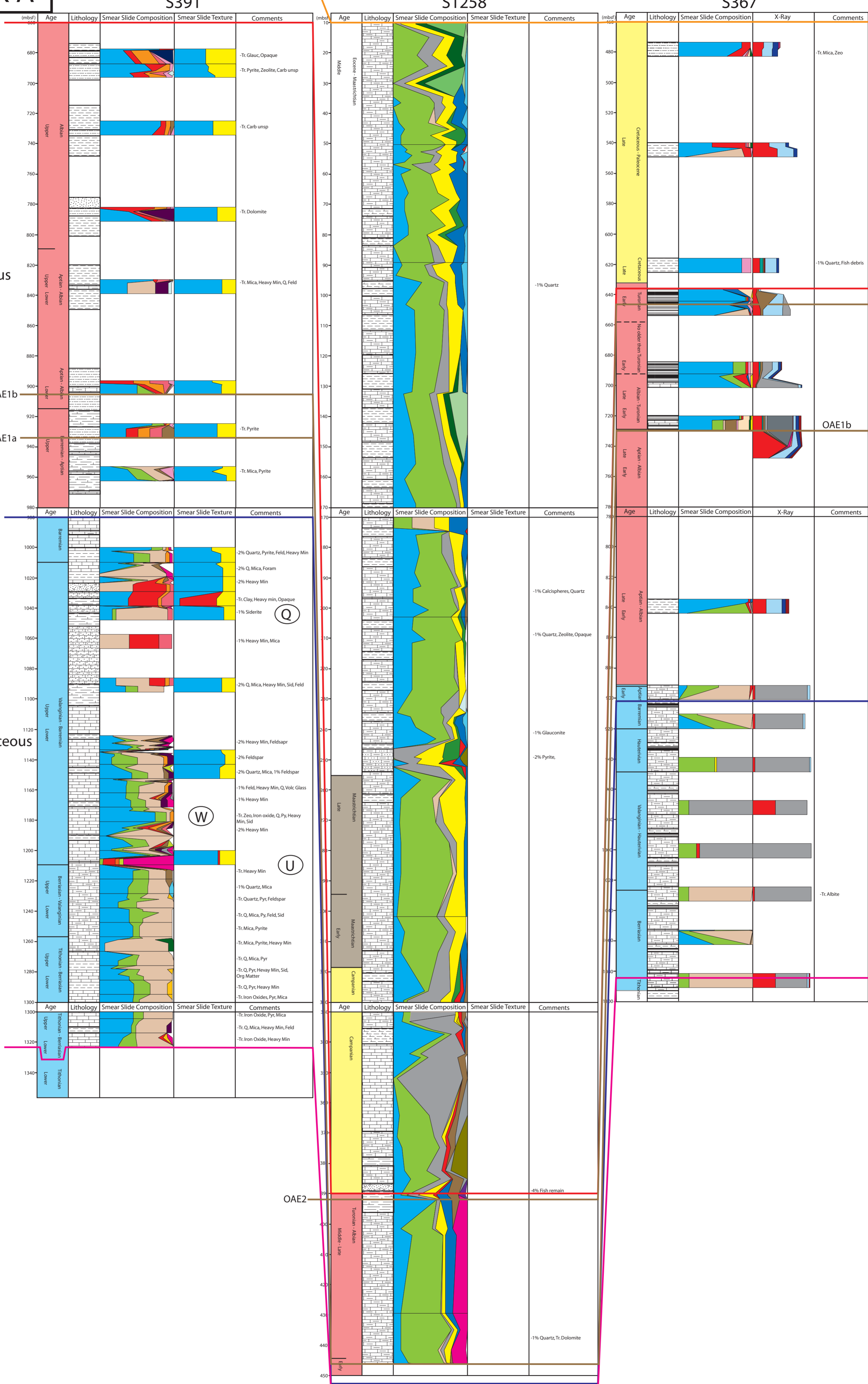
Upper Cretaceous S391

S1258

S367

Mid Cretaceous

Lower Cretaceous



OAE2

OAE1b

OAE1a

Appendix B

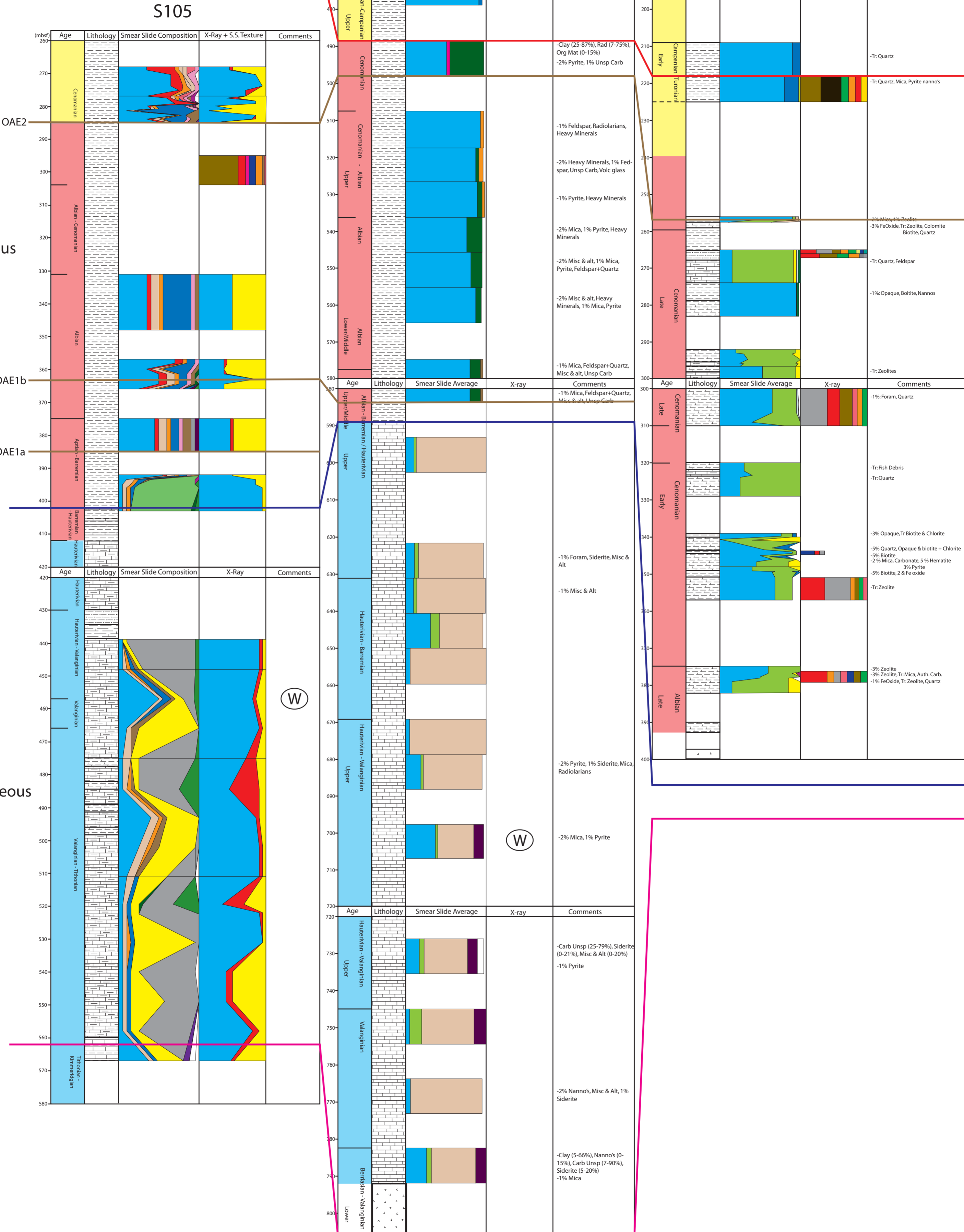
S387

S137

Upper Cretaceous

Mid Cretaceous

Lower Cretaceous



Appendix C

Ancona

S387

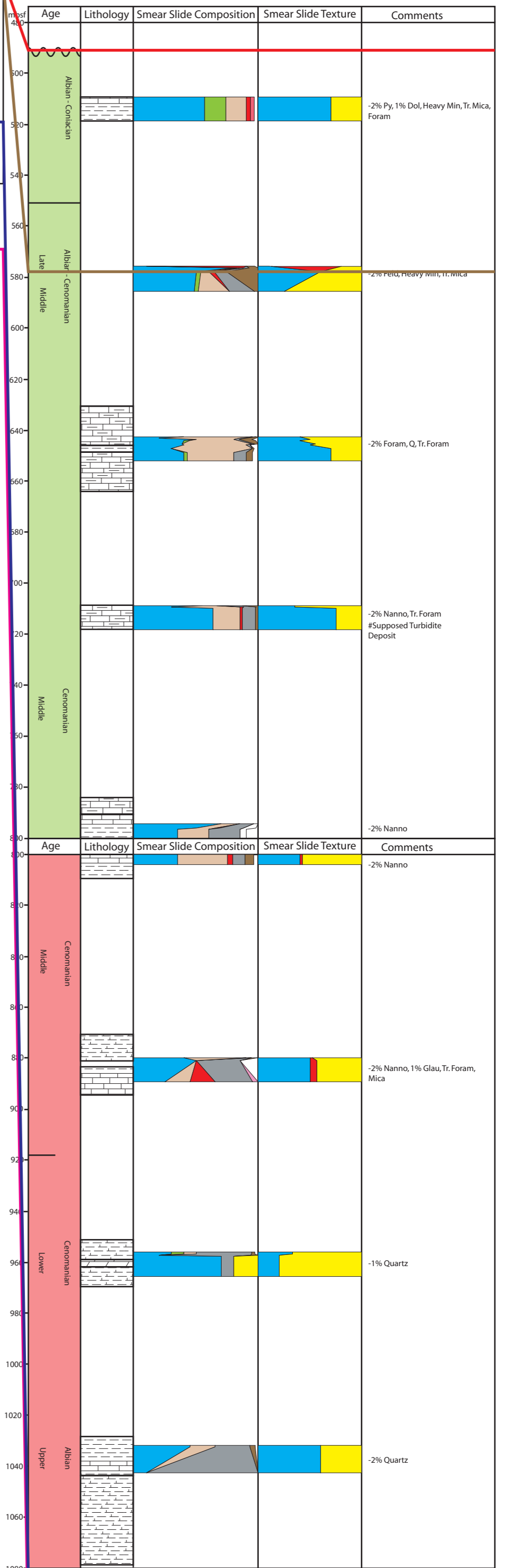
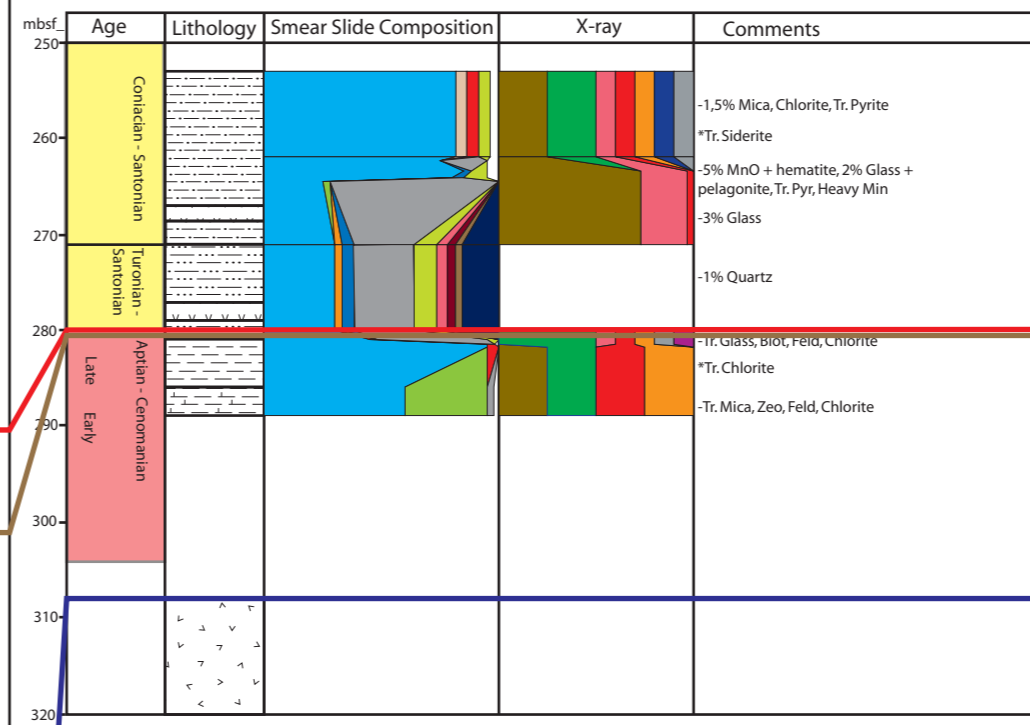
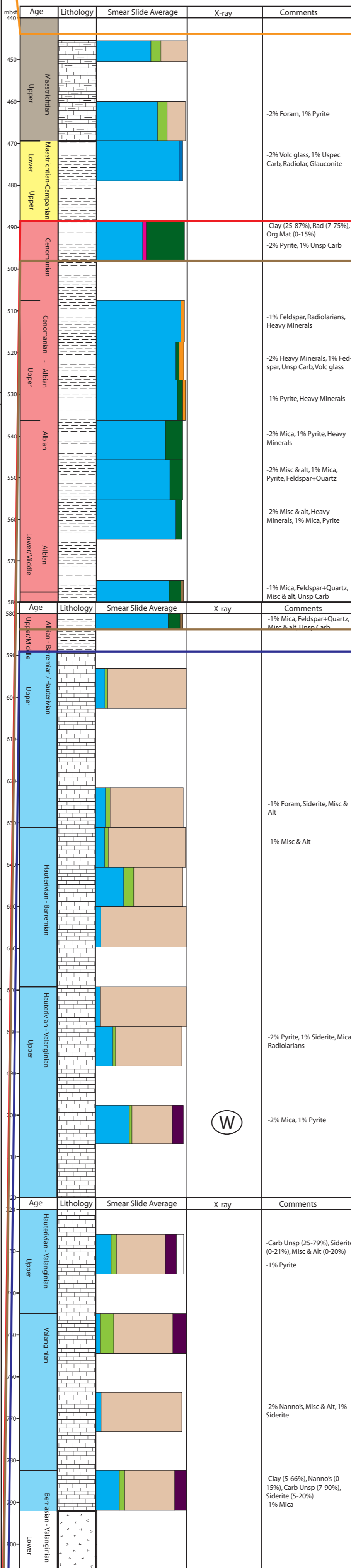
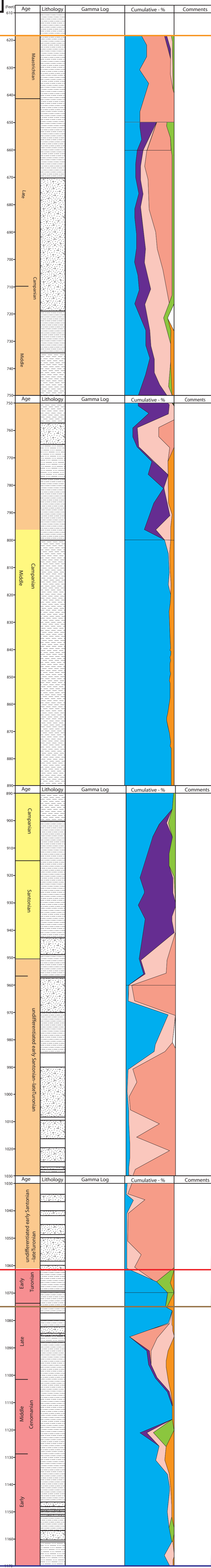
S136

S415

Upper Cretaceous

Mid Cretaceous

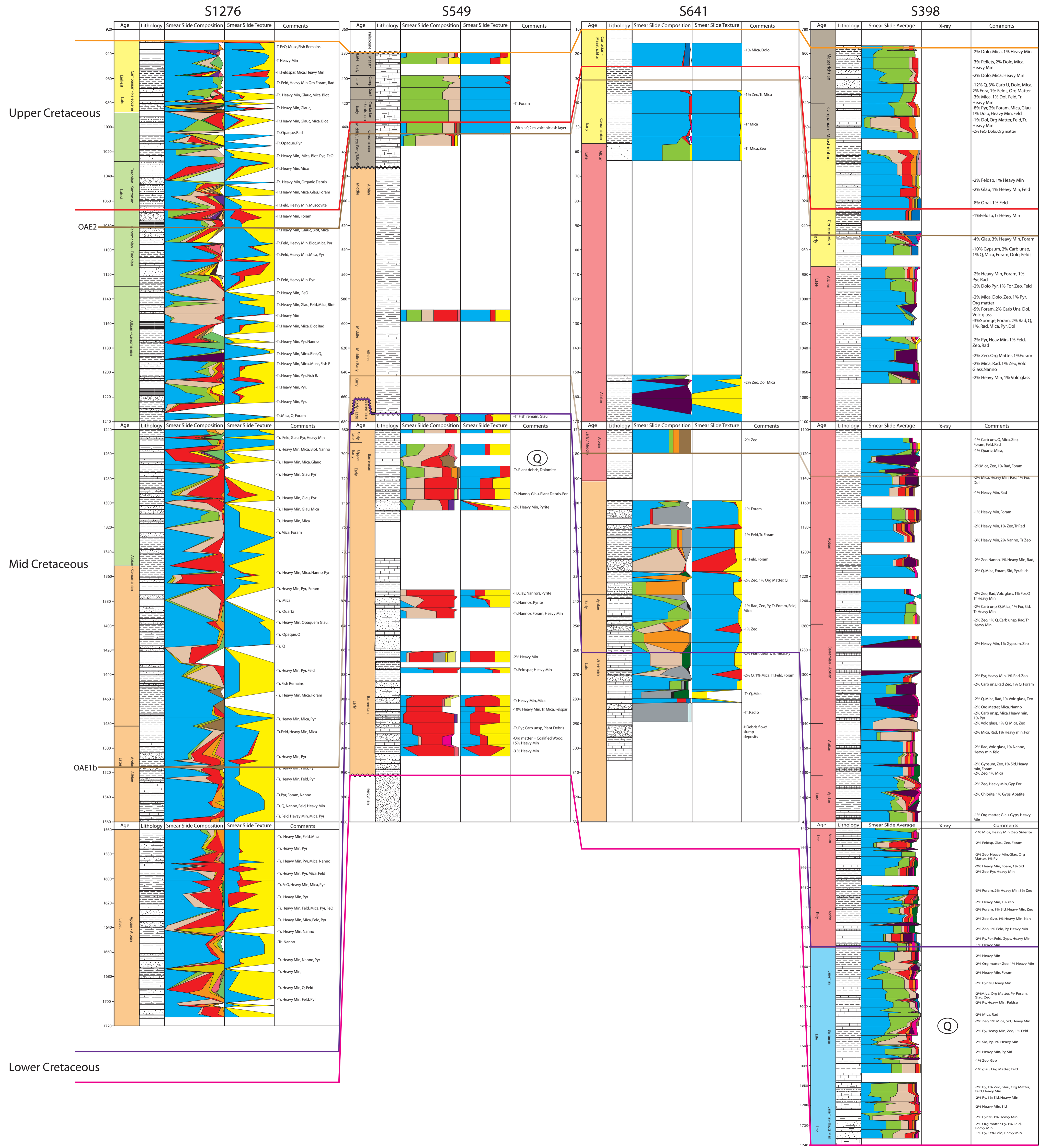
Lower Cretaceous



OAE1b

W

Appendix D

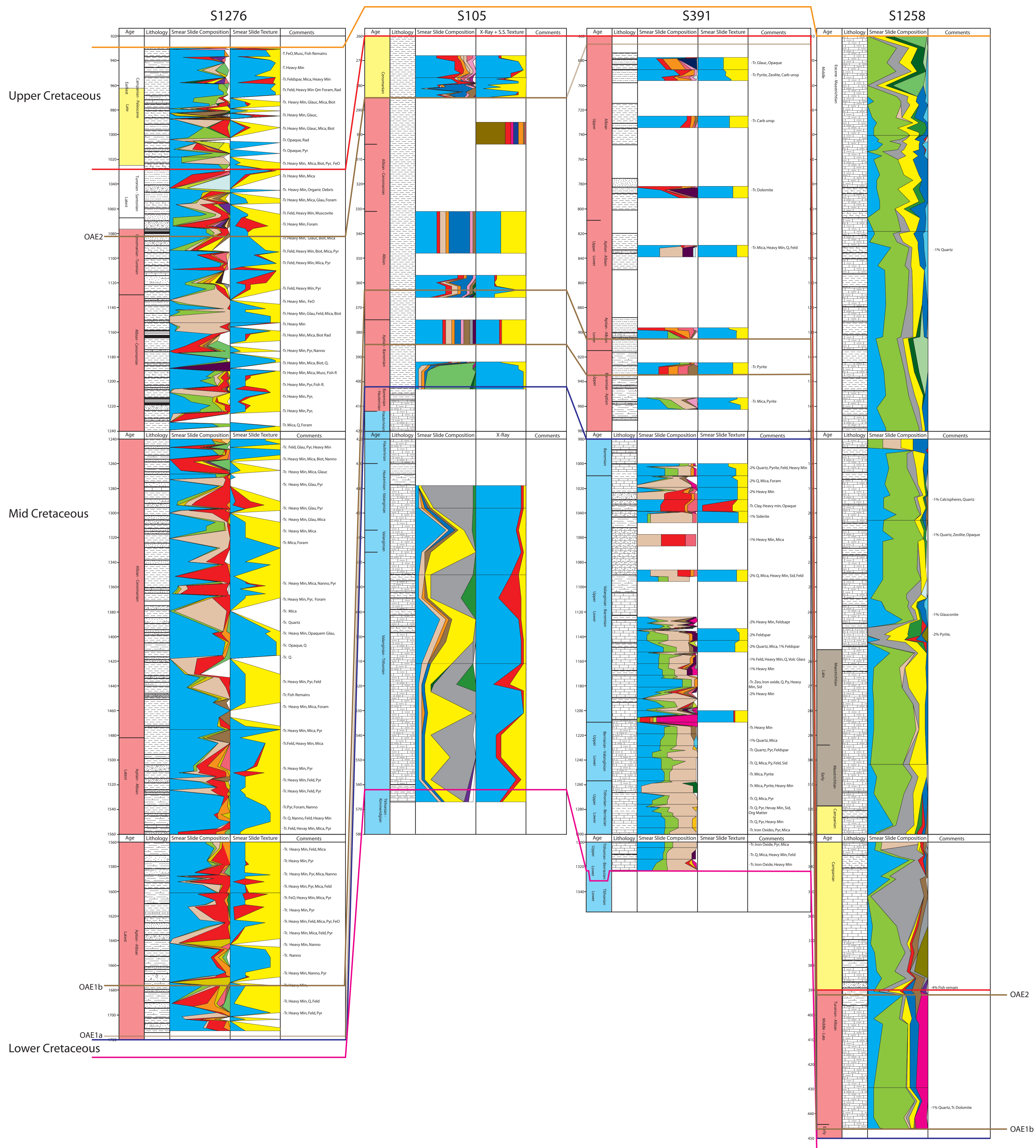


Upper Cretaceous

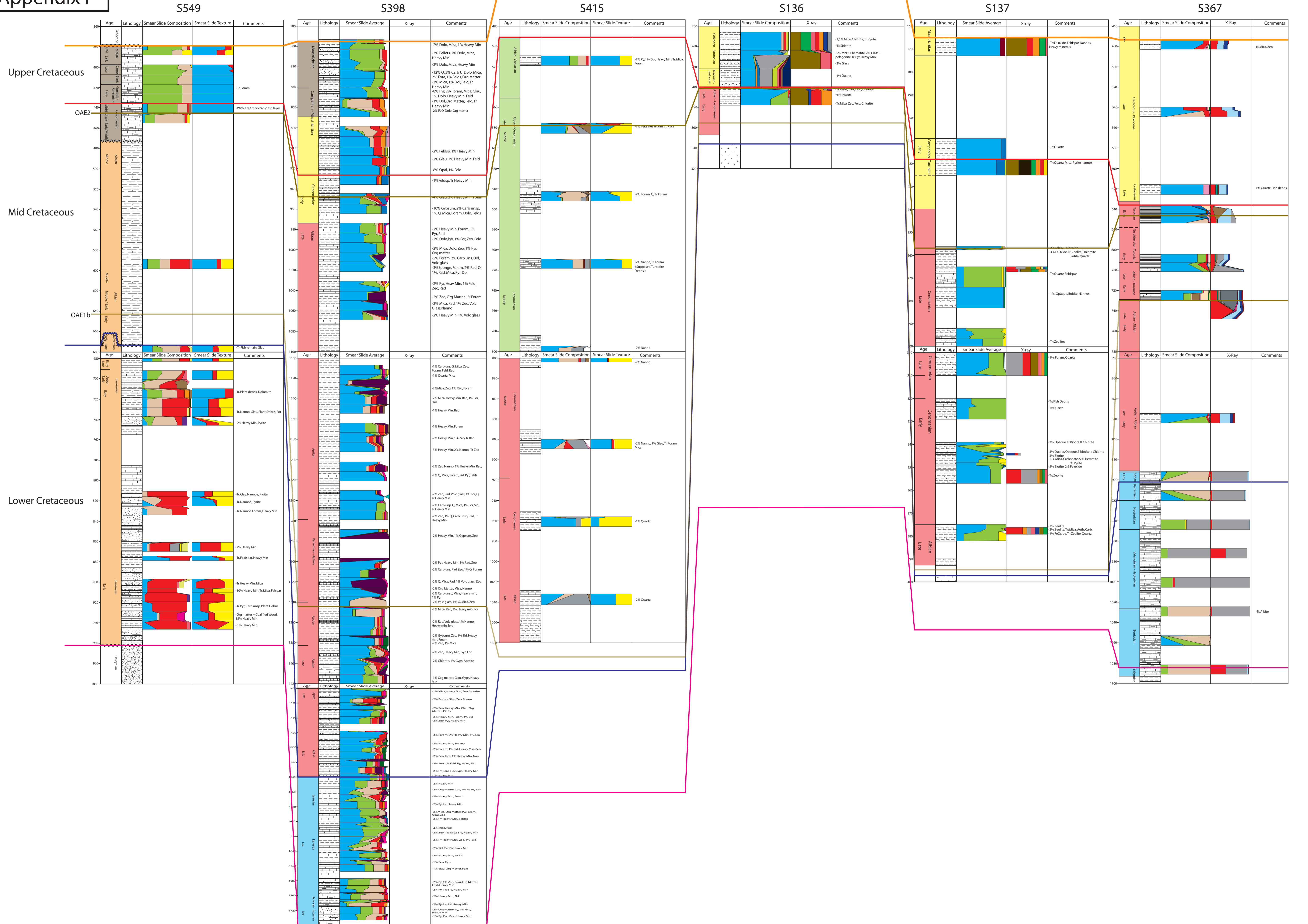
Mid Cretaceous

Lower Cretaceous

Appendix E



Appendix F



Upper Cretaceous

Mid Cretaceous

Lower Cretaceous

OAE2

OAE1b

S549

S398

S415

S136

S137

S367

Age	Lithology	Smear Slide Composition	Smear Slide Texture	Comments
360	Albanian			
380	Albanian			
400	Albanian			
420	Albanian			
440	Albanian			
460	Albanian			
480	Albanian			
500	Albanian			
520	Albanian			
540	Albanian			
560	Albanian			
580	Albanian			
600	Albanian			
620	Albanian			
640	Albanian			
660	Albanian			
680	Albanian			
700	Albanian			
720	Albanian			
740	Albanian			
760	Albanian			
780	Albanian			
800	Albanian			
820	Albanian			
840	Albanian			
860	Albanian			
880	Albanian			
900	Albanian			
920	Albanian			
940	Albanian			
960	Albanian			
980	Albanian			
1000	Albanian			

Age	Lithology	Smear Slide Average	X-ray	Comments
360	Albanian			
380	Albanian			
400	Albanian			
420	Albanian			
440	Albanian			
460	Albanian			
480	Albanian			
500	Albanian			
520	Albanian			
540	Albanian			
560	Albanian			
580	Albanian			
600	Albanian			
620	Albanian			
640	Albanian			
660	Albanian			
680	Albanian			
700	Albanian			
720	Albanian			
740	Albanian			
760	Albanian			
780	Albanian			
800	Albanian			
820	Albanian			
840	Albanian			
860	Albanian			
880	Albanian			
900	Albanian			
920	Albanian			
940	Albanian			
960	Albanian			
980	Albanian			
1000	Albanian			

Age	Lithology	Smear Slide Composition	Smear Slide Texture	Comments
360	Albanian			
380	Albanian			
400	Albanian			
420	Albanian			
440	Albanian			
460	Albanian			
480	Albanian			
500	Albanian			
520	Albanian			
540	Albanian			
560	Albanian			
580	Albanian			
600	Albanian			
620	Albanian			
640	Albanian			
660	Albanian			
680	Albanian			
700	Albanian			
720	Albanian			
740	Albanian			
760	Albanian			
780	Albanian			
800	Albanian			
820	Albanian			
840	Albanian			
860	Albanian			
880	Albanian			
900	Albanian			
920	Albanian			
940	Albanian			
960	Albanian			
980	Albanian			
1000	Albanian			

Age	Lithology	Smear Slide Composition	X-ray	Comments
360	Albanian			
380	Albanian			
400	Albanian			
420	Albanian			
440	Albanian			
460	Albanian			
480	Albanian			
500	Albanian			
520	Albanian			
540	Albanian			
560	Albanian			
580	Albanian			
600	Albanian			
620	Albanian			
640	Albanian			
660	Albanian			
680	Albanian			
700	Albanian			
720	Albanian			
740	Albanian			
760	Albanian			
780	Albanian			
800	Albanian			
820	Albanian			
840	Albanian			
860	Albanian			
880	Albanian			
900	Albanian			
920	Albanian			
940	Albanian			
960	Albanian			
980	Albanian			
1000	Albanian			

Age	Lithology	Smear Slide Average	X-ray	Comments
360	Albanian			
380	Albanian			
400	Albanian			
420	Albanian			
440	Albanian			
460	Albanian			
480	Albanian			
500	Albanian			
520	Albanian			
540	Albanian			
560	Albanian			
580	Albanian			
600	Albanian			
620	Albanian			
640	Albanian			
660	Albanian			
680	Albanian			
700	Albanian			
720	Albanian			
740	Albanian			
760	Albanian			
780	Albanian			
800	Albanian			
820	Albanian			
840	Albanian			
860	Albanian			
880	Albanian			
900	Albanian			
920	Albanian			
940	Albanian			
960	Albanian			
980	Albanian			
1000	Albanian			

Age	Lithology	Smear Slide Composition	X-Ray	Comments
360	Albanian			
380	Albanian			
400	Albanian			
420	Albanian			
440	Albanian			
460	Albanian			
480	Albanian			
500	Albanian			
520	Albanian			
540	Albanian			
560	Albanian			
580	Albanian			
600	Albanian			
620	Albanian			
640	Albanian			
660	Albanian			
680	Albanian			
700	Albanian			
720	Albanian			
740	Albanian			
760	Albanian			
780	Albanian			
800	Albanian			
820	Albanian			
840	Albanian			
860	Albanian			
880	Albanian			
900	Albanian			
920	Albanian			
940	Albanian			
960	Albanian			
980	Albanian			
1000	Albanian			

Age	Lithology	Smear Slide Average	X-Ray	Comments
360	Albanian			
380	Albanian			
400	Albanian			
420	Albanian			
440	Albanian			
460	Albanian			
480	Albanian			
500	Albanian			
520	Albanian			
540	Albanian			
560	Albanian			
580	Albanian			
600	Albanian			
620	Albanian			
640	Albanian			
660	Albanian			
680	Albanian			
700	Albanian			
720	Albanian			
740	Albanian			
760	Albanian			
780	Albanian			
800	Albanian			
820	Albanian			
840	Albanian			
860	Albanian			
880	Albanian			
900	Albanian			
920	Albanian			
940	Albanian			
960	Albanian			
980	Albanian			
1000	Albanian			